



Royal Military Academy
Signal and Image Centre
Brussels — Belgium

Scatterometer Algorithm Review

Technical Report no: RMA-SIC-011109

X. Neyt, P. Pettiaux, N. Manise, A. Elyouncha,
M. De Smet, E. Cuvelier and M. Acheroy

March 1, 2012

ESA Study Manager: P. Lecomte
EUROPEAN SPACE AGENCY CONTRACT REPORT
The study was performed under ESA contract: 15183/01/I-LG.
Responsibility for contents resides in the author or organisation that prepared it.

Contents

1	Scope	7
2	Notations and acronyms	8
3	Reference documents	10
I	SCATT/ERS-2 Algorithm Description	12
4	Overall Scatterometer description	13
4.1	Scatterometer Principle	13
5	Ground processing description	14
5.1	Functional block diagram	14
5.2	Signal preprocessing	14
5.2.1	Resampling and Refiltering	14
5.2.1.1	On-board filtering and sampling	14
5.2.1.2	Resampling	15
5.2.1.3	Refiltering	16
5.2.2	Doppler compensation	17
5.2.3	Low Pass Filtering — Butterworth filter	18
5.2.4	Envelope detection	18
5.3	Signal processing	19
5.3.1	Kp Calculation	19
5.3.2	Block Averaging	19
5.3.3	ADC Nonlinearity Correction	19
5.3.4	Noise Subtraction	20
5.3.5	Internal Calibration Correction	20
5.3.6	Normalization	21
5.3.7	Spatial Filtering	21
5.3.8	Geometry Parameters Calculation	22
5.3.8.1	The GEM-6 Model	22
5.3.8.2	The Orbit Propagator	23
5.3.8.3	The Different Coordinate Systems Used	23
5.3.8.3.1	Inertial Frame: γ -frame	23
5.3.8.3.2	Latitude-Longitude Frame: g -frame	24
5.3.8.3.3	Geocentric Orbital Frame: $geoorb$ -frame	25
5.3.8.3.4	Satellite Centred Orbital Frame: $satorb$ -frame	26
5.3.8.3.5	Relative Satellite Centred Orbital Frame: $relsat$ -frame	27
5.3.8.3.6	Platform Frame: $plat$ -frame	28
5.3.8.3.7	Antenna Frames: a -frames = for , mid , aft -frames	29
5.3.8.4	The Transformations between the Coordinate Systems	30

5.3.8.4.1	Inertial frame to Latitude-Longitude frame Transformation . . .	30
5.3.8.4.2	Inertial frame to Geocentric Orbital frame Transformation . . .	31
5.3.8.4.3	Geocentric Orbital frame to Satellite Centered Orbital frame Transformation	33
5.3.8.4.4	Inertial frame to Satellite Centered Orbital frame Transformation	33
5.3.8.4.5	Satellite Centered Orbital frame to Relative Satellite Centered Orbital frame Transformation	34
5.3.8.4.6	Inertial frame to Relative Satellite Centered Orbital frame Transformation	36
5.3.8.4.7	Relative Satellite Centered Orbital frame to Platform frame Transformation	36
5.3.8.4.8	Inertial frame to Platform frame Transformation	38
5.3.8.4.9	Satellite Centered Orbital frame to Platform frame Transformation	38
5.3.8.4.10	Platform frame to Antenna frame Transformation	38
5.3.8.4.11	Inertial frame to Antenna frame Transformation	40
5.3.8.5	Steering Modes	40
5.3.8.5.1	Yaw Steering Mode	40
5.3.8.5.2	Fine Pointing Mode	41
5.3.8.6	Determination of the Point Position	41
5.3.8.6.1	Exact solution	41
5.3.8.6.2	Approached solution	45
5.3.8.7	Determination of the Point Speed Vector	45
5.3.8.8	Determination of the Doppler Shift	45
5.3.8.9	Node location	45
5.4	Quality control and monitoring	46
5.4.1	High Power Amplifier Monitoring	46
5.4.2	Power spectrum monitoring	46
5.4.3	I/Q Imbalance Monitoring	47
5.4.4	Internal Calibration Level Monitoring	47

II ASCAT/METOP Algorithm Description 48

6 Overall Scatterometer description 49

6.1	General description	49
6.2	Measurement Mode	49
6.3	On-board echo processing	50
6.3.1	Pulse generation	51
6.3.2	De-chirping principle	51
6.3.3	Narrow Band Filters	52
6.3.4	Spatial averaging (range)	53
6.3.5	Spatial averaging (azimuth)	53
6.4	Calibration on-board processing	54
6.5	Noise on-board processing	54

7 Ground processing description 56

7.1	Ground processing principle	56
7.2	Measurement data correction	56
7.2.1	R_x filter shape estimation	56
7.2.2	Noise power estimation	57
7.2.3	Power gain product estimation	57
7.2.4	Data correction	58
7.3	Sample geometric localisation	58

7.3.1	Exact solution	58
7.3.2	Approached solution	59
7.4	Power to σ^o conversion	59
7.5	Spatial filtering	60
7.5.1	Node geometry	60
7.5.2	Sample selection	60
7.5.3	Sample weight	60
7.6	K_p computation	60
 III SCATT/ERS algorithm review		 61
8	Preprocessing	62
8.1	ADC Non-linearity correction (signal)	62
8.2	I/Q imbalance correction	62
8.3	Theoretical modelling	63
8.4	On-board anti-aliasing filter	64
8.5	Amplitude correction filter	64
8.5.1	Constant power spectral density	64
8.5.2	Pulse-power spectral density	65
8.5.3	Current filter	67
8.5.4	Discussion and comparison with the current filter	67
8.6	Doppler compensation	68
8.7	Low-pass filter	68
8.7.1	The signal bandwidth	68
8.7.2	The Butterworth filter	68
9	Yaw angle estimation	70
9.1	Introduction	70
9.2	Doppler frequency shift measurements	70
9.2.1	Frequency-shift measurement	70
9.2.2	Spectral correction	71
9.3	Yaw angle model	72
9.3.1	Constant speed-field model	72
9.3.2	Circular-orbit model	72
9.3.3	Comparison	74
9.4	Influence of Yaw misestimation	74
9.4.1	Influence on the normalization factor	74
9.4.2	Geometric influence	75
10	Along-track filtering	77
10.1	Introduction	77
10.2	Filters	77
10.2.1	Gaussian filter	77
10.2.2	Moving-average filter	78
10.2.3	Dirac-filter	78
10.2.4	Recursive filter	79
10.3	Gap-filling	79
11	Node geometry	81
11.1	Formulas for the node row geometry	81
11.1.1	The position of the node 10	81
11.1.2	The ellipse center in the g frame	82
11.1.3	The unit vectors in the direction of the ellipse axes	83

11.1.4	The lengths of the semi-axes	83
11.1.5	The other 18 nodes positions	83
11.1.6	The latitude and the longitude	84
11.1.7	The subsatellite track heading	85
11.2	The sample selection	85
11.2.1	The node local normal	86
11.2.2	The two square window unit vectors	86
11.2.3	The tangential plane	86
11.2.3.1	Determination of the projection point P'	87
11.2.4	The sample projections	87
11.2.5	The criteria of sample appurtenance to a node	87
11.3	The samples pre-selection	88
11.3.1	Hypothesis	88
11.3.2	The node parameters	88
11.3.3	The node limits depending on the beam	88
11.3.3.1	Determination of the Earth's point from a point of the tangential plane	89
11.3.3.2	Range to index conversion	89
11.3.3.3	Fore beam	90
11.3.3.4	Mid beam	91
11.3.3.5	Aft beam	92
11.4	The location of the nodes rows	93
11.5	Incidence angle and look-angle	94
11.5.1	The incidence angle of an Earth's point	94
11.5.2	The incidence angle of a node	94
11.5.3	The look-angle of an Earth's point	94
11.5.3.1	Projection of the vector from the satellite position to P onto the local tangential plane	94
11.5.3.2	Vector tangent to the local meridian at an Earth's point	95
11.5.3.3	The look-angle of an Earth's point	95
11.5.4	The look-angle of a node	96
12	K_p computation	97
12.1	Introduction	97
12.2	Expected σ^0 value	97
12.2.1	Sample value σ_{ij}^0	97
12.2.2	Node value σ^0	98
12.3	Variance of σ^0	98
12.3.1	Direct estimation	98
12.3.2	Indirect estimation	98
13	Ingestion	100
13.1	Introduction	100
13.2	EWIC file merging	100
13.2.1	Introduction	100
13.2.2	Initialization phase	101
13.2.3	Timecode correction phase	101
13.2.4	Source packet quality assessment	101
13.2.4.1	Corrupted beam-field	101
13.2.4.2	Corrupted Doppler coefficients	101
13.2.4.3	Frame checksum flag set	102
13.2.5	Source packet selection and merging	102
13.3	EWIC file ingestion	102
13.3.1	Calibration packet rejection	102
13.3.2	Dummy packet rejection	102

13.3.3	Corrupted noise power	102
13.3.4	Corrupted calibration pulses	102
13.3.5	Calibration pulse missing	102
13.3.6	Wave gap	103
13.3.7	Data gap	103
13.3.8	Arcing event	103
IV	User provided grid processing	104
14	Introduction	105
15	Nodes generation and pre-selection	106
15.1	Generation of the grid nodes	106
15.2	Selection of the grid nodes	106
15.3	User-provided grid input format	106
16	Sample pre-selection and selection	107
17	Spatial filtering	109
17.1	Design of the spatial averaging window	109
17.1.1	Separable Hamming window	109
17.1.2	Circular Hamming window	109
17.2	Aliasing analysis	110
17.3	Spatial resolution	111

Chapter 1

Scope

Due to the partial failure of some of the gyroscopes on board of ERS-2, a gyro-less Attitude and Orbit Control System is used to pilot the attitude of the satellite since January 2001. The resulting degraded spacecraft attitude, and in particular the yaw depointing leads to a degradation of the quality of the σ^0 -data. The reason of the data quality degradation is that the algorithm currently used to process the ERS-2 scatterometer raw data, defined in the period 1985-1987, heavily relies on pre-computed look-up tables and is thus not able to handle data acquired in degraded attitude conditions.

This document reports on the study performed in order to analyse the existing algorithm, evaluates the impact of the gyro-less piloting on that algorithm and suggests improvements to be included in the upgraded processing chain.

The first part of this document reviews the current ground processing chain of the ERS-2 Scatterometer (AMI in Wind mode) up to σ^0 -triplets. Special care is devoted to the discussion of the assumptions that were made within the current ground processing, particularly regarding the assumption of a correct yaw steering (minimum mid-beam Doppler shift). The mathematical part of the processing steps is only described at the level of detail needed to discuss the assumptions made.

The second part briefly describes the METOP scatterometer (ASCAT). The on-board and the on-ground processing, being largely different from the AMI/ERS-one are also briefly described.

In the third and last part of this document, specific points of the AMI/ERS ground processing are reviewed. The focus is put on processing steps affected by the degraded attitude steering, such as the yaw angle estimation, influence of yaw angle estimation errors and geometric characterization of the nodes. Other points that might benefit from advances in signal processing methods and processing power, such as the amplitude correction filter and the estimation of the K_p are furthermore discussed.

Chapter 2

Notations and acronyms

ESA	European Space Agency
ERS	European Remote Sensing satellite
METOP	Meteorological Operational satellite
SCAT	Scatterometer
ASCAT	Advanced Scatterometer
AMI	Active Microwave Instrument
AOCS	Attitude and Orbit Control System
ADC	Analog to Digital Converter
A/D	Analog to Digital
DC	Doppler Compensation
IC	Internal Calibration
HPA	High Power Amplifier
Rx	Receiver
Tx	Transmitter
for(e) antenna	antenna looking forward
mid antenna	antenna looking sideward
aft antenna	antenna looking backward
FMA	for(e)-, mid-, aft-
YSM	Yaw Steering Mode
FPM	Fine Pointing Mode
GEM	Goddard Earth Model
RF	Radio Frequency
LFM	Linear Frequency Modulation
PRF	Pulse Repetition Frequency
FPF	Frequency Power profile
σ^0	sigma-nought (absolute normalized radar cross-section)
Kp	normalized standard deviation of σ^0
γ -frame	inertial frame
g-frame	latitude-longitude frame
georb-frame	geocentric orbital frame
satorb-frame	satellite centred frame
relsat-frame	relative satellite centred frame
plat-frame	platform frame
a-frame	antenna frame

I/Q	In-phase/ Quadrature
COG	Center Of Gravity
GHA	Greenwich Hour Angle
PSD	Power Spectral Density
SNR	Signal to Noise Ratio
IIR filter	Infinite Impulse Response filter
FT	Fourier Transform
FFT	Fast Fourier Transform

Chapter 3

Reference documents

- [1] Ers-2 satellite system requirements specification. Technical Report ER-RS-DSF-SA-0000, Dornier ESA, September 1992.
- [2] Ers-2 satellite to ground segment interface specification. Technical Report ER-IS-ESA-GS-0002, ESA ESTEC, December 1993. ERS-2 Programme.
- [3] H. C. Andrews and B. R. Hunt. *Digital Image Restoration*. Prentice Hall, Inc., Englewood Cliffs, New-Jersey, USA, 1977.
- [4] E. P. W. Attema. The active microwave instrument on-board the ERS-1 satellite. In *Proc. of the IEEE*, volume 79, pages 791–799. IEEE, June 1991.
- [5] K. Brinz, Dr.L. Schmieder, and S. Schuetz. Description of simulation model (scatterometer system simulator). Technical Report ER-MA-DSF-SY-0006, Dornier ESA, September 1989. Project ERS-1.
- [6] J. C. Curlander and R. N. McDonough. *Synthetic Aperture Radar*. John Wiley & Sons, New-York, 1991.
- [7] L. B. Jackson. *Digital Filters and Signal Processing*. Kluwer Academic Publishers, 1995.
- [8] A. K. Katsaggelos. *Digital Image Restoration*. Springer-Verlag, 1991.
- [9] S. Lauchaud. Scatterometer kp - calculation from echo samples. Technical Report ER-PL-DSF-FL-0004, Dornier Daimler-Benz Aerospace, September 1995.
- [10] P. Lecomte. The ERS scatterometer instrument and the on-ground processing of its data. In *Proc. of a Joint ESA-Eumetsat Workshop on Emerging Scatterometer Applications*, pages 241–260, Noordwijk, The Netherlands, November 1998. ESTEC.
- [11] Dr.C. Lin, D. Miller, and Dr.R. Zahn. Ers-1 wind scatterometer impulse response - engineering manual to the scatt design modelling -. Technical Report ER-RP-DOS-AM-3009, Dornier ESA, 1986. ERS-1 AMI SUB.
- [12] D. G. Long and M. W. Spencer. Radar backscatter measurement accuracy for a spaceborne pencil-beam wind scatterometer with transmit modulation. *IEEE Trans. on Geoscience and Remote Sensing*, 35(1):102–114, January 1997.
- [13] R. M. Mersereau. The processing of hexagonally sampled two-dimensional signals. In *Proceedings of the IEEE*, volume 67, pages 930–949, June 1979.
- [14] Dr.H. Munz and S. Schutz. Wind scatterometer ground processing requirements up to σ^0 - triplets. Technical Report ER-RP-DSF-SY-0006, Dornier ESA, December 1987. Project ERS-1.

- [15] X. Neyt, P. Pettiaux, M. De Smet, and M. Acheroy. Scatterometer algorithm review for gyro-less operation. Technical Report RMA-SIC-011109, RMA, December 2001.
- [16] R. K. Raney. Doppler properties of radars in circular orbits. *Int. J. Remote Sensing*, 7(9):1153–1162, September 1986.
- [17] F. Rostan, M. Kuntz, and S. Schutz. The advanced scatterometer (ASCAT) ground processing prototype. In *Proceedings of the IEEE International Geoscience and Remote Sensing Symposium*, volume 1, pages 224–226, June 1999.
- [18] K. Sahr, D. White, and A. J. Kimerling. Geodesic discrete global grid systems. *Cartography and Geographic Information Science*, 30(2):121–134, April 2003.
- [19] G. Seeber. *Satellite Geodesy*. Walter de Gruyter, Berlin, 1993.
- [20] M. Suess, P. Matos, A. Gutierrez, M. Zundo, and M. Martin-Neira. Processing of SMOS level 1C data onto a discrete global grid. In *Proceedings of the IEEE International Geoscience and Remote Sensing Symposium*, volume 3, pages 1914–1917, September 2004.
- [21] J. Wollrab and R. Kulzer. Description of geometry modelling - engineering manual -. Technical Report ER-SR-DOS-AM-3002, Dornier ESA, November 1986. Project ERS-1 AMI SUB.
- [22] Marta Woodward and Francis Muir. Hexagonal Sampling. Technical report, Stanford Exploration Project - Report no 38, Stanford, CA, 1984.

The documents [1], [2], [5], [11], [14] and [21] are not available to external users.

Part I

SCATT/ERS-2 Algorithm Description

Chapter 4

Overall Scatterometer description

4.1 Scatterometer Principle

The scatterometer is a radar sending sequentially RF pulses with a carrier frequency of 5.3 GHz.

The backscattered signal is measured to determine the wind speed and direction at the sea surface and for ice and land monitoring. The wind characteristics are determined using a model which relates the sea surface backscattered signal after ground processing, ie the absolute normalized radar cross-section σ^0 , to the wind speed and direction relative to the radar beam.

Each Earth's area has to be illuminated under at least three different directions to obtain unambiguous wind characteristics. Consequently, the scatterometer has three antennas, one looking forward (the fore antenna), one looking sideward (the mid antenna) and one looking backward (the aft antenna) with respect to the spacecraft flight direction.

The swath of approximately 500 km width is parallel to the subsatellite track (approximately 220 km separate the subsatellite track from the nearest side of the swath). A regular grid of points, called nodes, is defined inside the swath. The spacing of the grid nodes is approximately 25 km. A σ^0 -triplets is associated to each node, after a weighted average of all the radar echoes received from the neighborhood of that node. The final products, wind speed and direction, are given at each of these nodes.

Due to the motion of the spacecraft and due to the Earth's rotation, the received signal is Doppler shifted. The Doppler shift varies significantly over the elliptical orbit and has to be compensated to keep the signal into the passband of the system. It is different for the three antennas. In the Yaw Steering Mode (YSM), the satellite is steered in roll and pitch to achieve a local normal pointing on the oblate Earth and in yaw to compensate the Doppler shift of the mid antenna. In the Fine pointing Mode (FPM), the satellite is steered to achieve a pointing parallel to the axis Earth's center-Satellite's center of gravity (COG) and to keep the mid antenna orientation parallel to the absolute spacecraft's velocity direction.

A more detailed general description of the Scatterometer can be found in the document [5], pp 6-19, with a short description of the on-board processing and of the content of the echo signal.

Chapter 5

Ground processing description

5.1 Functional block diagram

A Ground Processing Functional Block Diagram can be found in the document [14], p 19.

5.2 Signal preprocessing

The aim of the low-pass filtering operation is to increase the signal to noise ratio by rejecting frequency components bearing no useful information. This low-pass filtering operation can only efficiently be performed if the useful signal spectrum is centered in the filter window, such that the filter only keeps the useful signal and rejects the noise.

Centering the signal implies performing a compensation of the Doppler frequency shift induced by the relative motion of the satellite w.r.t. the Earth. This Doppler frequency shift compensation is partially performed on-board so the useful signal would fit in the bandwidth of the on-board amplifier and ADC. A second, finer, Doppler shift compensation is performed on ground. This Doppler frequency shift compensation requires taking some precaution, resampling, against aliasing artefacts, that would increase the noise content of the signal.

Moreover since one wants to measure the energy of the signal, it is required that the spectral characteristic of the system is flat (0dB) inside the system pass-band. A compensation filter, aiming at correcting the spectral behavior of the on-board anti-aliasing filter is thus required before the Doppler shift compensation.

5.2.1 Resampling and Refiltering

5.2.1.1 On-board filtering and sampling

The sampling frequency of the on-board ADC is 30kHz. Hence, a discrete anti-aliasing filter has to be used with the aim of reducing the power of signal components above 15kHz. The on-board anti-aliasing filter used is a Bessel filter (see [11], p106) that can be modelled with equation

$$H(p) = \frac{1}{(1 + a_1p + b_1p^2)(1 + a_2p + b_2p^2)} \quad (5.1)$$

with $a_1 = 1.3397$, $b_1 = 0.4889$, $a_2 = 0.7743$ and $b_2 = 0.3890$. The parameter $p = j\frac{f}{f_c}$ is a normalized frequency where f_c is the considered cut-off frequency. According to the filter characteristic mask (given in [1], p 240, fig 3.5.2.3.2.3-5), the cut-off frequency must be between 11.5kHz and 12.5kHz. A cut-off frequency of 12kHz was considered in this document. The frequency response of the filter is given by the blue curve in figure 5.1.

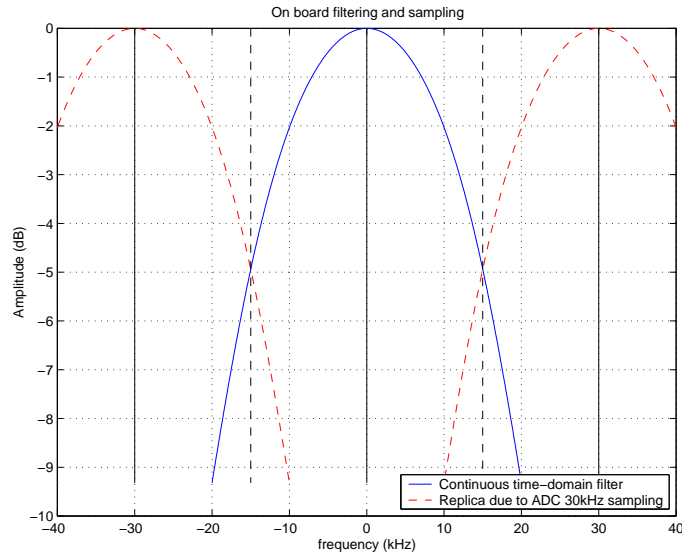


Figure 5.1: Illustration of the effect of the on-board sampling (ADC).

The sampling of the ADC causes aliasing. The part of the spectrum located at frequencies higher than 15kHz, half the sampling frequency, is aliased back. This is illustrated by the red dashed curves in figure 5.1. These aliased components have to be interpreted as noise.

5.2.1.2 Resampling

Increasing the sampling frequency (upsampling) is needed to avoid frequency-leakage when the signal will be shifted in frequency as part of the Doppler Compensation (DC) operation.

Upsampling involves introducing more information in the signal. Obviously, the new frequency components of the signal are unknown. It was chosen to consider the signal coming from the space-segment as band-limited to $\pm 15\text{kHz}$ (half the on-board sampling frequency). A band-limited signal with higher sampling frequency is thus obtained by synthesizing a new signal having the same spectrum for $f \leq 15\text{kHz}$ and zero for $f > 15\text{kHz}$. I.e.

$$S_r(f) = \begin{cases} S(f) & f \leq 15\text{kHz} \\ 0 & f > 15\text{kHz} \end{cases} \quad (5.2)$$

where $S(f)$ is the spectrum of the original signal and $S_r(f)$ is the spectrum of the upsampled signal. This is illustrated on figure 5.2

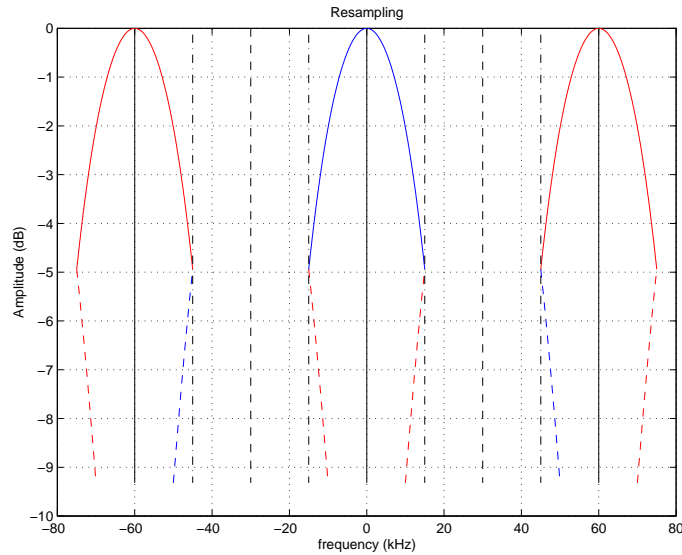


Figure 5.2: Illustration of the effect of the resampling in the frequency domain.

The main advantages of making the band-limited hypothesis when upsampling are 1) simplicity of implementation and 2) that the goal of avoiding frequency-leakage in the future DC operation is reached. In the case here, the upsampling operation should only be considered as a mean to avoid future problems. The upsampling performed here is not meant to actually increase the useful information content of the signal and the frequency components above half the original sampling frequency (above 15kHz) should be considered as wrong.

5.2.1.3 Refiltering

The refiltering step performed at the same time as the resampling aims at compensating the spectral behaviour of the on-board anti-aliasing filter. The goal is to have a flat spectrum (0dB) in the pass-band.

The spectral behaviour of the resampling filter is thus

$$H_r(f) = \begin{cases} \frac{1}{H(f)} & f \leq 15\text{kHz} \\ 0 & f > 15\text{kHz} \end{cases} \quad (5.3)$$

where $H(f)$ and $H_r(f)$ are the spectra of respectively the on-board filter and the on-ground pre-DC filter.

While the filter is implemented in the frequency domain, it is defined using a truncated impulse response (inverse Fourier transform of $H_r(f)$). The coefficients of the filter are given in table 5.1 (see [1], p198).

n	$h(n)$
0	11.7648
-1,1	-0.1100
-2,2	-0.5776
-3,3	0.5187
-4,4	-0.3169
-5,5	0.1034

Table 5.1: Non normalized amplitude correction filter time-domain coefficients at original sampling frequency (30kHz)

This leads to an approximation, where the 0dB overall characteristic is only obtained in part of the spectrum (see figure 5.3).

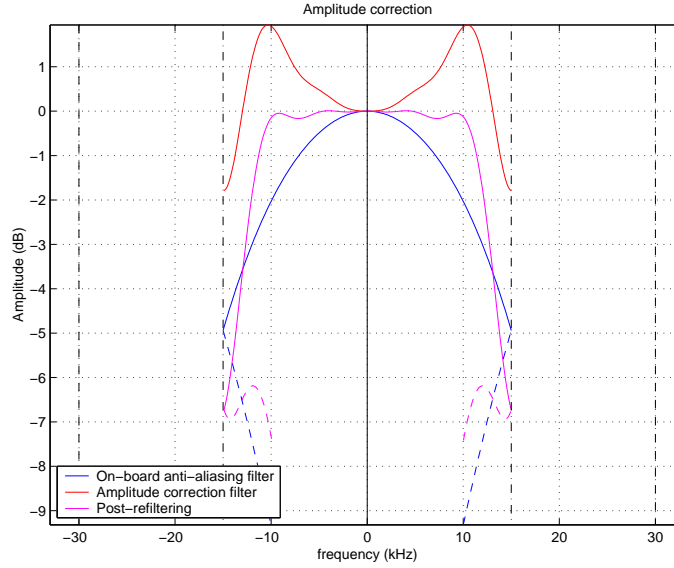


Figure 5.3: Amplitude correction filter and the resulting overall spectral behaviour

5.2.2 Doppler compensation

The relative motion between the satellite and the Earth surface causes, depending on the relative speed, a frequency shift of the returned echo signal. Due to their different orientation, this Doppler frequency shift is different for the three antennas.

In order to have the signal spectrum fit in the on-board anti-aliasing filter pass-band of ± 12 kHz, a coarse compensation of this frequency shift is performed on-board. The on-board compensation laws are different for the fore/aft and mid antennas (see [2], p4.1-65 for the actual formulas and numerical parameter values). Moreover, in Wind Calibration mode (when the antenna beam passes over ground transponders), an additional frequency shift of 540 kHz is applied.

The on-board Doppler compensation is not precise enough to perfectly center the signal within the receiver band. A second Doppler compensation stage is thus required on ground to correct the residual Doppler frequency shift. The frequency shift applied on-ground is given by

$$F_g(\tau, T) = F_{th}(\tau, T) - F_d(\tau, T) \quad (5.4)$$

where F_g , F_{th} and F_d are the on-ground residual Doppler shift, the theoretical Doppler shift and the on-board Doppler compensation respectively (τ is the echo time and T is the orbit time). The theoretical Doppler shift (see section 5.3.8.8) is computed from geometry relations and depends on the position and speed of the satellite w.r.t. the Earth (orbit time) and on the echo time.

The on-ground compensation law is implemented by a multiplication of the signal in the time-domain with a Doppler compensation function

$$s_c(n) = e(n)s(n) \quad n = 0, \dots, N-1 \quad (5.5)$$

with

$$e(n) = e^{-j2\pi F_g(\tau, T)\tau} \quad (5.6)$$

where $\tau = n/F_s$ and F_s is the on-board ADC sampling frequency (30 kHz). $s(n)$ and $s_c(n)$ denote the samples of respectively the original signal and the frequency-shifted signal. In the actual implementation, the phasors $\theta = -2\pi F_g(\tau, T)\tau$ are actually interpolated (both in slow and in fast time) from values found in a LUT.

The equivalent of equation (5.5) in the frequency domain is a convolution between $E(k)$ and $S(k)$, respectively the discrete Fourier transform of $e(n)$ and $s(n)$:

$$S_c(k) = E(k) * S(k) \quad k = 0, \dots, N-1 \quad (5.7)$$

The frequency sweep of $e(n)$ is quite small but is not null and hence the corresponding spectrum is not a Dirac impulse $E(k) \neq \delta(F_g/F_s N)$ with as consequence that the support of $E(k)$ is not null. Hence, if the spectrum $S(k)$ is not zero for some $k > N_s$, with $N - N_s > N_e$, leakage will occur in the frequency domain (N_s and N_e are the size of the support of the signal and the Doppler compensation function respectively).

This frequency leakage is due to the fact that implementing a convolution using a multiplication in the discrete Fourier-transformed domain implies the hypothesis of a circulant filter (samples past the last samples are again the first samples, hence the name ‘‘circulant’’).

Since the signal $S(k)$ was upsampled in the Fourier-transformed domain, the spectrum of the signal is zero for some frequency on and there is no problem of frequency leakage.

5.2.3 Low Pass Filtering — Butterworth filter

The aim of this filter is to keep only the useful signal while rejecting the other components (considered as noise) in order to increase the signal to noise ratio.

The filter currently chosen is a low-pass 4th order Butterworth filter with cut-off frequencies (-3dB) of 8.8kHz and 6.4kHz for respectively the Mid and Fore/Aft beams (see [1], table 3.5.2.2.2.1, p198). The behaviour of the filter is illustrated in figure 5.4.

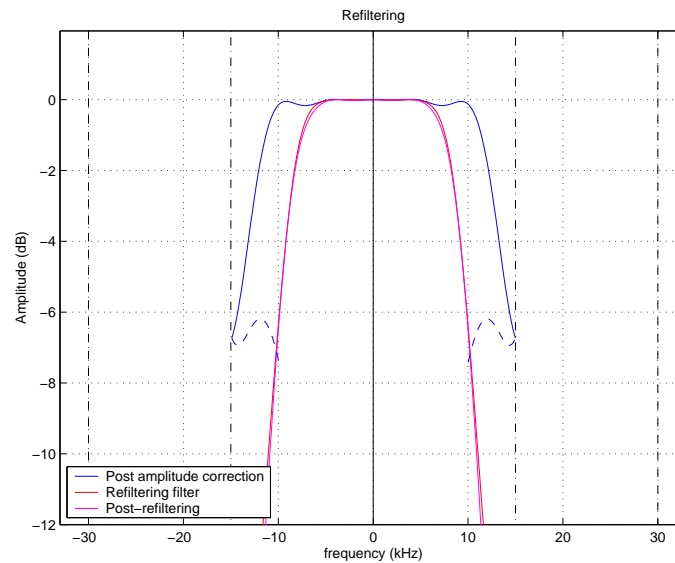


Figure 5.4: Low-pass filter and its effect on the overall spectral behaviour of the system

This filter is implemented in the frequency domain. It is expected that due to the way the previous modules are implemented, and particularly due to the signal extension (adding zeros in the time domain) to 256 samples as part of the resampling and refiltering operation, no particular care should be taken regarding the time-leakage phenomenon. The time-leakage indeed depends on the size of the support of both the signal to be filtered and the impulse response of the filter itself. To avoid aliasing, it is required that $N_f + N_s < N$ where N_f and N_s are the number of non-zero samples (size of the support) of respectively the filter’s impulse response and the signal to be filtered, and N the total number of samples of the output signal.

5.2.4 Envelope detection

The signal received on ground is to be considered as a complex-valued signal (actually, the in-phase and in-quadrature parts)

$$s(n) = s_I(n) + js_Q(n)^2 \quad (5.8)$$

where $s_I(n)$, $s_Q(n)$ and $s(n)$ are the real (in-phase), imaginary (in-quadrature) and the complex-valued signal, respectively. The envelope detection involves taking the modulus of this complex-valued signal i.e.

$$p(n) = |s(n)|^2 = s_I(n)^2 + s_Q(n)^2 \quad (5.9)$$

where $p(n)$ represents the signal instantaneous power.

5.3 Signal processing

5.3.1 K_p Calculation

Complementary data relative to the accuracy of the σ^o values will be needed as input to the σ^o to wind conversion. This accuracy information is contained in the K_p parameter, which is determined for each node and each beam.

A first approach, described in [14], p44, bases the estimation of the K_p value on the noise to signal ratio with the following expression:

$$K_p = \frac{1}{\sqrt{M}} \left(1 + \frac{\sigma_{noise}^o}{\sigma^o} \right) \quad (5.10)$$

where M is the effective number of independent signal samples, and σ_{noise}^o is the σ^o equivalent of the receiver noise power.

Another approach calculates K_p by determining the standard deviation of the derived σ^o values themselves. The algorithm used to compute the standard deviation (see [9], p6) requires the unaveraged measurement block $\sigma_{i,j,p}$ samples. An estimation for K_p can be deduced with:

$$K_p = 100 \times \frac{SD(\sigma^o)}{\sigma^o} \quad (5.11)$$

The first approach is based on the computation of the K_p on the noise power taking into account the correlation between samples, while the second is based on a statistical study of the standard deviation of the σ^o . The second approach requiring $\sigma_{i,j,p}$ values for the computation of variance, correlation coefficients and thus standard deviation, this step must be executed before block averaging.

The first approach takes only into account the noise level measured on-board while the second approach considers the variations of the σ^o and thus is also able to take into account the noise due to speckle, inherent to coherent imaging systems.

5.3.2 Block Averaging

Block averaging consists in averaging the power of corresponding samples of all the echoes (nominally 32) part of one measurement block. The aim of this averaging is to reduce the variance of the signal due to the noise. This is justified by the fact that the area imaged by each of the pulse of the same measurement block is approximately the same, given the duration of these 32 pulses.

The variance of the signal is only effectively reduced if the power (or intensity) of independent signals samples are averaged. If the independence assumption is not valid, the variance reduction will be smaller. This averaging has to be performed incoherently, i.e. on the power (or intensity) signal (squared amplitude). If the signal samples were really independent, their phase would bear no relationship and hence a coherent averaging (taking the complex phase into account) would provide a meaningless result.

5.3.3 ADC Nonlinearity Correction

Radiometric sampling errors may occur due to nonlinearities of the Analogical-to-Digital Converter. Indeed the signal power may be such that a significant proportion of samples exceeds the ADC maximum level or is below the least significant bit level. The correction of these nonlinearities, based on a statistical correction of the power, occurs after block averaging.

The correction factor is defined as the ratio of expected ADC output power to the expected ADC input power in function of the expected ADC output power for a Rayleigh distributed input signal:

$$C(P_{out}) = \frac{P_{out}}{P_{in}(P_{out})} \quad (5.12)$$

and is contained in a look-up table. This correction factor is used to evaluate the expected input power P_{in} in function of the expected ADC output P_{out} :

$$P_{in} = \frac{P_{out}}{C(P_{out})} \quad (5.13)$$

The ADC nonlinearity correction has to be performed for the block averaged target echo as well as for the noise averages. For the block averaged echo, one has

$$s^{ADC}(n) = \frac{s(n)}{C(P_{out})} \quad (5.14)$$

where $s(n)$ and $s^{ADC}(n)$ are the real signal power after block averaging and after ADC-nonlinearity correction, respectively. The P_{out} used is computed by making a running average of the signal power after block averaging on the N last measurement block, where N is a parameter.

For the noise samples,

$$s_N^{ADC} = \frac{s_N}{C(s_N)} \quad (5.15)$$

where $s_N = s_N^I + s_N^Q$ is the sum of the noise power respectively for the I- and Q-channel and s_N^{ADC} is the noise power after ADC-nonlinearity correction.

In both cases, the correction coefficient C in function of the output power is logarithmically interpolated (see [14], p 86 for the details).

5.3.4 Noise Subtraction

In reality, the target signal plus the receiver noise power is measured rather than the target signal alone. To improve the instrument accuracy the receiver noise power is measured separately and then subtracted from the sum of both.

The noise correction is performed by subtracting from each target sample of one measurement block, the averaged noise power estimate P_N corresponding to that measurement block:

$$s_c(n) = s_u(n) - C_N P_N \quad (5.16)$$

where s_u is the square of the averaged uncorrected target signal and s_c the corresponding noise-corrected target signal. P_N is the average of the noise power estimates of the corresponding measurement block.

C_N is the noise correction factor. It is constant and depends on the noise processing chain (see [14], p34) but is different for each beam.

5.3.5 Internal Calibration Correction

Internal calibration consists in injecting a small fraction of the transmit signal directly into the receiver low noise amplifier. During each block, 4 calibration measurements take place. These calibration measurements are received on-ground as I and Q samples.

On-ground, these I and Q samples are first corrected for I/Q imperfection (gain imbalance, non-orthogonality and DC-bias), see [14] p94. The samples corresponding to one calibration pulse are averaged together (using a weighting function) to give the energy of that pulse. The energies of the 4 pulses corresponding to one measurement block are averaged together. In order to reduce quantization noise, the result is further low pass filtered across several measurement blocks by an exponential (recursive) filter (see [14], p96).

Finally, the correction factor is computed

$$g_c = \mathcal{E}/g_{c_0} \quad (5.17)$$

where \mathcal{E} is the filtered calibration pulse energy and g_{c_0} is the reference internal calibration pulse energy.

The correction factor is then applied to the signal and to the noise:

$$s_c(n) = s(n)/g_c \quad (5.18)$$

where $s(n)$ and $s_c(n)$ denote the signal samples respectively before and after IC correction. The formula is similar for the noise IC correction.

5.3.6 Normalization

The signal power at the output of the block averaging is proportional to the instantaneous power. It has to be related to the backscattered coefficient to obtain the σ^0 . This operation is called normalization.

The normalization factor f_N from the echo power profile to the surface backscatter coefficient is (see [11], p17 and p70; see also [6]):

$$f_N(n) = \frac{R^3 \sin \theta}{G_{el}^2(\theta_{el})} \quad (5.19)$$

where

- R = slant range, ie the distance between the spacecraft and the target point: $= ct/2$
- $\theta(n)$ = incidence angle at the target point
- $G_{el}(\theta_{el}(n))$ = one-way antenna gain in the beam elevation plane at the look-angle $\theta_{el}(n)$

These values are interpolated in slow-time, $f_N(n)$ being kept constant for several FMA sequences (see [14], p97). The factor G_{el} takes into account antenna gain variation around the orbit due to thermal variations (see [5], p206, p549).

The normalized power is thus obtained by multiplying the signal power by this normalization coefficient

$$\sigma^0(n) = f_N(n)s_c(n) \quad (5.20)$$

$$= f_N(n)s(n)/g_c \quad (5.21)$$

$$= s(n)/N(n) \quad (5.22)$$

where $\sigma^0(n)$ is the backscattering coefficient (normalized echo power signal sample), $s(n)$ is the unnormalized echo power signal sample before the IC correction, $s_c(n)$ is the unnormalized echo power signal sample after the IC correction, and $N(n) = g_c/f_N(n)$.

5.3.7 Spatial Filtering

Spatial filtering denotes here the operation of computing the spatially averaged σ^0 values at the node locations. The spatial filtering is used to make the impulse response of the scatterometer system match the requirements. Moreover, it is also necessary to reduce the aliasing artefacts due to the coarse along-track sampling.

The spatial averaging at the node location can be seen as a spatial filtering of irregularly sampled data, the filtered result being resampled at the node locations.

The spatial weighting function used to perform the spatial averaging is given by (see [5], p583)

$$w_L(l) = \begin{cases} \beta + (1 - \beta) \cos\left(\frac{2\pi l}{L}\right) & -L/2 < l < L/2 \\ 0 & \text{elsewhere} \end{cases} \quad (5.23)$$

where L is the size of the window and β is a coefficient. For $\beta = 1$, one has a plain rectangular window; for $\beta = 0.54$, one has a Hamming window. The size of the window L has a direct influence on the spatial and spectral resolution.

A two-dimensional window is obtained by making the separability assumption

$$w(x,y) = w_L(x)w_L(y) \quad (5.24)$$

The σ^o value at a node will thus be

$$\sigma_n^o(x_n, y_n) = \frac{\sum_{(x,y) \in \mathcal{D}} w(x,y) \sigma^o(x+x_n, y+y_n)}{\sum_{(x,y) \in \mathcal{D}} w(x,y)} \quad (5.25)$$

where σ_n^o is the averaged σ^o value at the node located in (x_n, y_n) and \mathcal{D} is the set of samples located inside the weighting window ($|x-x_n| < L/2$ and $|y-y_n| < L/2$). For the ease of implementation, the weighting function was sampled, thus leading to possibly having a filter weight being used by several samples. Hence the normalization factor, $w_{\mathcal{D}}(x_n, y_n) = \sum_{(x,y) \in \mathcal{D}} w(x,y)$, needed to be re-computed for each node, even if the weighting function $w(x,y)$ is normalized.

The node location is further discussed in section 5.3.8.9.

5.3.8 Geometry Parameters Calculation

5.3.8.1 The GEM-6 Model

In order to calculate surface related quantities, a geometrical reference model of the Earth is used. This model, the GEM-6 (Goddard Earth Model 6) describes an Earth reference ellipsoid. This ellipsoid is obtained by the rotation of an ellipse around the Earth's rotation axis. It can be thought of as an oblate spheroid. The GEM-6 approximates the Earth surface over the oceans better than ± 100 m.

The equation for the GEM-6 Earth model (ellipsoid) is given by :

$$\frac{x^2 + y^2}{a^2} + \frac{z^2}{b^2} = 1 \quad (5.26)$$

In this equation, there are two constants, a and b . To increase the numerical precision, these parameters are specified as

- equatorial Earth radius: $a = 6378.144$ km
- oblateness coefficient: $f = 1/298.257$

and the polar Earth radius b can be deduced from these values

$$b = a(1 - f) \quad (5.27)$$

The eccentricity of the meridian cross-section can also be defined as

$$e = \sqrt{2f - f^2} = \sqrt{\frac{a^2 - b^2}{a^2}} \quad (5.28)$$

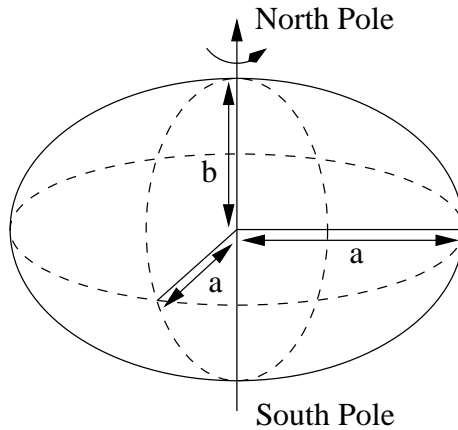


Figure 5.5: The GEM-6 Model

This definition is coherent with the documents:

- [21] p 19
- [14] p 102 : Earth model
- [2] p A.2-3

5.3.8.2 The Orbit Propagator

The basis for the geometry modeling is the ERS Orbit propagator combined with the Earth reference model GEM-6. The orbit propagator delivers spacecraft position and velocity vectors at given time.

The combination of the orbit propagator and the GEM-6 model is assumed to model the real world. Any difference between the models and the true world is out of the present consideration.

5.3.8.3 The Different Coordinate Systems Used

There are a lot of intermediate coordinate systems used to transform the expression of a vector given in one of the three antenna frames to its corresponding expression in the inertial frame, or to make the inverse transformation.

The reference documents do not always use the same intermediate coordinate systems to calculate this global transformation. See [5], pp 224 to 234 and [21], pp 10 to 18 for the transformation matrices between the coordinate systems used in these documents. Besides these two documents, there are other documents that use different frames ([21], p 40).

But of course, the intermediate coordinate systems may not have an influence on the result: the expression from the same vector given in the inertial frame or in one of the antenna frames must be the same whatever the intermediate coordinate systems used are. These intermediate coordinate systems only exist to make the transformations between the inertial frame and the three antenna (FOR, MID, AFT) frames easier.

For the simplicity the coordinate systems used in [5] will be adhered to in this description. The naming convention used in [5] is not always coherent with the one used in the other reference documents. To avoid ambiguity, the name of some of the frames defined in [5] was changed in this description.

The definition and main characteristics of each frame will first be presented in the next section, followed by the transformation between these coordinate systems.

All the coordinate systems are right-handed Cartesian coordinate systems.

5.3.8.3.1 Inertial Frame: γ -frame

This frame is commonly used as the basic astronomical system for orbit calculations. In reality, this frame is not totally inertial but must be considered as a quasi inertial system. In this study, it is nevertheless considered as an inertial frame.

It is an Earth centered (or geocentric) system, with the (x_γ, y_γ) -plane merging the Earth's equatorial plane and the x_γ -axis pointing to the vernal equinox. The slow precession of the x_γ -axis is neglected. The z_γ -axis completes the right-handed Cartesian coordinate system and is pointing to the north pole.

5.3.8.3.1.1 Main characteristics

- geocentric system
- (x_γ, y_γ) -plane lying in the Earth's equatorial plane
- x_γ -axis pointing to the vernal equinox (γ)
- z_γ -axis pointing to the north

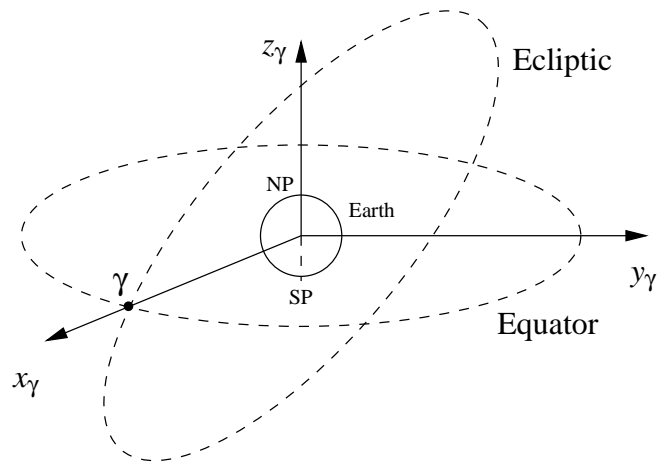


Figure 5.6: Inertial frame: γ -frame

5.3.8.3.1.2 References

This definition is coherent with:

- [5] p 214: Right Ascension Declination Frame (γ -frame)
- [21] p 7: Geocentric Inertial Coordinate System (GI -frame)
- [14] p 103: Right Ascension Declination Frame (γ -frame)

5.3.8.3.2 Latitude-Longitude Frame: g -frame

This geocentric frame is fixed to the rotating Earth, with the (x_g, y_g) -plane lying in the Earth's equatorial plane and the x_g -axis pointing to the Greenwich meridian. The z_g -axis points to the north and completes the right-handed Cartesian frame.

5.3.8.3.2.1 Comment

This g -frame is compliant with the inertial γ -frame once a day, when the Greenwich hour angle is equal to zero.

5.3.8.3.2.2 Main characteristics

- geocentric system
- Earth fixed system
- (x_g, y_g) -plane lying in the Earth's equatorial plane
- x_g -axis pointing to the Greenwich meridian
- z_g -axis pointing to the north pole

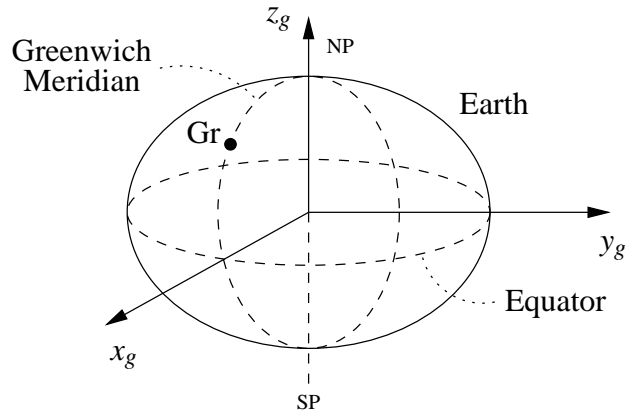


Figure 5.7: Latitude-Longitude frame: g -frame

5.3.8.3.2.3 References

This definition is coherent with:

- [5] pp 218-219: Latitude-Longitude frame (g -frame)
- [21] p 9: Latitude-Longitude Coordinate System (G -frame)
- [14] pp 103-104 : Latitude-Longitude frame (g -frame)

5.3.8.3.3 Geocentric Orbital Frame: $geoorb$ -frame

This is a geocentric system. The (x_{geoorb}, y_{geoorb}) -plane lies in the satellite's orbit plane. The x_{geoorb} -axis is pointing away from the Earth's centre to the satellite's centre of gravity (COG). The y_{geoorb} -axis is perpendicular to the x_{geoorb} -axis and in the plane containing the absolute velocity vector of the satellite, \vec{v}_{sc} , such that the velocity vector of the satellite is approximately along the y_{geoorb} -axis:

$$\cos(\vec{v}_{sc}, \vec{1}_{y_{geoorb}}) > 0 \quad (5.29)$$

The z_{geoorb} -axis completes the right-handed Cartesian coordinate system.

5.3.8.3.3.1 Main characteristics

- geocentric system
- (x_{geoorb}, y_{geoorb}) -plane lying in the momentary orbit plane
- x_{geoorb} -axis pointing in the direction from geocenter to satellite
- in the $geoorb$ -frame, the spacecraft velocity vector has a positive y_{geoorb} -component.

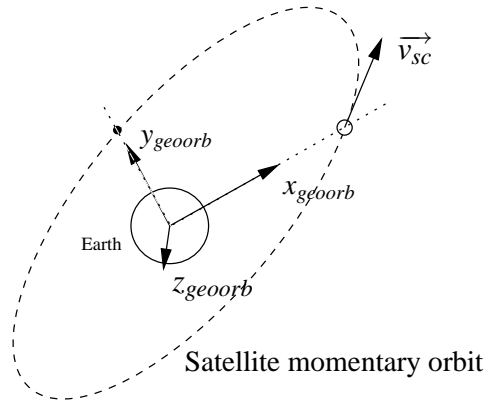


Figure 5.8: Geocentric Orbital frame: *georb*-frame

5.3.8.3.2 References

This definition is coherent with:

- [5] p 214 : Satellite reference frame (*SA*)

5.3.8.3.4 Satellite Centred Orbital Frame: *satorb*-frame

This frame has its origin in the spacecraft's COG. The (x_{satorb}, z_{satorb}) -plane lies in the satellite's orbit plane. The z_{satorb} -axis is pointing away from the Earth's centre to the satellite's COG. The x_{satorb} -axis is perpendicular to the z_{satorb} -axis and in the plane containing the absolute velocity vector, \vec{v}_{sc} , of the satellite such that the velocity vector of the satellite is approximately along the x_{satorb} -axis:

$$\cos(\vec{v}_{sc}, \vec{1}_{x_{satorb}}) > 0 \quad (5.30)$$

The y_{satorb} -axis completes the right-handed Cartesian coordinate system.

5.3.8.3.4.1 Comments

The main difference between the geocentric orbital frame and the satellite centred orbital frame is that these frames don't have the same origin. Apart from this translation between the frame's origins (Earth's centre and satellite's COG, respectively), there is only a transformation between the axes:

$$(x_{satorb}, y_{satorb}, z_{satorb}) = (y_{georb}, z_{georb}, x_{georb}) \quad (5.31)$$

5.3.8.3.4.2 Fine Pointing Mode

This frame is normally used as a reference frame for the satellite's attitude steering: it defines the absolute pointing of the satellite for the fine pointing mode.

5.3.8.3.4.3 Main characteristics

- spacecraft's COG centred system
- (x_{satorb}, z_{satorb}) -plane lying in the momentary orbit plane
- z_{satorb} -axis pointing in the direction from geocenter to satellite's COG
- in the *satorb*-frame, the spacecraft's velocity vector has a positive x_{satorb} -component.

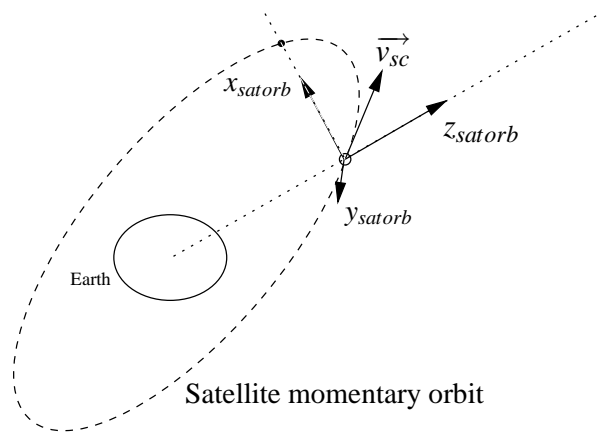


Figure 5.9: Satellite Centred Orbital frame: *satorb*-frame

5.3.8.3.4.4 References

This definition is coherent with:

- [21] p 7: Orbit Coordinate System (Orbit-Frame)
- [2] p A.2-2: Local Orbital Reference Frame (T, R, L)

5.3.8.3.5 Relative Satellite Centred Orbital Frame: *relsat*-frame

This frame has its origin in the spacecraft's centre of gravity (COG). The z_{relsat} -axis is pointing in the direction of the outward local normal of the Earth's reference ellipsoid defined by the GEM-6 model. The y_{relsat} -axis is in the direction of the velocity vector \vec{v}'_{sc} of the subsatellite point relative to the Earth model surface, taking into account a plane elliptical orbit with the orbital elements of the ERS-2 Reference Orbit (see [2], p 3-1). The x_{relsat} -axis completes the right-handed Cartesian coordinate system.

5.3.8.3.5.1 Comments

The unit vectors of this frame are close to the unit vectors of the *satorb*-frame (not taking into account a rotation of 270° around the z -axis). The main difference is that the y_{relsat} -axis is now by construction aligned with the relative ground track velocity of the satellite but still perpendicular to the z_{relsat} -axis, which is close but not compliant with the z_{satorb} -axis. The x_{satorb} -axis is not, in general, perfectly parallel with the velocity vector of the satellite.

5.3.8.3.5.2 Yaw Steering Mode

This frame is normally used as a reference frame for the satellite's attitude steering: it defines the absolute pointing of the satellite for the yaw-steering mode with $x_{relsat}, y_{relsat}, z_{relsat}$ being the pitch, roll and yaw axes respectively.

5.3.8.3.5.3 Main characteristics

- spacecraft's COG centred system
- z_{relsat} -axis pointing in the direction of the outward local normal in the geodetic subsatellite position (nadir)
- y_{relsat} -axis pointing in the direction of the relative ground trace velocity vector
- x_{relsat} -axis completing the right-handed Cartesian coordinate system

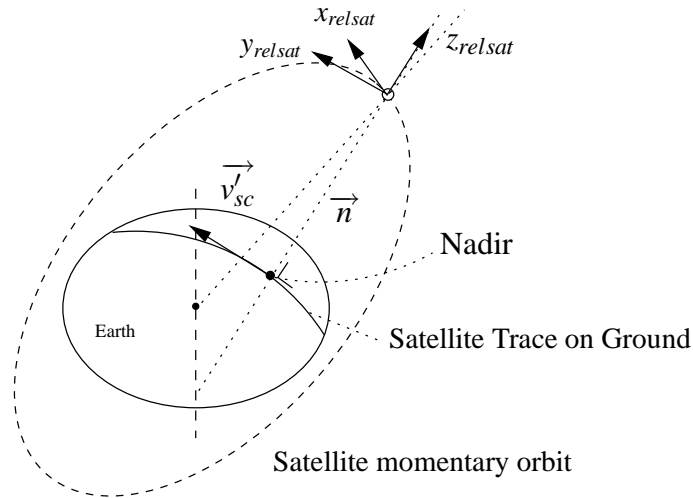


Figure 5.10: Relative Satellite Centred Orbital Frame: *relsat*-frame

5.3.8.3.5.4 References

This definition is coherent with:

- [5] p 215: Local relative orbital frame 2 (*L*-frame)
- [2] p A.2-3: Local Relative Orbital Reference Frame (T', R', L')

5.3.8.3.6 Platform Frame: *plat*-frame

This frame is fixed on the spacecraft.

Its origin is at the spacecraft's COG. The z_{plat} -axis is parallel to the outward normal to the surface carrying the stowed solar array. The x_{plat} -axis is parallel to the longitudinal (downward vertical) axis of the satellite on the launch vehicle. The y_{plat} -axis completes the right-handed Cartesian coordinate system and is such that:

$$\cos(\vec{v}_{sc}, \vec{1}_{y_{plat}}) > 0 \quad (5.32)$$

5.3.8.3.6.1 Yaw Steering Mode and Fine Pointing Mode

This frame is, if the pointing errors are neglected, respectively merging the Relative Satellite Centred Orbital Frame in the Yaw Steering Mode, and the Satellite Centred Orbital Frame in the Fine Pointing Mode (up to a rotation of 270° around the z -axis).

5.3.8.3.6.2 Main characteristics

- spacecraft's COG centred system
- fixed on the spacecraft
- z_{plat} -axis parallel to the outward normal to the surface carrying the stowed solar array
- x_{plat} -axis parallel to the longitudinal (downward vertical) axis of the satellite on the launch vehicle
- y_{plat} -axis completes the right-handed Cartesian frame

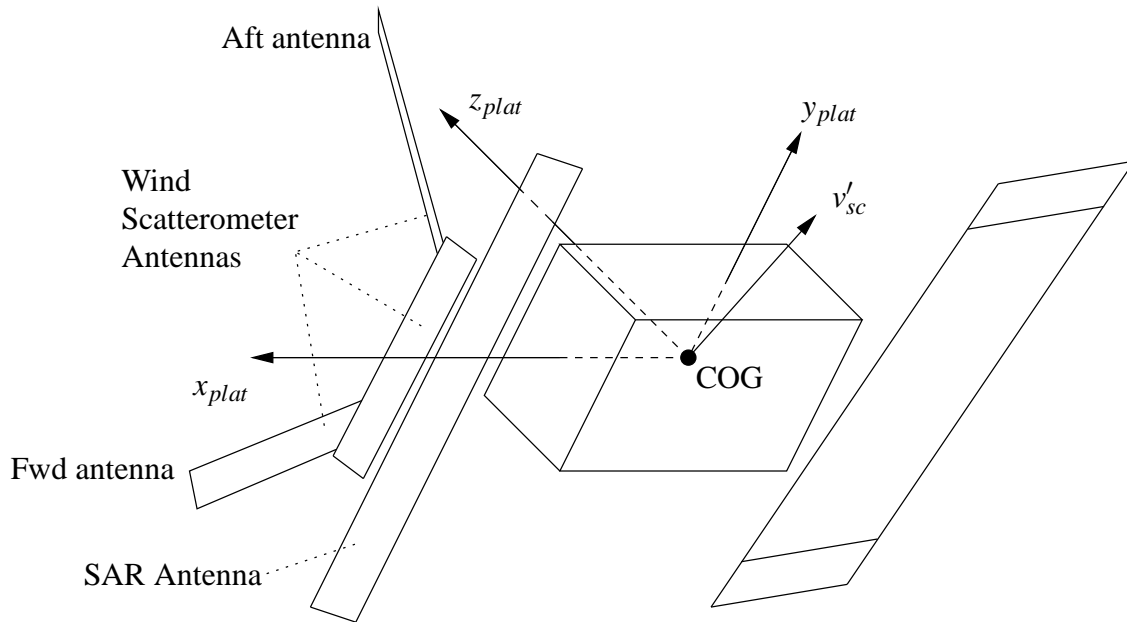


Figure 5.11: Platform frame: *plat*-frame

5.3.8.3.6.3 References

This definition is coherent with

- [5] p 215: Platform frame (*P*-frame)
- [21] p 8: Platform Coordinate System (Platform-Frame), except that pitch= y -axis (in stead of x -axis) and roll= x -axis (in stead of y -axis)
- [2] p A.2-6: Attitude (Piloting) Reference Frame (X_p, Y_p, Z_p), except for the origin of the frames

5.3.8.3.7 Antenna Frames: *a*-frames = *for*, *mid*, *aft*-frames

There are three antenna frames, one for each beam: *for*, *mid* and *aft*-beam.

For each of the AMI antenna frames, the (x_a, y_a) -plane is parallel to the antenna reflecting surfaces, with the x_a -axis parallel to the longitudinal side of the antenna, the z_a -axis is in the direction of the normal to the surface, to the mechanical boresight direction, and the satellite's velocity vector has a positive x_a -component:

$$\cos(\vec{v}_{sc}, \vec{1}_{x_a}) > 0 \quad (5.33)$$

These frames are thus in a fixed orientation in regard with the platform frame.

The offset between the origin (centre of the antenna) of these antenna frames and the satellite's COG is constant, and noted $\vec{r}_{plat_{ac}}$, in the *platform*-frame.

5.3.8.3.7.1 Main characteristics

- antenna centered system
- fixed on the spacecraft
- (x_a, y_a) -plane parallel to the antenna radiating surface
- (y_a, z_a) -plane representing the elevation plane
- in the *a*-frames, the spacecraft's velocity vector has a positive x_a -component; for the *mid*-beam, the x_{mid} -axis is pointing approximately in the flight direction of the satellite

- z_a -axis pointing in the direction of the normal to the surface

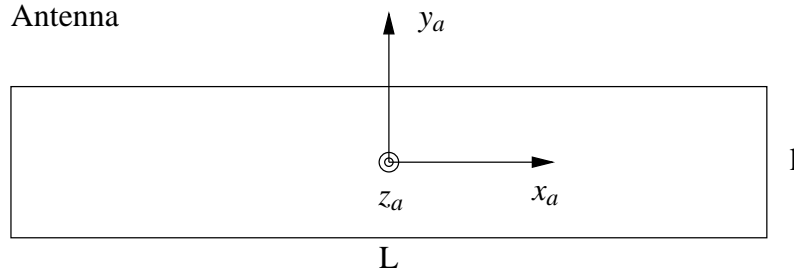


Figure 5.12: Antenna frames: a -frames

5.3.8.3.7.2 References

This definition is coherent with:

- [5] p 216: Antenna frame (A)
- [21] pp 8-9: Scan Coordinate Systems (Scan-Frames), except that the z -axis of these refers to the electrical boresight direction and not to the mechanical boresight direction
- [2] pp A.2-8 - A.2-9: Antenna Local Reference Frames ($X_{ANT}, Y_{ANT}, Z_{ANT}$)

5.3.8.4 The Transformations between the Coordinate Systems

5.3.8.4.1 Inertial frame to Latitude-Longitude frame Transformation

The transformation matrix from the Inertial frame to the Latitude-Longitude frame is a rotation matrix around the common z -axis of these two frames. The rotation angle, noted GHA , is the Greenwich hour angle. The value of GHA depends of the orbit time and is calculated by the ERS orbit propagator.

Notation $\mathcal{T}_{\gamma 2g}$

Expression

$$\mathcal{T}_{\gamma 2g} = \begin{pmatrix} \cos GHA & \sin GHA & 0 \\ -\sin GHA & \cos GHA & 0 \\ 0 & 0 & 1 \end{pmatrix} \quad (5.34)$$

Property If \vec{r}_γ is a vector given in the Inertial frame, then the corresponding vector in the Latitude-Longitude frame, \vec{r}_g , is given by:

$$\vec{r}_g = \mathcal{T}_{\gamma 2g} \cdot \vec{r}_\gamma \quad (5.35)$$

Inverse transformation Because of the general property that the inverse matrix A^{-1} of a rotation matrix A , is equal to the transposed matrix A^t , the inverse matrix of $\mathcal{T}_{\gamma 2g}$, noted $\mathcal{T}_{g 2\gamma}$, is easily deduced.

$$\mathcal{T}_{g 2\gamma} = \mathcal{T}_{\gamma 2g}^{-1} = \mathcal{T}_{\gamma 2g}^t \quad (5.36)$$

In the same way, if \vec{r}_g is a vector given in the Latitude-Longitude frame, then the corresponding vector in the Inertial frame, \vec{r}_γ , is given by:

$$\vec{r}_\gamma = \mathcal{T}_{g 2\gamma} \cdot \vec{r}_g \quad (5.37)$$

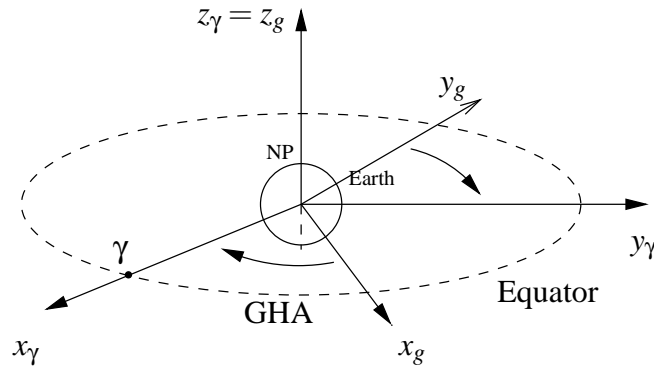


Figure 5.13: γ_{2g} -transformation

5.3.8.4.2 Inertial frame to Geocentric Orbital frame Transformation

The transformation matrix from the Inertial frame to the Geocentric Orbital frame is a matrix composed by three successive rotation matrices.

- rotation by an angle Ω around the z_γ -axis: the first intermediate coordinate system is noted (x_1, y_1, z_1) and the transformation matrix from the Inertial frame to this first intermediate frame, noted $\mathcal{T}_{\gamma_{2int_1}}$, is:

$$\mathcal{T}_{\gamma_{2int_1}} = \begin{pmatrix} \cos\Omega & \sin\Omega & 0 \\ -\sin\Omega & \cos\Omega & 0 \\ 0 & 0 & 1 \end{pmatrix} \quad (5.38)$$

- rotation by an angle i around the x_1 -axis: the second intermediate coordinate system is noted (x_2, y_2, z_2) and the transformation matrix from the first intermediate frame to this second intermediate frame, noted $\mathcal{T}_{int_1 2int_2}$, is:

$$\mathcal{T}_{int_1 2int_2} = \begin{pmatrix} 1 & 0 & 0 \\ 0 & \cos i & \sin i \\ 0 & -\sin i & \cos i \end{pmatrix} \quad (5.39)$$

- rotation by an angle $u = v + \omega$ around the z_2 -axis: the third coordinate system merges the Geocentric Orbital coordinate system. The transformation matrix from the second intermediate frame to the Geocentric Orbital frame, noted $\mathcal{T}_{int_2 2geoorb}$, is:

$$\mathcal{T}_{int_2 2geoorb} = \begin{pmatrix} \cos u & \sin u & 0 \\ -\sin u & \cos u & 0 \\ 0 & 0 & 1 \end{pmatrix} \quad (5.40)$$

The three rotation angles Ω , i and $u = v + \omega$ are respectively:

- Ω := the longitude of the ascending node
- i := the orbital inclination
- $u = v + \omega$:= the spacecraft angle in orbit plane from the equator at the ascending node:
 - v := the true anomaly
 - ω := the argument of perigee

The values of Ω , i and u depend of the orbit time and are given by the ERS orbit propagator.

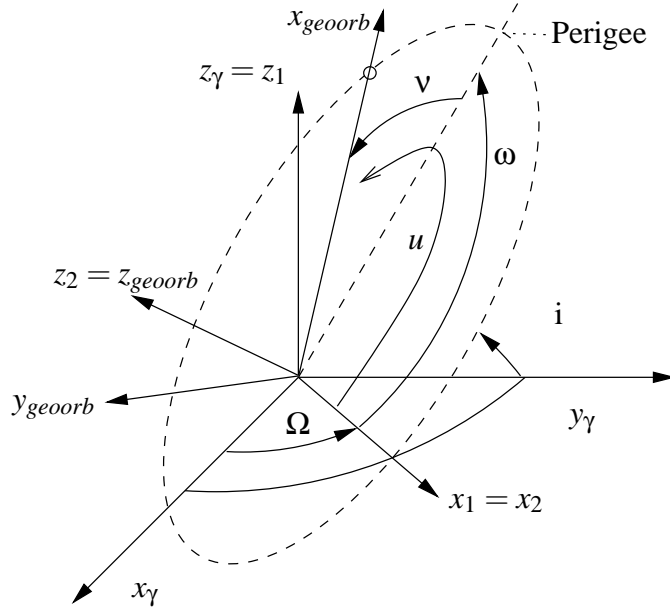


Figure 5.14: γ_{2georb} -transformation

Notation $\mathcal{T}_{\gamma_{2georb}}$

Expression

$$\begin{aligned} \mathcal{T}_{\gamma_{2georb}} &= \mathcal{T}_{int_2 2georb} \cdot \mathcal{T}_{int_1 2int_2} \cdot \mathcal{T}_{\gamma 2int_1} \\ &= \begin{pmatrix} \cos u & \sin u & 0 \\ -\sin u & \cos u & 0 \\ 0 & 0 & 1 \end{pmatrix} \begin{pmatrix} 1 & 0 & 0 \\ 0 & \cos i & \sin i \\ 0 & -\sin i & \cos i \end{pmatrix} \begin{pmatrix} \cos \Omega & \sin \Omega & 0 \\ -\sin \Omega & \cos \Omega & 0 \\ 0 & 0 & 1 \end{pmatrix} \end{aligned} \quad (5.41)$$

Property If \vec{r}_γ is a vector given in the Inertial frame, then the corresponding vector in the Geocentric Orbital frame, \vec{r}_{georb} , is given by:

$$\vec{r}_{georb} = \mathcal{T}_{\gamma_{2georb}} \cdot \vec{r}_\gamma \quad (5.42)$$

Inverse transformation

$$\begin{aligned} \mathcal{T}_{georb 2\gamma} &= \mathcal{T}_{\gamma_{2georb}}^{-1} \\ &= (\mathcal{T}_{int_2 2georb} \cdot \mathcal{T}_{int_1 2int_2} \cdot \mathcal{T}_{\gamma 2int_1})^{-1} \\ &= \mathcal{T}_{\gamma 2int_1}^{-1} \cdot \mathcal{T}_{int_1 2int_2}^{-1} \cdot \mathcal{T}_{int_2 2georb}^{-1} \\ &= \mathcal{T}_{int_1 2\gamma} \cdot \mathcal{T}_{int_2 2int_1} \cdot \mathcal{T}_{georb 2int_2} \\ &= \mathcal{T}_{\gamma 2int_1}^t \cdot \mathcal{T}_{int_1 2int_2}^t \cdot \mathcal{T}_{int_2 2georb}^t \end{aligned} \quad (5.43)$$

So, if \vec{r}_{georb} is a vector given in the Geocentric Orbital frame, then the corresponding vector in the Inertial frame, \vec{r}_γ , is given by:

$$\vec{r}_\gamma = \mathcal{T}_{georb 2\gamma} \cdot \vec{r}_{georb} \quad (5.44)$$

Remark The transformation matrix from the Inertial frame to the Geocentric Orbital frame can also be expressed using the vector position of the satellite's COG $\vec{r}_{\gamma sc}$ and the absolute velocity vector of the satellite's COG $\vec{v}_{\gamma sc}$, given in the γ frame:

$$\mathcal{T}_{\gamma_{2georb}} = \begin{pmatrix} \vec{u}_{1\gamma} \cdot \vec{e}_x & \vec{u}_{2\gamma} \cdot \vec{e}_x & \vec{u}_{3\gamma} \cdot \vec{e}_x \\ \vec{u}_{1\gamma} \cdot \vec{e}_y & \vec{u}_{2\gamma} \cdot \vec{e}_y & \vec{u}_{3\gamma} \cdot \vec{e}_y \\ \vec{u}_{1\gamma} \cdot \vec{e}_z & \vec{u}_{2\gamma} \cdot \vec{e}_z & \vec{u}_{3\gamma} \cdot \vec{e}_z \end{pmatrix} \quad (5.45)$$

where

$$\vec{u}_{1\gamma} = \vec{r}_{\gamma sc} / \|\vec{r}_{\gamma sc}\| \quad (5.46)$$

$$\vec{u}_{3\gamma} = \vec{r}_{\gamma sc} \times \vec{v}_{\gamma sc} / \|\vec{r}_{\gamma sc} \times \vec{v}_{\gamma sc}\| \quad (5.47)$$

$$\vec{u}_{2\gamma} = \vec{u}_{3\gamma} \times \vec{u}_{1\gamma} / \|\vec{u}_{3\gamma} \times \vec{u}_{1\gamma}\| \quad (5.48)$$

5.3.8.4.3 Geocentric Orbital frame to Satellite Centered Orbital frame Transformation

The transformation from the Geocentric Orbital frame to the Satellite Centered Orbital frame is the composition of a matrix of transformation and of a translation from the Earth' centre, centre of the Geocentric Orbital frame, to the satellite's COG, centre of the Satellite Centered Orbital frame.

Notation $\mathcal{T}_{georb2satorb}$ and $\vec{r}_{georb_{sc}}$

Expression

$$\mathcal{T}_{georb2satorb} = \begin{pmatrix} 0 & 1 & 0 \\ 0 & 0 & 1 \\ 1 & 0 & 0 \end{pmatrix} \quad (5.49)$$

$\vec{r}_{georb_{sc}}$ is a vector exprimed in the *georb*-frame, from the Earth'centre to the satellite's COG. Reducing the spacecraft to its COG, this vector corresponds to the spacecraft position given in the *georb*-frame.

Property If \vec{r}_{georb} is a vector given in the Geocentric Orbital frame, then the corresponding vector in the Satellite Centered Orbital frame, \vec{r}_{satorb} , is given by:

$$\vec{r}_{satorb} = \mathcal{T}_{georb2satorb} \cdot (\vec{r}_{georb} - \vec{r}_{georb_{sc}}) \quad (5.50)$$

Inverse tranformation

$$\begin{aligned} \mathcal{T}_{satorb2georb} &= \mathcal{T}_{georb2satorb}^{-1} \\ &= \begin{pmatrix} 0 & 0 & 1 \\ 1 & 0 & 0 \\ 0 & 1 & 0 \end{pmatrix} \end{aligned} \quad (5.51)$$

So, if \vec{r}_{satorb} is a vector given in the Satellite Centered Orbital frame, then the corresponding vector in the Geocentric Orbital frame, \vec{r}_{georb} , is given by:

$$\vec{r}_{georb} = \mathcal{T}_{satorb2georb} \cdot \vec{r}_{satorb} + \vec{r}_{georb_{sc}} \quad (5.52)$$

5.3.8.4.4 Inertial frame to Satellite Centered Orbital frame Transformation

The transformation from the Inertial frame to the Satellite Centered Orbital frame can be easily deduced from the previous sections (5.3.8.4.2) and (5.3.8.4.3).

Notation $\mathcal{T}_{\gamma 2satorb}$ and $\vec{r}_{\gamma sc}$

Expression

$$\begin{aligned} \mathcal{T}_{\gamma 2satorb} &= \mathcal{T}_{georb2satorb} \cdot \mathcal{T}_{\gamma 2georb} \\ &= \mathcal{T}_{georb2satorb} \cdot (\mathcal{T}_{int_2 2georb} \cdot \mathcal{T}_{int_1 2int_2} \cdot \mathcal{T}_{\gamma 2int_1}) \end{aligned} \quad (5.53)$$

$\vec{r}_{\gamma sc}$ is a vector expressed in the γ -frame, from the Earth'centre to the satellite's COG. Identifying the spacecraft to its COG, this vector corresponds to the spacecraft position, position given in the γ -frame.

Property If \vec{r}_γ is a vector given in the Inertial frame, then the corresponding vector in the Satellite Centered Orbital frame, \vec{r}_{satorb} , is given by:

$$\vec{r}_{satorb} = \mathcal{T}_{\gamma 2satorb} \cdot (\vec{r}_\gamma - \vec{r}_{\gamma sc}) \quad (5.54)$$

Inverse transformation

$$\begin{aligned} \mathcal{T}_{satorb 2\gamma} &= \mathcal{T}_{\gamma 2satorb}^{-1} \\ &= (\mathcal{T}_{georb 2satorb} \cdot \mathcal{T}_{\gamma 2georb})^{-1} \\ &= \mathcal{T}_{\gamma 2georb}^{-1} \cdot \mathcal{T}_{georb 2satorb}^{-1} \\ &= \mathcal{T}_{georb 2\gamma} \cdot \mathcal{T}_{satorb 2georb} \\ &= (\mathcal{T}_{\gamma 2int_1}^t \cdot \mathcal{T}_{int_1 2int_2}^t \cdot \mathcal{T}_{int_2 2georb}^t) \cdot \mathcal{T}_{satorb 2georb} \end{aligned} \quad (5.55)$$

So, if \vec{r}_{satorb} is a vector given in the Satellite Centered Orbital frame, then the corresponding vector in the Inertial frame, \vec{r}_γ , is given by:

$$\vec{r}_\gamma = \mathcal{T}_{satorb 2\gamma} \cdot \vec{r}_{satorb} + \vec{r}_{\gamma sc} \quad (5.56)$$

5.3.8.4.5 Satellite Centered Orbital frame to Relative Satellite Centered Orbital frame Transformation

These two frames have the same origin. The transformation matrix from the Satellite Centered Orbital frame to the Relative Satellite Centered Orbital frame is determined with the help of two vectors, the outward local normal in the nadir and the relative ground trace velocity. These vectors depend on the orbit time. They are calculated by the ERS orbit propagator and they are given in the Inertial frame (or in the latitude-Longitude frame).

Notation $\mathcal{T}_{satorb 2relsat}$, $\vec{r}_{\gamma n}$ and \vec{v}'_γ

Expression To calculate the rotation matrix $\mathcal{T}_{satorb 2relsat}$, the rotation matrices $\mathcal{T}_{georb 2relsat}$ and $\mathcal{T}_{georb 2satorb}$ will be used. The rotation matrix $\mathcal{T}_{georb 2relsat}$ is easily calculated with the help of the two vectors $\vec{r}_{\gamma n}$ and \vec{v}'_γ , as explained below.

- $\vec{r}_{\gamma n}$ = the outward local normal in the nadir, expressed in the γ -frame
- \vec{v}'_γ = the relative ground trace velocity, expressed in the γ -frame

The first step consists in expressing these vectors in the Geocentric Orbital frame, with the help of the corresponding transformation.

$$\vec{r}_{georb n} = \mathcal{T}_{\gamma 2georb} \cdot \vec{r}_{\gamma n} \quad (5.57)$$

$$\vec{v}'_{georb} = \mathcal{T}_{\gamma 2georb} \cdot \vec{v}'_\gamma \quad (5.58)$$

With these two orthogonal (by definition) vectors, a right-handed Cartesian coordinate system can be built. To have an orthonormal coordinate system, these vectors have to be normalized.

$$\vec{1}_{r_{georb n}} = \frac{\vec{r}_{georb n}}{\|\vec{r}_{georb n}\|} \quad (5.59)$$

$$\vec{1}_{v'_{georb}} = \frac{\vec{v}'_{georb}}{\|\vec{v}'_{georb}\|} \quad (5.60)$$

The third vector, completing the right-handed Cartesian coordinate system, is:

$$\vec{1}_{v'_{georb}} \times \vec{1}_{r_{georb n}} \quad (5.61)$$

These three vectors, expressed in the Geocentric Orbital frame, define the unit vectors ($\vec{1}_x, \vec{1}_y, \vec{1}_z$) of the Relative Satellite Centered Orbital frame:

$$\vec{1}_{x_{geoorb}} = \vec{1}_{v'_{geoorb}} \times \vec{1}_{r_{geoorbn}} \quad (5.62)$$

$$\vec{1}_{y_{geoorb}} = \vec{1}_{v'_{geoorb}} \quad (5.63)$$

$$\vec{1}_{z_{geoorb}} = \vec{1}_{r_{geoorbn}} \quad (5.64)$$

Hence, the rotation matrix between the Geocentric Orbital frame and the Relative Satellite Centered Orbital frame is formed by these unit vectors, and the matrix expression is:

$$\begin{aligned} \mathcal{T}_{geoorb2relsat} &= \begin{pmatrix} \vec{1}_{v'_{geoorb}} \times \vec{1}_{r_{geoorbn}} \\ \vec{1}_{v'_{geoorb}} \\ \vec{1}_{r_{geoorbn}} \end{pmatrix} \quad (5.65) \\ &= \begin{pmatrix} \vec{1}_{v'_{geoorb}} \times \vec{1}_{r_{geoorbn}} \downarrow_x & \vec{1}_{v'_{geoorb}} \times \vec{1}_{r_{geoorbn}} \downarrow_y & \vec{1}_{v'_{geoorb}} \times \vec{1}_{r_{geoorbn}} \downarrow_z \\ \vec{1}_{v'_{geoorb}} \downarrow_x & \vec{1}_{v'_{geoorb}} \downarrow_y & \vec{1}_{v'_{geoorb}} \downarrow_z \\ \vec{1}_{r_{geoorbn}} \downarrow_x & \vec{1}_{r_{geoorbn}} \downarrow_y & \vec{1}_{r_{geoorbn}} \downarrow_z \end{pmatrix} \end{aligned}$$

The rotation matrix between the Satellite Centered Orbital frame and the Relative Satellite Centered Orbital frame can now be deduce with the help of the following relation:

$$\mathcal{T}_{geoorb2relsat} = \mathcal{T}_{satorb2relsat} \cdot \mathcal{T}_{geoorb2satorb} \quad (5.66)$$

Or,

$$\begin{aligned} \mathcal{T}_{satorb2relsat} &= \mathcal{T}_{geoorb2relsat} \cdot \mathcal{T}_{geoorb2satorb}^{-1} \quad (5.67) \\ &= \mathcal{T}_{geoorb2relsat} \cdot \mathcal{T}_{satorb2geoorb} \\ &= \begin{pmatrix} \vec{1}_{v'_{geoorb}} \times \vec{1}_{r_{geoorbn}} \downarrow_y & \vec{1}_{v'_{geoorb}} \times \vec{1}_{r_{geoorbn}} \downarrow_z & \vec{1}_{v'_{geoorb}} \times \vec{1}_{r_{geoorbn}} \downarrow_x \\ \vec{1}_{v'_{geoorb}} \downarrow_y & \vec{1}_{v'_{geoorb}} \downarrow_z & \vec{1}_{v'_{geoorb}} \downarrow_x \\ \vec{1}_{r_{geoorbn}} \downarrow_y & \vec{1}_{r_{geoorbn}} \downarrow_z & \vec{1}_{r_{geoorbn}} \downarrow_x \end{pmatrix} \end{aligned}$$

Property If \vec{r}_{geoorb} is a vector given in the Geocentric Orbital frame, then the corresponding vector in the Relative Satellite Centered Orbital frame, \vec{r}_{relsat} , is given by:

$$\vec{r}_{relsat} = \mathcal{T}_{geoorb2relsat} \cdot (\vec{r}_{geoorb} - \vec{r}_{geoorb_{sc}}) \quad (5.68)$$

where $\vec{r}_{geoorb_{sc}}$ is the vector expressed in the *geoorb*-frame, from the Earth's centre to the satellite's COG.

And, if \vec{r}_{satorb} is a vector given in the Satellite Centered Orbital frame, then the corresponding vector in the Relative Satellite Centered Orbital frame, \vec{r}_{relsat} , is given by:

$$\vec{r}_{relsat} = \mathcal{T}_{satorb2relsat} \cdot \vec{r}_{satorb} \quad (5.69)$$

Inverse transformation

$$\begin{aligned} \mathcal{T}_{relsat2satorb} &= \mathcal{T}_{satorb2relsat}^{-1} \\ &= (\mathcal{T}_{geoorb2relsat} \cdot \mathcal{T}_{satorb2geoorb})^{-1} \\ &= \mathcal{T}_{satorb2geoorb}^{-1} \cdot \mathcal{T}_{geoorb2relsat}^{-1} \\ &= \mathcal{T}_{geoorb2satorb} \cdot \mathcal{T}_{relsat2geoorb} \quad (5.70) \end{aligned}$$

where

$$\begin{aligned}\mathcal{T}_{georb2relsat}^{-1} &= \mathcal{T}_{relsat2georb} \\ &= \mathcal{T}_{georb2relsat}^t\end{aligned}\quad (5.71)$$

Thus,

$$\mathcal{T}_{relsat2satorb} = \mathcal{T}_{georb2satorb} \cdot \mathcal{T}_{georb2relsat}^t \quad (5.72)$$

So, if $\overrightarrow{r_{relsat}}$ is a vector given in the Relative Satellite Centered Orbital frame, then the corresponding vector in the Satellite Centered Orbital frame, $\overrightarrow{r_{satorb}}$, is given by:

$$\overrightarrow{r_{satorb}} = \mathcal{T}_{relsat2satorb} \cdot \overrightarrow{r_{relsat}} \quad (5.73)$$

5.3.8.4.6 Inertial frame to Relative Satellite Centered Orbital frame Transformation

The transformation from the Inertial frame to the Relative Satellite Centered Orbital frame can be easily deduced from the previous sections 5.3.8.4.4 and 5.3.8.4.5.

Notation $\mathcal{T}_{\gamma 2relsat}$ and $\overrightarrow{r_{\gamma sc}}$

Expression

$$\begin{aligned}\mathcal{T}_{\gamma 2relsat} &= \mathcal{T}_{satorb2relsat} \cdot \mathcal{T}_{\gamma 2satorb} \\ &= (\mathcal{T}_{georb2relsat} \cdot \mathcal{T}_{satorb2georb}) \cdot (\mathcal{T}_{georb2satorb} \cdot \mathcal{T}_{\gamma 2georb}) \\ &= \mathcal{T}_{georb2relsat} \cdot \mathcal{T}_{\gamma 2georb} \\ &= \mathcal{T}_{georb2relsat} \cdot (\mathcal{T}_{int_2 2georb} \cdot \mathcal{T}_{int_1 2int_2} \cdot \mathcal{T}_{\gamma 2int_1})\end{aligned}\quad (5.74)$$

$\overrightarrow{r_{\gamma sc}}$ is the vector exprimed in the γ -frame, from the Earth' centre to the satellite's COG.

Property If $\overrightarrow{r_{\gamma}}$ is a vector given in the Inertial frame, then the corresponding vector in the Relative Satellite Centered Orbital frame, $\overrightarrow{r_{relsat}}$, is given by:

$$\overrightarrow{r_{relsat}} = \mathcal{T}_{\gamma 2relsat} \cdot (\overrightarrow{r_{\gamma}} - \overrightarrow{r_{\gamma sc}}) \quad (5.75)$$

Inverse tranformation

$$\begin{aligned}\mathcal{T}_{relsat 2\gamma} &= \mathcal{T}_{\gamma 2relsat}^{-1} \\ &= (\mathcal{T}_{satorb2relsat} \cdot \mathcal{T}_{\gamma 2satorb})^{-1} \\ &= \mathcal{T}_{\gamma 2satorb}^{-1} \cdot \mathcal{T}_{satorb2relsat}^{-1} \\ &= \mathcal{T}_{satorb 2\gamma} \cdot \mathcal{T}_{relsat 2satorb} \\ &= (\mathcal{T}_{\gamma 2int_1}^t \cdot \mathcal{T}_{int_1 2int_2}^t \cdot \mathcal{T}_{int_2 2georb}^t) \cdot \mathcal{T}_{satorb 2georb} \cdot \mathcal{T}_{georb 2satorb} \cdot \mathcal{T}_{relsat 2georb}^t \\ &= (\mathcal{T}_{\gamma 2int_1}^t \cdot \mathcal{T}_{int_1 2int_2}^t \cdot \mathcal{T}_{int_2 2georb}^t) \cdot \mathcal{T}_{relsat 2georb}^t\end{aligned}\quad (5.76)$$

So, if $\overrightarrow{r_{relsat}}$ is a vector given in the Relative Satellite Centered Orbital frame, then the corresponding vector in the Inertial frame, $\overrightarrow{r_{\gamma}}$, is given by:

$$\overrightarrow{r_{\gamma}} = \mathcal{T}_{relsat 2\gamma} \cdot \overrightarrow{r_{relsat}} + \overrightarrow{r_{\gamma sc}} \quad (5.77)$$

5.3.8.4.7 Relative Satellite Centered Orbital frame to Platform frame Transformation

The transformation from the Relative Satellite Centered Orbital frame to the Platform frame is determined by the AOCS pointing errors when the satellite is beeing yaw steered.

The transformation matrix from the Relative Satellite Centered Orbital frame to the Platform frame is a matrix composed by three successive rotation matrices. The angles to be considered for these rotation matrices are the AOCS pointing errors.

- rotation by an angle Δ_y around the x_{relsat} -axis: the first intermediate coordinate system is noted (x_6, y_6, z_6) and the transformation matrix from the Relative Satellite Centered Orbital frame to this first intermediate frame, noted $\mathcal{T}_{relsat2int_6}$, is:

$$\mathcal{T}_{relsat2int_6} = \begin{pmatrix} 1 & 0 & 0 \\ 0 & \cos\Delta_y & \sin\Delta_y \\ 0 & -\sin\Delta_y & \cos\Delta_y \end{pmatrix} \quad (5.78)$$

- rotation by an angle Δ_r around the y_6 -axis: the second intermediate coordinate system is noted (x_7, y_7, z_7) and the transformation matrix from the first intermediate frame to this second intermediate frame, noted $\mathcal{T}_{int_62int_7}$, is:

$$\mathcal{T}_{int_62int_7} = \begin{pmatrix} \cos\Delta_r & 0 & -\sin\Delta_r \\ 0 & 1 & 0 \\ \sin\Delta_r & 0 & \cos\Delta_r \end{pmatrix} \quad (5.79)$$

- rotation by an angle Δ_p around the z_7 -axis: the third coordinate system merges the Platform coordinate system. The transformation matrix from the second intermediate frame to the Platform frame, noted \mathcal{T}_{int_72plat} , is:

$$\mathcal{T}_{int_72plat} = \begin{pmatrix} \cos\Delta_p & \sin\Delta_p & 0 \\ -\sin\Delta_p & \cos\Delta_p & 0 \\ 0 & 0 & 1 \end{pmatrix} \quad (5.80)$$

where the Δ_y , Δ_r and Δ_p are respectively:

- Δ_{pitch} is the error in pitch
- Δ_{roll} is the error in roll
- Δ_{yaw} is the error in yaw

Notation $\mathcal{T}_{relsat2plat}$

Expression

$$\begin{aligned} \mathcal{T}_{relsat2plat} &= \mathcal{T}_{int_72plat} \cdot \mathcal{T}_{int_62int_7} \cdot \mathcal{T}_{relsat2int_6} \\ &= \begin{pmatrix} \cos\Delta_p & \sin\Delta_p & 0 \\ -\sin\Delta_p & \cos\Delta_p & 0 \\ 0 & 0 & 1 \end{pmatrix} \begin{pmatrix} \cos\Delta_r & 0 & -\sin\Delta_r \\ 0 & 1 & 0 \\ \sin\Delta_r & 0 & \cos\Delta_r \end{pmatrix} \begin{pmatrix} 1 & 0 & 0 \\ 0 & \cos\Delta_y & \sin\Delta_y \\ 0 & -\sin\Delta_y & \cos\Delta_y \end{pmatrix} \end{aligned} \quad (5.81)$$

Property If \vec{r}_{relsat} is a vector given in the Relative Satellite Centered Orbital frame, then the corresponding vector in the Platform frame, \vec{r}_{plat} , is given by:

$$\vec{r}_{plat} = \mathcal{T}_{relsat2plat} \cdot \vec{r}_{relsat} \quad (5.82)$$

Inverse transformation

$$\begin{aligned} \mathcal{T}_{plat2relsat} &= \mathcal{T}_{relsat2plat}^{-1} \\ &= (\mathcal{T}_{int_72plat} \cdot \mathcal{T}_{int_62int_7} \cdot \mathcal{T}_{relsat2int_6})^{-1} \\ &= (\mathcal{T}_{relsat2int_6})^{-1} \cdot (\mathcal{T}_{int_62int_7})^{-1} \cdot (\mathcal{T}_{int_72plat})^{-1} \\ &= \mathcal{T}_{int_62relsat} \cdot \mathcal{T}_{int_72int_6} \cdot \mathcal{T}_{plat2int_7} \\ &= \mathcal{T}_{relsat2int_6}^t \cdot \mathcal{T}_{int_62int_7}^t \cdot \mathcal{T}_{int_72plat}^t \end{aligned} \quad (5.83)$$

So, if \vec{r}_{plat} is a vector given in the Platform frame, then the corresponding vector in the Relative Satellite Centered Orbital frame, \vec{r}_{relsat} , is given by:

$$\vec{r}_{relsat} = \mathcal{T}_{plat2relsat} \cdot \vec{r}_{plat} \quad (5.84)$$

5.3.8.4.8 Inertial frame to Platform frame Transformation

The transformation from the Inertial frame to the Platform can easily be deduced from the previous sections 5.3.8.4.6 and 5.3.8.4.7.

Notation $\mathcal{T}_{\gamma 2 plat}$ and $\vec{r}_{\gamma sc}$

Expression

$$\begin{aligned}\mathcal{T}_{\gamma 2 plat} &= \mathcal{T}_{rels at 2 plat} \cdot \mathcal{T}_{\gamma 2 relsat} \\ &= \left(\mathcal{T}_{int_7 2 plat} \cdot \mathcal{T}_{int_6 2 int_7} \cdot \mathcal{T}_{rels at 2 int_6} \right) \\ &\quad \left(\mathcal{T}_{geoorb 2 relsat} \cdot \left(\mathcal{T}_{int_2 2 geoorb} \cdot \mathcal{T}_{int_1 2 int_2} \cdot \mathcal{T}_{\gamma 2 int_1} \right) \right)\end{aligned}\quad (5.85)$$

$\vec{r}_{\gamma sc}$ is the vector exprimed in the γ -frame, from the Earth's centre to the satellite's COG.

Property If \vec{r}_{γ} is a vector given in the Inertial frame, then the corresponding vector in the Platform frame, \vec{r}_{plat} , is given by:

$$\vec{r}_{plat} = \mathcal{T}_{\gamma 2 plat} \cdot \left(\vec{r}_{\gamma} - \vec{r}_{\gamma sc} \right) \quad (5.86)$$

Inverse tranformation

$$\begin{aligned}\mathcal{T}_{plat 2 \gamma} &= \mathcal{T}_{\gamma 2 plat}^{-1} \\ &= \left(\mathcal{T}_{rels at 2 plat} \cdot \mathcal{T}_{\gamma 2 relsat} \right)^{-1} \\ &= \mathcal{T}_{\gamma 2 relsat}^{-1} \cdot \mathcal{T}_{rels at 2 plat}^{-1} \\ &= \mathcal{T}_{rels at 2 \gamma} \cdot \mathcal{T}_{plat 2 relsat} \\ &= \left(\left(\mathcal{T}_{\gamma 2 int_1}^t \cdot \mathcal{T}_{int_1 2 int_2}^t \cdot \mathcal{T}_{int_2 2 geoorb}^t \right) \cdot \mathcal{T}_{rels at 2 geoorb}^t \right) \\ &\quad \left(\mathcal{T}_{rels at 2 int_6}^t \cdot \mathcal{T}_{int_6 2 int_7}^t \cdot \mathcal{T}_{int_7 2 plat}^t \right)\end{aligned}\quad (5.87)$$

So, if \vec{r}_{plat} is a vector given in the Platform frame, then the corresponding vector in the Inertial frame, \vec{r}_{γ} , is given by:

$$\vec{r}_{\gamma} = \mathcal{T}_{plat 2 \gamma} \cdot \vec{r}_{plat} + \vec{r}_{\gamma sc} \quad (5.88)$$

5.3.8.4.9 Satellite Centered Orbital frame to Platform frame Transformation

A similar transformation can be found for the transformation matrix $T_{satorb 2 plat}$ which can be useful when the satellite is in fine pointing mode. The three angles will be also determined by the AOCS pointing errors when the satellite is in this mode.

5.3.8.4.10 Platform frame to Antenna frame Transformation

The transformation from the Platform Frame into an Antenna Frame is determined by the antenna mounting angles: α_z , α_x and α_y , and by the vector, $\vec{r}_{plat ac}$, exprimed in the *plat*-frame, from the satellite's COG to the antenna's centre.

Notation $\mathcal{T}_{plat 2 a}$ and $\vec{r}_{plat ac}$

Expression The transformation matrix from the Platform frame to an Antenna frame is a matrix composed by three successive rotation matrices.

The last of the three rotations is characterized by a very small angle, so the corresponding matrix is approximately the unit matrix. Neglecting this rotation, the (y_{mid}, z_{mid}) -plane is the (x_{plat}, z_{plat}) -plane while the (y_{aft}, z_{aft}) and (y_{for}, z_{for}) -planes are inclined at 45° w.r.t. the (x_{plat}, z_{plat}) -plane.

The z_{mid} -axis is inclined w.r.t. the platform (y_{plat}, z_{plat}) -plane by approximately 30° , and w.r.t. the z_{for} and z_{aft} -axes by approximately 40° .

- rotation by an angle α_z around the z_{plat} -axis: the intermediate coordinate system is noted (x_3, y_3, z_3) and the transformation matrix from the Platform frame to this intermediate frame, noted $\mathcal{T}_{plat2int_3}$, is:

$$\mathcal{T}_{plat2int_3} = \begin{pmatrix} \cos\alpha_z & \sin\alpha_z & 0 \\ -\sin\alpha_z & \cos\alpha_z & 0 \\ 0 & 0 & 1 \end{pmatrix} \quad (5.89)$$

- rotation by an angle α_x around the x_3 -axis: the intermediate coordinate system is noted (x_4, y_4, z_4) and the transformation matrix from the intermediate frame 3 to this frame 4, noted $\mathcal{T}_{int_32int_4}$, is:

$$\mathcal{T}_{int_32int_4} = \begin{pmatrix} 1 & 0 & 0 \\ 0 & \cos\alpha_x & \sin\alpha_x \\ 0 & -\sin\alpha_x & \cos\alpha_x \end{pmatrix} \quad (5.90)$$

- rotation by an angle α_y around the y_4 -axis: this coordinate system merges the Antenna coordinate system. The transformation matrix from the intermediate frame 4 to this Antenna frame, noted \mathcal{T}_{int_42a} , is:

$$\mathcal{T}_{int_42a} = \begin{pmatrix} \cos\alpha_y & 0 & -\sin\alpha_y \\ 0 & 1 & 0 \\ \sin\alpha_y & 0 & \cos\alpha_y \end{pmatrix} \quad (5.91)$$

$$\mathcal{T}_{plat2a} = \mathcal{T}_{int_42a} \cdot \mathcal{T}_{int_32int_4} \cdot \mathcal{T}_{plat2int_3} \quad (5.92)$$

$$= \begin{pmatrix} \cos\alpha_y & 0 & -\sin\alpha_y \\ 0 & 1 & 0 \\ \sin\alpha_y & 0 & \cos\alpha_y \end{pmatrix} \begin{pmatrix} 1 & 0 & 0 \\ 0 & \cos\alpha_x & \sin\alpha_x \\ 0 & -\sin\alpha_x & \cos\alpha_x \end{pmatrix} \begin{pmatrix} \cos\alpha_z & \sin\alpha_z & 0 \\ -\sin\alpha_z & \cos\alpha_z & 0 \\ 0 & 0 & 1 \end{pmatrix} \quad (5.93)$$

$\overrightarrow{r_{platac}}$ is a vector exprimed in the *plat*-frame, from the satellite's COG to the antenna's centre.

Property If $\overrightarrow{r_{plat}}$ is a vector given in the Platform frame, then the corresponding vector in the Antenna frame, $\overrightarrow{r_a}$, is given by:

$$\overrightarrow{r_a} = \mathcal{T}_{plat2a} \cdot (\overrightarrow{r_{plat}} - \overrightarrow{r_{platac}}) \quad (5.94)$$

Inverse tranformation

$$\begin{aligned} \mathcal{T}_{a2plat} &= (\mathcal{T}_{int_42a} \cdot \mathcal{T}_{int_32int_4} \cdot \mathcal{T}_{plat2int_3})^{-1} \\ &= \mathcal{T}_{plat2int_3}^{-1} \cdot \mathcal{T}_{int_32int_4}^{-1} \cdot \mathcal{T}_{int_42a}^{-1} \\ &= \mathcal{T}_{plat2int_3}^t \cdot \mathcal{T}_{int_32int_4}^t \cdot \mathcal{T}_{int_42a}^t \end{aligned} \quad (5.95)$$

So, if $\overrightarrow{r_a}$ is a vector given in an Antenna frame, then the corresponding vector in the Platform frame, $\overrightarrow{r_{plat}}$, is given by:

$$\overrightarrow{r_{plat}} = \mathcal{T}_{a2plat} \cdot \overrightarrow{r_a} + \overrightarrow{r_{platac}} \quad (5.96)$$

Remark In the document [2], p A.2-9, the three rotation angles α_z , α_x and α_y are respectively:

	for	mid	aft
α_z	135.0°	90.0°	45.0°
α_x	140.650°	150.150°	140.650°
α_y	0.0°	0.0°	0.0°

Table 5.2: Antenna orientation angles

5.3.8.4.11 Inertial frame to Antenna frame Transformation

The transformation from the Inertial frame to an Antenna frame can easily be deduced from the previous sections 5.3.8.4.8 and 5.3.8.4.10.

Notation $\mathcal{T}_{\gamma 2a}$ and $\vec{r}_{\gamma ac}$

Expression From the relations (5.94) and (5.86), one can write

$$\begin{aligned}\vec{r}_a &= \mathcal{T}_{plat2a} \cdot (\vec{r}_{plat} - \vec{r}_{platac}) \\ &= \mathcal{T}_{plat2a} \cdot (\mathcal{T}_{\gamma 2plat} \cdot (\vec{r}_{\gamma} - \vec{r}_{\gamma sc}) - \mathcal{T}_{\gamma 2plat} \cdot (\vec{r}_{\gamma ac} - \vec{r}_{\gamma sc})) \\ &= \mathcal{T}_{plat2a} \cdot \mathcal{T}_{\gamma 2plat} \cdot (\vec{r}_{\gamma} - \vec{r}_{\gamma ac})\end{aligned}\quad (5.97)$$

where $\vec{r}_{\gamma ac}$ is the vector expressed in the γ -frame, from the Earth' centre to antenna centre and hence

$$\begin{aligned}\mathcal{T}_{\gamma 2a} &= \mathcal{T}_{plat2a} \cdot \mathcal{T}_{\gamma 2plat} \\ &= (\mathcal{T}_{int_4 2a} \cdot \mathcal{T}_{int_3 2int_4} \cdot \mathcal{T}_{plat 2int_3}) \cdot \\ &\quad ((\mathcal{T}_{int_7 2plat} \cdot \mathcal{T}_{int_6 2int_7} \cdot \mathcal{T}_{relsat 2int_6}) \cdot (\mathcal{T}_{geoorb 2relsat} \cdot (\mathcal{T}_{int_2 2geoorb} \cdot \mathcal{T}_{int_1 2int_2} \cdot \mathcal{T}_{\gamma 2int_1})))\end{aligned}\quad (5.98)$$

Property If \vec{r}_{γ} is a vector given in the Inertial frame, then the corresponding vector in the Antenna frame, \vec{r}_a , is given by:

$$\vec{r}_a = \mathcal{T}_{\gamma 2a} \cdot (\vec{r}_{\gamma} - \vec{r}_{\gamma ac})\quad (5.99)$$

Inverse transformation

$$\begin{aligned}\mathcal{T}_{a 2\gamma} &= \mathcal{T}_{\gamma 2a}^{-1} \\ &= (\mathcal{T}_{plat2a} \cdot \mathcal{T}_{\gamma 2plat})^{-1} \\ &= \mathcal{T}_{\gamma 2plat}^{-1} \cdot \mathcal{T}_{plat2a}^{-1} \\ &= \mathcal{T}_{plat 2\gamma} \cdot \mathcal{T}_{a 2plat} \\ &= (((\mathcal{T}_{\gamma 2int_1}^t \cdot \mathcal{T}_{int_1 2int_2}^t \cdot \mathcal{T}_{int_2 2geoorb}^t) \cdot \mathcal{T}_{relsat 2geoorb}^t) \cdot (\mathcal{T}_{relsat 2int_6}^t \cdot \mathcal{T}_{int_6 2int_7}^t \cdot \mathcal{T}_{int_7 2plat}^t)) \\ &\quad \cdot (\mathcal{T}_{plat 2int_3}^t \cdot \mathcal{T}_{int_3 2int_4}^t \cdot \mathcal{T}_{int_4 2a}^t)\end{aligned}\quad (5.100)$$

So, if \vec{r}_a is a vector given in an Antenna frame, then the corresponding vector in the Inertial frame, \vec{r}_{γ} , is given by:

$$\vec{r}_{\gamma} = \mathcal{T}_{a 2\gamma} \cdot \vec{r}_a + \vec{r}_{\gamma ac}\quad (5.101)$$

5.3.8.5 Steering Modes

5.3.8.5.1 Yaw Steering Mode

In orbit, when the satellite is being yaw-steered, the satellite orientation shall be such that:

- the z_{plat} -axis is aligned close to the upward local normal (nadir), ie z_{relsat}
- the y_{plat} -axis is aligned close to the ground track relative velocity direction, so close to y_{relsat} -direction
- the x_{plat} is thus aligned close to the x_{relsat} -direction

The angles between the unit vectors $(\vec{1}_{x_{plat}}, \vec{1}_{y_{plat}}, \vec{1}_{z_{plat}})$ of this Platform frame and the unit vectors $(\vec{1}_{x_{relsat}}, \vec{1}_{y_{relsat}}, \vec{1}_{z_{relsat}})$ of the Relative Satellite Centred Orbital Frame are the pointing errors due to the Attitude and Orbit Control System (AOCS) in yaw steering mode. So, if these pointing errors are neglected, the Relative Satellite Centred Orbital Frame is merging the Platform Frame in the Yaw Steering Mode and the z_{plat} -axis coincides with the normal to the GEM-6 surface.

5.3.8.5.2 Fine Pointing Mode

In the Fine Pointing Mode, in orbit, the satellite orientation shall be such that:

- the z_{plat} -axis is aligned close with the direction from the Earth's centre to the satellite's COG, ie z_{satorb}
- the y_{plat} -axis is aligned close to the x_{satorb}
- the $-x_{plat}$ -axis is aligned close to the y_{satorb}

The angles between the unit vectors $(-\vec{1}_{x_{plat}}, \vec{1}_{y_{plat}}, \vec{1}_{z_{plat}})$ of this Platform frame and the unit vectors $(\vec{1}_{y_{satorb}}, \vec{1}_{x_{satorb}}, \vec{1}_{z_{satorb}})$ of the Satellite Centred Orbital Frame are the pointing errors due to the Attitude and Orbit Control System (AOCS) in fine pointing mode. So, if these pointing errors are neglected, the Satellite Centred Orbital Frame is merging the Platform Frame, rotated around the z -axis by a rotation of 270° , in the Fine Pointing Mode, and the z_{plat} -axis is pointing away from the Earth's centre to the satellite.

5.3.8.6 Determination of the Point Position

The measurement node position has to be determined for each given orbit "position" time at a specific azimuth angle Φ in an Antenna frame.

5.3.8.6.1 Exact solution

The problem of calculating this Earth point target corresponding to a specific range R and azimuth Φ in the Antenna frame is equivalent to the problem of determining the points of intersection between an ellipsoid, a sphere and a plane in the γ -frame.

A point is characterized by a vector given in the γ -frame. The origin of the vector is the origin of the γ -frame, ie the Earth's centre, while the end-point of the vector is this point.

Point coordinate A point is characterized by a vector given in the γ -frame. The origin of the vector is the origin of the γ -frame, ie the Earth's centre, while the end-point of the vector is this point.

Notation: $\vec{r}_\gamma = (x, y, z)$

Equation of the plane The plane of constant azimuth Φ is passing through the Antenna's center and is spanned by the two following vectors, given in the corresponding Antenna's frame:

$$\vec{r}_{a_1} = \begin{pmatrix} \sin\Phi \\ 0 \\ \cos\Phi \end{pmatrix} \quad (5.102)$$

$$\vec{r}_{a_2} = \begin{pmatrix} 0 \\ 1 \\ 0 \end{pmatrix} \quad (5.103)$$

In the γ -frame, the corresponding vectors are (cf 5.3.8.4.11):

$$\vec{r}_{\gamma_1} = \mathcal{T}_{a2\gamma} \cdot \vec{r}_{a_1} + \vec{r}_{\gamma_{ac}} \quad (5.104)$$

$$\vec{r}_{\gamma_2} = \mathcal{T}_{a2\gamma} \cdot \vec{r}_{a_2} + \vec{r}_{\gamma_{ac}} \quad (5.105)$$

So the plane spanned by these two vectors and passing through the Antenna's centre has the following equation, in the γ -frame:

$$\vec{r}_\gamma = \vec{r}_{\gamma_{ac}} + m \cdot \vec{r}_{\gamma_1} + n \cdot \vec{r}_{\gamma_2} \quad (5.106)$$

where $\vec{r}_{\gamma_{ac}} = (x_{ac}, y_{ac}, z_{ac})$ is the vector exprimed in the γ -frame, from the Earth's centre to antenna centre, and m and n are two real parameters.

Equation of the sphere The sphere is centered at the Antenna's centre and has a radius R determined by the echo sample time t . The slant range is given by:

$$R = \frac{c \cdot t}{2} \quad (5.107)$$

where c is the speed of light.

The equation of the sphere is thus:

$$(x - x_{ac})^2 + (y - y_{ac})^2 + (z - z_{ac})^2 = R^2 \quad (5.108)$$

Equation of the ellipsoid The ellipsoid is given by the GEM-6 model (see 5.3.8.1).

$$\frac{x^2 + y^2}{a^2} + \frac{z^2}{b^2} = 1 \quad (5.109)$$

The system to solve is thus formed by the three equations (5.106), (5.108) and (5.109).

Firstly, the coordinate (x, y, z) are substituted by their respective expression from (5.106) into the equation (5.108). Using the fact that the two vectors \vec{r}_{γ_1} and \vec{r}_{γ_2} are orthogonal unit vectors:

$$\|\vec{r}_{\gamma_1}\| = 1 \quad (5.110)$$

$$\|\vec{r}_{\gamma_2}\| = 1 \quad (5.111)$$

$$\vec{r}_{\gamma_1} \cdot \vec{r}_{\gamma_2} = 0 \quad (5.112)$$

a simple scalar relation between the two parameters, m and n , is obtained:

$$\begin{aligned} (x - x_{ac})^2 + (y - y_{ac})^2 + (z - z_{ac})^2 &= R^2 \\ \Leftrightarrow \|\vec{r}_\gamma - \vec{r}_{\gamma_{ac}}\| &= R^2 \\ \Leftrightarrow \|m \cdot \vec{r}_{\gamma_1} + n \cdot \vec{r}_{\gamma_2}\| &= R^2 \\ \Leftrightarrow m^2 + n^2 &= R^2 \end{aligned} \quad (5.113)$$

Then, substituting the coordinate (x, y, z) by their respective expression from (5.106) and using the relation between the two parameters m and n (5.113), a quartic equation in the variable m is obtained:

$$Am^4 + Bm^3 + Cm^2 + Dm + E = 0 \quad (5.114)$$

where the five coefficients are:

$$\begin{aligned}
A &= \left(\left(\frac{x_{\gamma_1}^2 + y_{\gamma_1}^2}{a^2} + \frac{z_{\gamma_1}^2}{b^2} \right) - \left(\frac{x_{\gamma_2}^2 + y_{\gamma_2}^2}{a^2} + \frac{z_{\gamma_2}^2}{b^2} \right) \left(\frac{\|\vec{r}_{\gamma_1}\|}{\|\vec{r}_{\gamma_2}\|} \right)^2 \right)^2 \\
&\quad + 4 \left(z_{\gamma_1} \cdot z_{\gamma_2} \cdot \left(\frac{1}{b^2} - \frac{1}{a^2} \right) \right)^2 \left(\frac{\|\vec{r}_{\gamma_1}\|}{\|\vec{r}_{\gamma_2}\|} \right)^2 \\
B &= 4 \left(\frac{x \cdot x_{\gamma_1} + y \cdot y_{\gamma_1}}{a^2} + \frac{z \cdot z_{\gamma_1}}{b^2} \right) \left(\left(\frac{x_{\gamma_1}^2 + y_{\gamma_1}^2}{a^2} + \frac{z_{\gamma_1}^2}{b^2} \right) - \left(\frac{x_{\gamma_2}^2 + y_{\gamma_2}^2}{a^2} + \frac{z_{\gamma_2}^2}{b^2} \right) \left(\frac{\|\vec{r}_{\gamma_1}\|}{\|\vec{r}_{\gamma_2}\|} \right)^2 \right) \\
&\quad + 8 \left(\frac{x \cdot x_{\gamma_2} + y \cdot y_{\gamma_2}}{a^2} + \frac{z \cdot z_{\gamma_2}}{b^2} \right) \left(z_{\gamma_1} \cdot z_{\gamma_2} \cdot \left(\frac{1}{b^2} - \frac{1}{a^2} \right) \right) \left(\frac{\|\vec{r}_{\gamma_1}\|}{\|\vec{r}_{\gamma_2}\|} \right)^2 \\
C &= 4 \left(\frac{x \cdot x_{\gamma_1} + y \cdot y_{\gamma_1}}{a^2} + \frac{z \cdot z_{\gamma_1}}{b^2} \right)^2 + \\
&\quad 2 \left(\left(\frac{x_{\gamma_1}^2 + y_{\gamma_1}^2}{a^2} + \frac{z_{\gamma_1}^2}{b^2} \right) - \left(\frac{x_{\gamma_2}^2 + y_{\gamma_2}^2}{a^2} + \frac{z_{\gamma_2}^2}{b^2} \right) \left(\frac{\|\vec{r}_{\gamma_1}\|}{\|\vec{r}_{\gamma_2}\|} \right)^2 \right) \left(\left(\frac{x^2 + y^2}{a^2} + \frac{z^2}{b^2} \right) + \left(\frac{x_{\gamma_2}^2 + y_{\gamma_2}^2}{a^2} + \frac{z_{\gamma_2}^2}{b^2} \right) \left(\frac{R}{\|\vec{r}_{\gamma_2}\|} \right)^2 - 1 \right) \\
&\quad + 4 \left(\frac{x \cdot x_{\gamma_2} + y \cdot y_{\gamma_2}}{a^2} + \frac{z \cdot z_{\gamma_2}}{b^2} \right)^2 \left(\frac{\|\vec{r}_{\gamma_1}\|}{\|\vec{r}_{\gamma_2}\|} \right)^2 - 4 \left(z_{\gamma_1} \cdot z_{\gamma_2} \cdot \left(\frac{1}{b^2} - \frac{1}{a^2} \right) \right)^2 \left(\frac{R}{\|\vec{r}_{\gamma_2}\|} \right)^2 \\
D &= 4 \left(\frac{x \cdot x_{\gamma_1} + y \cdot y_{\gamma_1}}{a^2} + \frac{z \cdot z_{\gamma_1}}{b^2} \right) \left(\left(\frac{x^2 + y^2}{a^2} + \frac{z^2}{b^2} \right) + \left(\frac{x_{\gamma_2}^2 + y_{\gamma_2}^2}{a^2} + \frac{z_{\gamma_2}^2}{b^2} \right) \left(\frac{R}{\|\vec{r}_{\gamma_2}\|} \right)^2 - 1 \right) \\
&\quad - 8 \left(\frac{x \cdot x_{\gamma_2} + y \cdot y_{\gamma_2}}{a^2} + \frac{z \cdot z_{\gamma_2}}{b^2} \right) \left(z_{\gamma_1} \cdot z_{\gamma_2} \cdot \left(\frac{1}{b^2} - \frac{1}{a^2} \right) \right) \left(\frac{R}{\|\vec{r}_{\gamma_2}\|} \right)^2 \\
E &= \left(\left(\frac{x^2 + y^2}{a^2} + \frac{z^2}{b^2} \right) + \left(\frac{x_{\gamma_2}^2 + y_{\gamma_2}^2}{a^2} + \frac{z_{\gamma_2}^2}{b^2} \right) \left(\frac{R}{\|\vec{r}_{\gamma_2}\|} \right)^2 - 1 \right)^2 \\
&\quad - 4 \left(\frac{x \cdot x_{\gamma_2} + y \cdot y_{\gamma_2}}{a^2} + \frac{z \cdot z_{\gamma_2}}{b^2} \right)^2 \left(\frac{R}{\|\vec{r}_{\gamma_2}\|} \right)^2
\end{aligned}$$

- If A is not equal to 0, the preceding equation can be normalized:

$$a m^4 + b m^3 + c m^2 + d m + e = 0 \quad (5.115)$$

where the five coefficients are:

$$\begin{aligned}
a &= A/A = 1 \\
b &= B/A \\
c &= C/A \\
d &= D/A \\
e &= E/A
\end{aligned}$$

The roots of a quartic equation can be found analytically. To simplify the expression of these roots,

some constants are defined:

$$c_1 = c^2 - 3bd + 12e \quad (5.116)$$

$$c_2 = 2c^3 - 9bcd + 27d^2 + 27b^2e - 72ce \quad (5.117)$$

$$c_3 = \sqrt{-4c_1^3 + c_2^2} \quad (5.118)$$

$$c_4 = (c_2 + c_3)^{\frac{1}{3}} \quad (5.119)$$

$$c_5 = \frac{2^{\frac{1}{3}}c_1}{3c_4} + \frac{c_4}{32^{\frac{1}{3}}} \quad (5.120)$$

$$c_7 = \sqrt{\frac{b^2}{4} - \frac{2c}{3} + c_5} \quad (5.121)$$

$$c_8 = \frac{b^2}{2} - \frac{4c}{3} - c_5 \quad (5.122)$$

So the four roots are:

$$m = \begin{cases} \frac{-b}{4} - \frac{c_7}{2} - \frac{1}{2} \sqrt{c_8 - \frac{-b^3 + 4bc - 8d}{4c_7}} \\ \frac{-b}{4} - \frac{c_7}{2} + \frac{1}{2} \sqrt{c_8 - \frac{-b^3 + 4bc - 8d}{4c_7}} \\ \frac{-b}{4} + \frac{c_7}{2} - \frac{1}{2} \sqrt{c_8 + \frac{-b^3 + 4bc - 8d}{4c_7}} \\ \frac{-b}{4} + \frac{c_7}{2} + \frac{1}{2} \sqrt{c_8 + \frac{-b^3 + 4bc - 8d}{4c_7}} \end{cases} \quad (5.123)$$

- If $A = 0$, ie if $z_{\gamma_1} = z_{\gamma_2} = 0$, then $B = 0$, and the quartic equation degenerates in a second order equation:

$$Cm^2 + Dm + E = 0 \quad (5.124)$$

where the coefficients are:

$$\begin{aligned} C &= 4(x \cdot x_{\gamma_1} + y \cdot y_{\gamma_1})^2 + 4(x \cdot x_{\gamma_2} + y \cdot y_{\gamma_2})^2 \\ D &= 4(x^2 + y^2 + \frac{a^2 z^2}{b^2} - a^2 + R^2)(x \cdot x_{\gamma_1} + y \cdot y_{\gamma_1}) \\ E &= (x^2 + y^2 + \frac{a^2 z^2}{b^2} - a^2 + R^2)^2 - 4R^2(x \cdot x_{\gamma_2} + y \cdot y_{\gamma_2}) \end{aligned}$$

The two solutions are:

$$m = \begin{cases} \frac{-D + \sqrt{D^2 - 4CE}}{2C} \\ \frac{-D - \sqrt{D^2 - 4CE}}{2C} \end{cases} \quad (5.125)$$

In both cases, only the real solutions have to be kept. Moreover, since the parameter n has also to be real, m has to be smaller than R . And finally since the satellite is looking on his right, only the positive values of m must be kept. To resume, only the real, positive roots smaller than R , have to be kept. This root should be unique.

The coordinates of the Earth point target can thus be written as:

$$\vec{r}_\gamma = \vec{r}_{\gamma_{ac}} + m \cdot \vec{r}_{\gamma_1} + n \cdot \vec{r}_{\gamma_2} \quad (5.126)$$

5.3.8.6.2 Approached solution

An approximation to the exact solution exists, which consists in considering a locally spherical Earth (see document [5], pp 250-254, for more details).

An other approximation to the exact solution is based on the linear interpolation between two exact solutions. Indeed, the exact point position is easily determined from its elevation angle, the equation being of the second order. Doing so for a set of elevation angles values, a set of corresponding (elevation angle, range) is determined. For an arbitrary range, the method consists in interpolating the elevation angle between the two values whose ranges frame the given range. From this approximated elevation angle, the point position is then easily computed.

5.3.8.7 Determination of the Point Speed Vector

With the help of the orbit propagator software, the velocity of the point target on Earth can be determined: the input for this routine is the point position, given in the γ -frame or in the g -frame.

5.3.8.8 Determination of the Doppler Shift

Due to the motion of the spacecraft and to Earth rotation the received (reflected) echo signal of the scatterometer is Doppler shifted. This two-way frequency shift of the transmitted signal is given by (see [21], p 20) :

$$f_d = \frac{2 \cdot f_t}{c} (\vec{v}_{\gamma_{sc}} - \vec{v}_{\gamma}) \cdot \vec{r}_{\gamma_1} \quad (5.127)$$

where

- f_d : Doppler shift
- f_t : carrier frequency
- c : speed of light
- $\vec{v}_{\gamma_{sc}}$: velocity vector of the satellite in γ -frame
- \vec{v}_{γ} : velocity vector of the point on Earth in γ -frame
- \vec{r}_{γ_1} : unit vector from the point on Earth to the satellite

$$\vec{r}_{\gamma_1} = \frac{\vec{r}_{\gamma} - \vec{r}_{\gamma_{sc}}}{\|\vec{r}_{\gamma_{sc}} - \vec{r}_{\gamma}\|} \quad (5.128)$$

with :

- \vec{r}_{γ} : vector position of the point on Earth in γ -frame
- $\vec{r}_{\gamma_{sc}}$: vector position of the spacecraft in γ -frame

The Doppler shift depends on the position of the target on ground and the position of the spacecraft on its orbit, and hence is a function of the orbit time (T). The Doppler shift of the received signal is also a function of the echo time (τ) and therefore, the Doppler compensation frequency must also be a function of the echo time.

5.3.8.9 Node location

The measurement nodes form the regular grid at which the processed data σ^0 -triplets and their auxiliary data are given. These nodes are then used to generate the final products: the wind speed and direction.

The node grid is derived from:

- the initial orbit time

- the reference orbit time
- the FMA-repetition interval
- the along-track node distance factor, expressed in units of FMA-repetition intervals
- the gamma angle of node 10
- the across-track node angular distance

The first four parameters determine the location of the across track rows of nodes. An across-track row of nodes is defined at the time corresponding to the middle of a Mid beam measurement sequence. This yields a perpendicular orientation of the across-track row with respect to the ground trace in YSM. The along-track distance between two across-track rows of nodes corresponds to the along-track node distance factor multiplied by the FMA-repetition interval. This corresponds to one across-track row of nodes each four FMA-sequences.

The gamma angle defines the center node across track of each across track row of nodes. This angle is measured in the plane perpendicular to the relative ground trace velocity, from the nadir direction, the satellite's COG being the top of this angle.

Given the definition above, the nodes belonging to one across-track row are located on an ellipse, the intersection of the GEM-6 Earth model and the elevation plane of the Mid antenna. The center node of the across-track row determines the location of all the other nodes of the across track row, 9 having a smaller range than the mid-swath point and 9 having a greater range. The across-track angular distance, accounted from the center of that ellipse, between two adjacent nodes is constant. This means that in all rigor the across-track distance between two adjacent nodes is not constant. This method was probably chosen because the distance along an ellipse, being given by an elliptic integral, is much more difficult to compute in closed form.

This being said, the across-track distance variations between nodes is actually very small and remain below 100m. The explanation for these small differences is that the Earth, although not perfectly spherical — in which case a strictly constant across-track inter-node distance would be observed — is very close to a sphere. Hence the assumption of a constant across-track inter-node distance is reasonable.

More information can be found in [5] p63, p198 and p449.

5.4 Quality control and monitoring

The overall system behavior must be monitored to check the product confidence. For this purpose, several control parameters are computed and delivered in the source packet headers.

5.4.1 High Power Amplifier Monitoring

A possible cause to missing transmit pulses is HPA-arc-ing, leading to temporary shutdown of the amplifier. During these time intervals only noise will be recorded, hence the derived σ^o values are invalid and must be detected as such. This can be achieved by monitoring the HPA. The HPA-shutdown detection procedure, described in [14], p37, is based on the difference in energy level of the calibration pulses during normal HPA operation and shutdown. The averaged energy of the samples of the calibration pulses of a measurement block is compared to a threshold value, a flag being raised if the latter is greater.

When performing the spatial averaging, the flags of the samples contributing to a node are summed together, yielding the number of “arc-ing” samples that contributed to a particular node (see [14], p124 for the detailed formula).

5.4.2 Power spectrum monitoring

The Doppler compensation performed is subject to errors, in particular due to the yaw control inaccuracy. This may lead to a shift of the spectrum out of the low pass filter passband and thus to an alteration of the signal to noise ratio. The required monitoring is performed on the power spectrum at the input of

the low-pass filter by computation of the centre of gravity C_{cog} and the standard deviation C_{var} of the signal averaged over a monitoring interval. The algorithms used to determine these two control parameters are described in [14], p130a.

5.4.3 I/Q Imbalance Monitoring

Due to possible I/Q channel gain imbalances or DC-offsets, the I- and Q- channel noise power averages must be monitored. The monitoring parameters $C_{B,I}$ and $C_{B,Q}$ are used for that purpose. These parameters will be obtained by averaging the real noise power on 8 consecutive FMA sequences every 76th FMA sequence, and this respectively for the I- and Q-channel. Suitable expressions for these parameters, evaluated for each beam, are given by (see [14], p132)

$$C_{B,I} = \frac{1}{\Delta L} \sum_{l=L}^{L+\Delta L-1} \bar{s}_{N,I,l} \quad (5.129)$$

$$C_{B,Q} = \frac{1}{\Delta L} \sum_{l=L}^{L+\Delta L-1} \bar{s}_{N,Q,l} \quad (5.130)$$

respectively for the I- and Q-channel. The real noise power average for the I- and Q-channel are symbolized respectively by $\bar{s}_{N,I}$ and $\bar{s}_{N,Q}$. ΔL denotes the number of measurement blocks considered and L the start index.

5.4.4 Internal Calibration Level Monitoring

The internal calibration level is monitored by computing, for each beam, a control parameter denoted C_{CL} . This parameter is based on the energy of the internal calibration pulses samples, that is

$$p^C(n) = s_I^C(n)^2 + s_Q^C(n)^2 \quad (5.131)$$

A weighted sum of these values for a pulse is computed using a weighting function a_n as described in section 5.3.5. The pulse energies of the four calibration pulses per block and of several (ΔL) measurement blocks are then averaged.

$$C_{CL} = \frac{1}{4 \cdot \Delta L} \sum_{l=L}^{L+\Delta L-1} \sum_{\mu=1}^4 \sum_{n=N_1}^{N_2} a_n \cdot p^C(n) \quad (5.132)$$

where L denotes the monitoring start index and N_1 and N_2 respectively the lower and upper bounds of the used ADC samples.

Part II

ASCAT/METOP Algorithm Description

Chapter 6

Overall Scatterometer description

6.1 General description

As for the ERS scatterometer, the primary measurement objective of the Advanced Scatterometer (ASCAT) is the determination of wind fields at the ocean surface. The same principle is used, that is the dependence of radar backscatter upon the amplitude and orientation of the surface capillary and small gravity waves, themselves related to the wind velocity near sea surface.

ASCAT is aboard the METOP satellite on a sun-synchronous orbit with a 5-day repeat cycle, a 835 km nominal altitude and an Equator crossing time at 0930AM. For an enhanced spatial coverage, a large swath width is needed. It is obtained by implementing two sets of antennas providing 550 km wide swath left and right of the sub satellite track. An unambiguous determination of the wind direction requires observing the sea surface from three directions. Thus each antenna set consists in three antennas with three different azimuth look angles (45°, 90°, 135°). The swathes correspond to incidence angles ranging from 25° to 53.4° (Mid beam) and 33.7° to 64.3° (Fore and Aft beams).

As for the ERS scatterometer, ASCAT is a real aperture radar working in the C-band and vertically polarized. The principle of operation however differs from the ERS scatterometer in the pulse type used. While the ERS scatterometer relies on the emission of continuous-wave (CW) pulses with durations of around 100 μ sec and peak powers in the kW range, ASCAT's measurements are based on long transmit pulses (typically 10 msec) with Linear Frequency Modulation (LFM) called chirps, thus allowing low peak power (125 W).

In the ground processing, the ASCAT source packets are corrected for noise and instrument gain variations and processed to obtain the normalized backscatter measurements at the 25 km/50 km spatial resolution nodes. The ensemble of spatially averaged σ^o estimates from the three beams (Fore, Mid, Aft) is called σ^o triplet. These σ^o values correspond to measurements taken at different times: the fore beam measurement leads in time, followed by the mid beam and later by the aft beam. The distance between the measurement times depends on the node position within the swath, increasing from near range to far range.

6.2 Measurement Mode

The measurement mode is the nominal operational mode. In this mode, the ASCAT antennas are activated in a predefined sequence specified in the global parameter table and the sequencer parameter table. The default antenna sequence is

$$F_L M_L A_L F_R M_R A_R$$

where F_L represents fore beam left side transmit/receive cycle etc. Echo, calibration and noise samples are derived in a sequential way from the different antennas of the defined sequence.

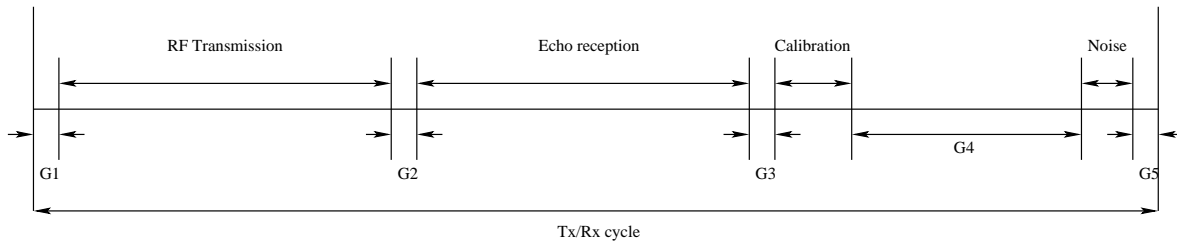


Figure 6.1: Instrument time lining

The time lining for one Tx/Rx cycle in the measurement mode is shown in Figure 6.1. The (default) total duration of each Tx/Rx cycle is 34.34ms and is independent of the actually operated antenna beam. However, the transmit pulse length and the chirp rate within each cycle are beam dependent.

The structure of a Tx/Rx cycle is defined by:

- **G1:** Set-up of switch matrix for transmission via antenna assigned to actual PRI; Set-up of chirp generator for transmission.
- **RF transmission:** Pulse transmission from the cycle beam.
- **G2:** Guard time to allow deactivation of the High Power Amplifier (HPA); Set-up of chirp generator for reception; Opening of receiver shutter at end of guard time.
- **Echo reception:** Reception via the same beam as transmission.
- **G3:** Scatterometer Front End (SFE) reconfiguration.
- **Internal Calibration:** Stimulus is coupled into the switch matrix (analogue processing as during echo reception).
- **G4:** SFE reconfiguration.
- **Noise:** Reception via a selected beam.
- **G5:** Closure of Pulse Repetition Interval (PRI) cycle (shutter closing).

6.3 On-board echo processing

ASCAT transmits chirps at a carrier frequency of 5.225 GHz. The received echo signal is de-chirped with an image of the transmitted pulse, filtered and down-converted to baseband (see on board preprocessing at Figure 6.2). The baseband signal is sampled and processed by the on-board digital signal processor. The on-board processing is basically a power spectrum estimation (transformation to frequency domain and square modulus detection) followed by (spatial) low pass filtering (in azimuth and in range). This results in echo power spectra, where each frequency f corresponds to a specific slant range distance. The effect of the on-board processing is a substantial reduction of the data rate required to record the science data. It does not require on-board knowledge of satellite positioning/pointing. Together with internal calibration data (containing information on relative gain variations within the instruments transmit and receive path) the echo power spectra are packed to nominal ASCAT source packets and transferred to the ground, where they serve as input data for the ASCAT ground processing. Besides the nominal ASCAT source packets also noise source packets are generated, which contain information on the instrument background noise [17].

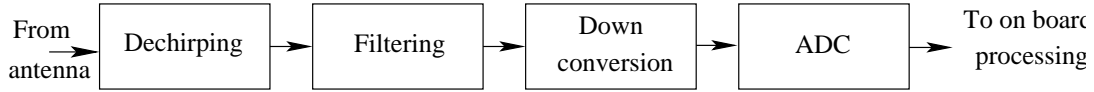


Figure 6.2: ASCAT on board preprocessing chain

6.3.1 Pulse generation

ASCAT generates LFM pulses with a pulse repetition frequency (PRF) of 29.12 Hz , corresponding to a pulse repetition interval of 34.34 ms . These pulses are transmitted at a carrier frequency of 5.255 GHz sequentially through the six antennas, hence the beam PRF is one sixth of the chirp generator PRF (4.8 Hz). The default pulse length are 8.03 ms for the mid beams and 10.10 ms for the fore and aft beams. The corresponding default chirp rates are -50 kHz/ms for the mid beams and -24 kHz/ms for the fore beams and $+24 \text{ kHz/ms}$ for the aft beams respectively. The generated chirps are then amplified to the required power level (approximately 125 W) and distributed to the individual antennas.

6.3.2 De-chirping principle

The received echo can be seen as a serie of superimposed echo pulses arriving over a time range corresponding to the width of the instrument swath. Figure (6.3) illustrates the mixing process for two echo pulses with respective flight times t_1 and t_2 . The linear frequency modulation causes a frequency offset between the pulses and the local oscillator pulse of respectively f_1 and f_2 . Signals originating at different ranges can thus be discriminated, based on this frequency difference. Hence, the spectral lines deduced by analyzing the mixer output are characterized by amplitude and frequency directly linked to power and range respectively.

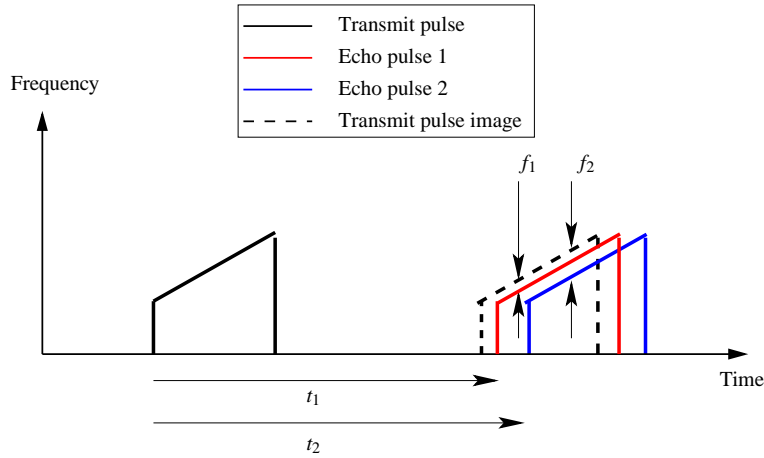


Figure 6.3: Principle of range discrimination with LFM.

The form of the transmitted linear chirp signal is given by:

$$s_t(t) = a_0 \text{rect}(t, \tau_{T_x}) \cos(2\pi f_c t + \pi K_c t^2) \quad (6.1)$$

where K_c is the chirp rate, f_c the carrier frequency, τ_{T_x} the pulse length and a_0 the signal amplitude.

The transmitted pulse is scattered at the sea surface and received back by the antenna. The received echo signal, for a scattering point target, is given by:

$$s_r(t) = s_0 \text{rect}\left(t - \frac{2R}{c}, \tau_{T_x}\right) \cos\left(2\pi f_c \left(t - \frac{2R}{c}\right) + \phi_0 + \pi K_c \left(t - \frac{2R}{c}\right)^2 + 2\pi f_D(R) \left(t - \frac{2R}{c}\right)\right) \quad (6.2)$$

where R is the slant range, $\frac{2R}{c}$ the time delay due to the two way propagation time between the radar and the target and $f_D(R)$ the Doppler shift due to the relative motion between the radar and the target.

Here the hypothesis is made that the Doppler frequency shift is independent of the instantaneous frequency of the chirp and equal to a mean Doppler shift that only depends on range (see also section 7.3).

The received signal is de-chirped with a conjugate image of the transmitted signal produced by restarting the chirp generator. It is then filtered and down-converted to the baseband. The de-chirping signal is given by:

$$s_{dc}(t) = \cos(2\pi f_0 t + 2\pi f_{off} t + \pi K_c t^2) \quad (6.3)$$

where f_{off} is the chirp start frequency. Multiplying the received echo (6.2) and the de-chirping signal (6.3) consists of an up-converted part and a down-converted part. Since the up-converted part is rejected by the filters, the de-chirped (and down-converted) echo of a single target point is given by:

$$s_d(t) = \frac{1}{2} s_0 \text{rect} \left(t - \frac{2R}{c}, \tau_{T_x} \right) \cos(\phi(t)) \quad (6.4)$$

where the phase term is given by:

$$\phi(t) = \alpha t + \phi_x = 2\pi(f_c - f_0 - f_{off})t + \phi_0 + \pi K_c \left(t - \frac{2R}{c} \right)^2 - \pi K_c t^2 + 2\pi f_D(R) \left(t - \frac{2R}{c} \right) - \frac{4\pi f_c R}{c} \quad (6.5)$$

Rearranging equation (6.5) leads to:

$$\phi(t) = \alpha t + \phi_x = \left(\phi_0 + \pi K_c \frac{4R^2}{c^2} - \pi f_D(R) \frac{4R}{c} - \frac{4\pi f_c R}{c} \right) + 2\pi \left(f_c - f_0 - f_{off} - K_c \frac{2R}{c} + f_D(R) \right) t \quad (6.6)$$

Equation (6.6) indicates that in the overall de-chirped and down-converted echo signal each point target appears as a single tone of finite duration with a specific frequency f determined by range R , Doppler shift f_D , baseband carrier frequency f_T ($f_c - f_0$) and chirp start frequency f_{off} . The specific frequency assigned to a slant range R is determined by differentiating the phase term $\phi(t)$ of the de-chirped signal (see equation (6.5)). The de-chirped frequency, function of the slant range R , is given by:

$$f(R) = \frac{1}{2\pi} \frac{\partial \phi(t)}{\partial t} = \alpha = f_c - f_0 - f_{off} - K_c \frac{2R}{c} + f_D(R) \quad (6.7)$$

Equation (6.7) indicates that:

- the bandwidths of the filters stages determine the width of the swath from which information is obtained;
- in order to keep the echo signals within the pass-bands of the filters, the chirp start frequency f_{off} and the chirp rate K_c have to be adjusted for each beam to take into account the beam dependent mean slant range and mean Doppler shifts.

This equation (6.7) is also used to determine the sample position (see section (7.3)).

6.3.3 Narrow Band Filters

Following the de-chirping, narrow band filters (NBF) are used to synthesize range-bins. In practice, these narrow band filters are implemented using the Fourier transform¹, acting as a filter bank.

¹The discrete Fourier transform of the sampled time domain signal $s(n)$ is given by

$$\mathcal{F}(s(n)) = S(l) = \frac{1}{\sqrt{L}} \sum_{n=0}^{L-1} s(n) e^{-j2\pi n l / L} \quad \text{with } l = 0 : \frac{L}{2} \quad (6.8)$$

All the time domain signals considered here are real, so their Fourier transform $S(l)$ are symmetrical and it is sufficient to consider only the first half of the L frequency bins.

6.3.4 Spatial averaging (range)

The on-board processing in across-track direction is similar to SAR multi-looking processing. The digitized signal within the reception window of total length τ_r is segmented in K overlapping segments of the length τ_w (nominal K values are 5 for the mid beam and 9 for the fore and aft beams). These segments are first separately processed:

1. by multiplying the segment with a window function (nominally a Tukey window);
2. by applying a NBF bank, implemented using the discrete Fourier transforms;
3. by doing a detection.

The power spectral density of the k^{th} segment is given by:

$$PSD_k(l) = |S_k(l)|^2 \quad (6.9)$$

where $S_k(l)$ is the discrete Fourier transform of the sampled time domain signal $s_k(n)$, after windowing, each segment consisting of L samples (nominally 512).

The power spectral densities of the segments are then averaged in order to decrease the intensity variance due to speckle or in other words to increase the radiometric resolution similarly to SAR multi-look processing. The power spectrum density average estimation is given by:

$$PSD(l) = \sum_{k=k_0(l)}^{k_1(l)} PSD_k(l) \quad (6.10)$$

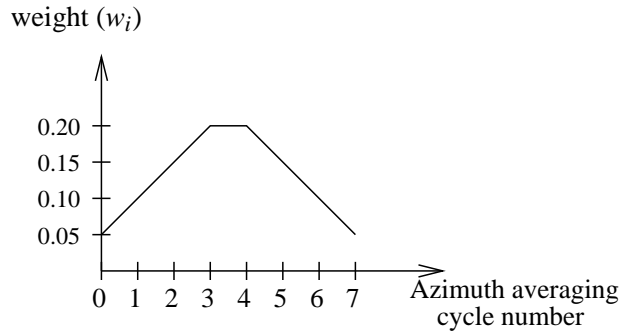
where $k_0(l)$ and $k_1(l)$ are antenna and segment dependent. The number $\chi(l) = (k_1(l) - k_0(l) + 1)$ of averaged power spectral densities for each value of l should be taken into account in the on ground processing.

6.3.5 Spatial averaging (azimuth)

Finally an azimuth averaging is performed to reduce the amount of data transmitted. It combines all the power spectral densities $PSD_i(l)$ obtained from the same antenna during A successive antenna cycles (nominally 8):

$$\underline{PSD}(l) = \sum_{i=0}^{A-1} w_i PSD_i(l) \quad (6.11)$$

with $w_i = [0.05, 0.1, 0.15, 0.2, 0.2, 0.15, 0.10, 0.05]$.



Here also the total weight of the azimuth averaging interval $\sum_{i=0}^{A-1} w_i$ should be taken into account in the on ground processing. In the nominal case, it is noticed that this total weight is equal to unity. This azimuth averaging takes place every $A/2$ antenna cycles so there is data overlap in the resulting data.

6.4 Calibration on-board processing

The internal calibration includes the generation of a calibration signal as well as the measurement of forward and reflected power. During the transmit phase of each Tx/Rx cycle the transmit power is measured at the forward power detector. The power reflected from the antenna is measured at the reflected power detector.

In the calibration phase of each Tx/Rx cycle a CW pulse is generated. The calibration signal experiences the same gain/loss variation as the nominal measurement data because the internal calibration path includes all the main elements like amplifiers, mixers, filters and ADC.

First the calibration signal is sampled and a windowing is applied with a dedicated calibration window function. The discrete Fourier transform is then taken:

$$S_{cal}(l) = \mathcal{F}(s_{cal}(n)) \quad (6.12)$$

with $s_{cal}(n)$ and $S_{cal}(l)$ being respectively the sampled time domain signal and the corresponding spectrum.

The spectrum amplitude is expected to exhibit a peak at the frequency of the calibration CW pulse used. The amplitude and phase of three (selectable) samples $S_{cal}(l_1)$, $S_{cal}(l_2)$ and $S_{cal}(l_3)$ around the expected peak of the calibration response are recorded in the ASCAT source packet without any azimuth averaging, resulting in $A/2$ sets (due to the $A/2$ azimuth averaging cycle) of calibration data per one set of azimuth compressed echo data in one source packet.

6.5 Noise on-board processing

The aim of the noise measurement is to measure the noise power at the output of the receiver without a receive signal at the input. In the on ground processing, the noise data are used to reconstruct the actual on-board filter shape for compensating the echo data for this filter shape, while the mean noise level is subtracted from the echo data.

The noise measurements are the last step of each transmit/receive cycle when all echoes have died away. The noise signal is mainly due to thermal noise. It includes also interferences from other instruments and the thermal radiation due to the actual surface temperature on the ground.

The noise signal is on board preprocessed like the echo signal and the calibration signal. It is first sampled by the ADC and a time noise window function is applied. Then a power spectrum density estimation is performed:

$$PSD_{noise}(l) = |\mathcal{F}(s_{noise}(n))|^2 = |S_{noise}(l)|^2 \quad (6.13)$$

Finally an azimuth averaging is performed to reduce the amount of data transmitted. It performs a moving average of all the noise power spectral densities obtained from the same antenna during N successive transmit/receive cycles:

$$\underline{PSD}_{noise}(l) = \frac{1}{N} \sum_{i=0}^{N-1} PSD_{noise_i}(l) \quad (6.14)$$

The number N of noise measurements per antenna is a parameter.

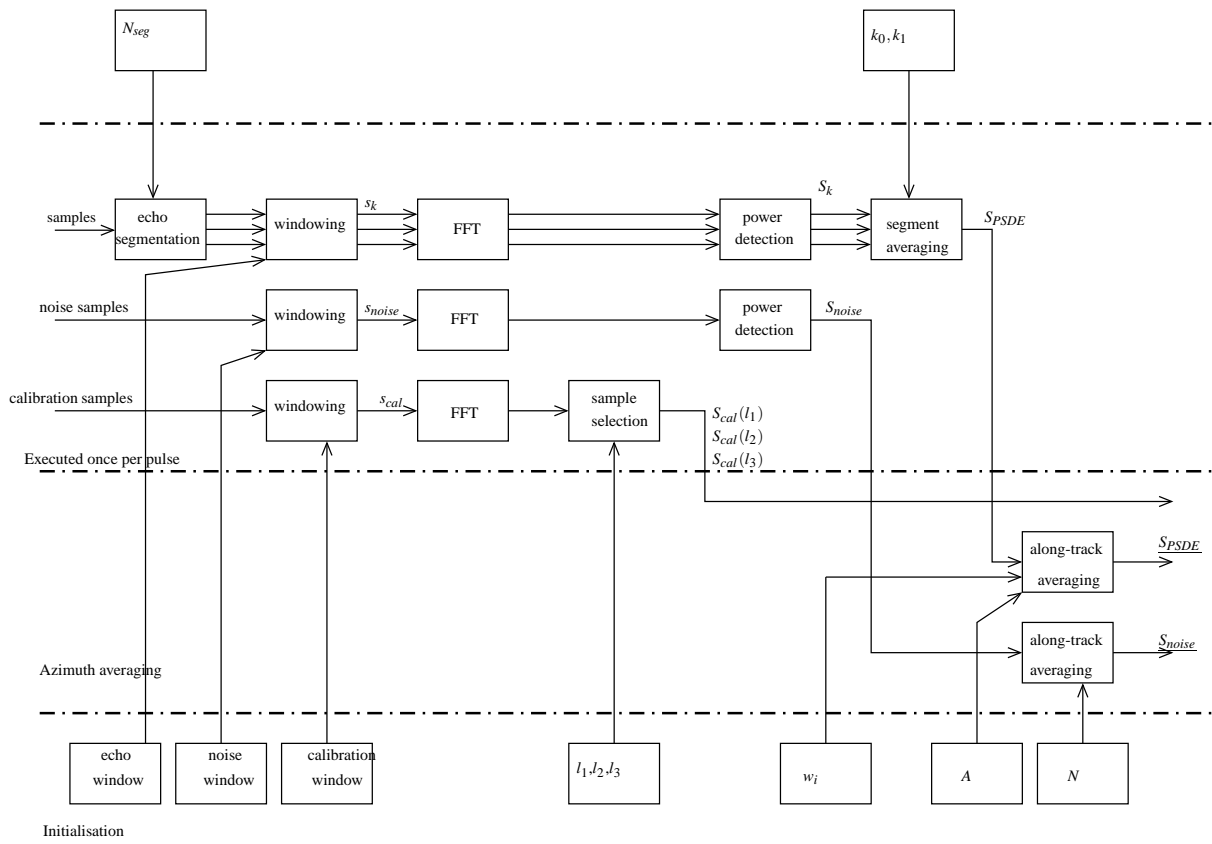


Figure 6.4: ASCAT on board processing chain

Chapter 7

Ground processing description

7.1 Ground processing principle

The main input to the ASCAT ground processor is the Frequency Power Profile $FPF(f, T)$ given in an orbit time-echo frequency coordinate system. After a first correction to the echo measurement data based on the noise and calibration measurements, the obtained values are associated to spatial coordinates. The σ -power values are then converted to σ^o values by applying normalization functions leading to full-resolution σ^o data. Generating the smoothed σ^o values at the desired spatial and radiometric resolution requires a final spatial filtering step. From the σ^o , the wind speeds and directions can be derived using a wind model. An overview of these processing steps is given at Figure 7.1.

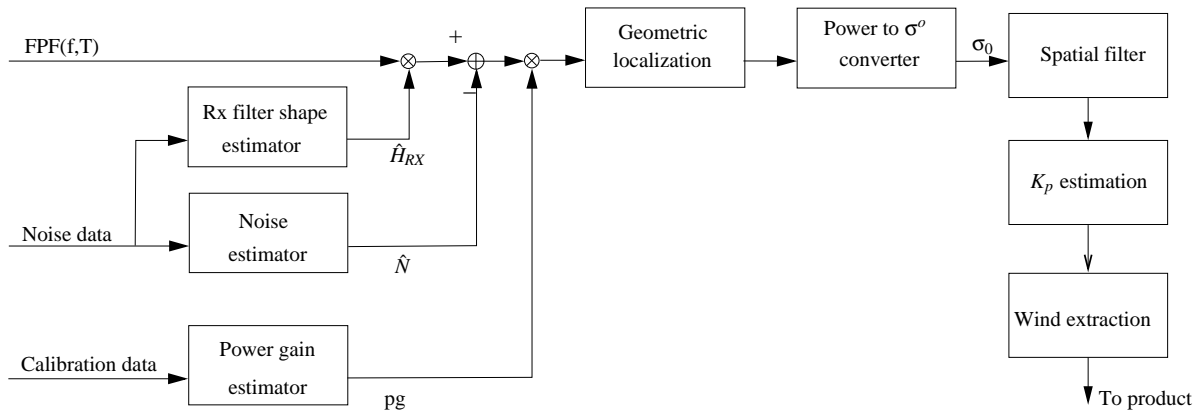


Figure 7.1: ASCAT ground processing chain

7.2 Measurement data correction

7.2.1 R_x filter shape estimation

The noise processor derives from the noise measurement source packets ($PSD_{noise}(l, T)$) a noise power estimate $\hat{N}(T)$ and an onboard filter shape estimate $\hat{H}_{RX}(l, T)$. The noise power estimate is specific for each antenna, while the onboard filter shape does not depend on the antenna. $\hat{H}_{RX}(l, T)$ is assumed identical for all beams. The onboard filter shape estimate $\hat{H}_{RX}(l, T)$ is computed by time averaging the noise power spectrum normalised with respect to the noise power at the calibration signal frequency f_0 (l_0 is the

corresponding sample)

$$\hat{H}_{RX}(l, T) = \frac{1}{M_1} \sum_{m=0}^{M_1-1} \left[\frac{1}{B} \sum_{b=1}^B \frac{PSD_{noise}^b(l, T_{k+m})}{PSD_{noise}^b(l_0, T_{k+m})} \right] \quad (7.1)$$

with M_1 the number of spectra incorporated in the averaging and B the number of beams. A filter shape is valid for a given period of time. If there is no filter shape available for a particular time T or if $\hat{H}_{RX}(l, T)$ cannot be estimated correctly, a default filter shape shall be used instead. The filter shape is further averaged in time.

7.2.2 Noise power estimation

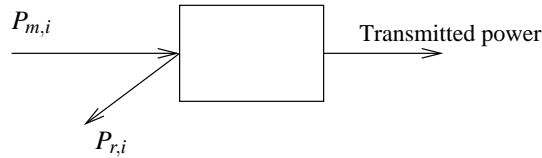
A receiver noise power estimate $\hat{N}(T)$ is computed by averaging with uniform weight noise samples from a selected range of discriminator frequencies. It is assumed that it is a white noise.

$$\hat{N}(T) = \frac{1}{M_2} \sum_{m=0}^{M_2-1} \frac{1}{(n_{stop} - n_{start} + 1)} \sum_{l=n_{start}}^{n_{stop}} \frac{PSD_{noise}(l, T_{k+m})}{\hat{H}_{RX}(l, T)} \quad (7.2)$$

with M_2 the number of spectra incorporated in the averaging. A noise estimate is valid for a given period of time. If there is no noise estimate available for a particular time T or if $\hat{N}(T)$ cannot be estimated correctly, a default noise estimate shall be used instead.

7.2.3 Power gain product estimation

Several power measurements are made by the instrument for internal-calibration purposes. During the RF pulse transmission, the transmitted power P_T is measured on the way to the antenna, and the reflected power P_R is measured on the way back from the antenna. The measurement of the transmitted power and reflected power together allow the power lost due to mismatch at the antenna port to be determined thereby allowing the actual power transmitted from the antenna to be monitored. $TPR(P_{m,i}, P_{r,i})$ is the transmission



power ratio, which may be approximated by

$$TPR(P_{m,i}, P_{r,i}) = \frac{P_{m,i} - P_{r,i}}{P_{m,i}} = 1 - \frac{P_{r,i}}{P_{m,i}} \quad (7.3)$$

Optionally the user may switch off the calculation of the transmission power ratio leading to $TPR(P_{m,i}, P_{r,i}) = 1$

The power gain product $pg(l_0, T)$ represents the power gain product valid for one frequency f_0 (corresponding sample l_0) (which is characteristic for the internal calibration) and for the orbit time T associated with the power spectrum.

$$pg(l_0) = C_0 \frac{1}{N} \sum_{i=0}^{N-1} P_{d,i} \frac{P_{m,i} TPR^2(P_{m,i}, P_{r,i})}{P_{c,i}} \quad (7.4)$$

$P_{m,i}$, $P_{r,i}$ and $P_{c,i}$ are the measured values for forward, reflected and calibration power derived from the digitised power detector values contained in the source packets. $P_{d,i}$ is the receiver detected power readout, which is the peak value of the power spectrum obtained during the internal calibration measurement 'i'. This peak value is determined by interpolating three values next to the expected peak of the spectrum with a parabola and determine the maximum thereof. The constant C_0 is correction factor that takes into account the conversion factors of the ADC.

7.2.4 Data correction

The echo samples within each source packet are corrected for the variations of:

- the shape of the receiver filter characteristic,
- the receiver noise power,
- the transmitted RF power.

Figure 7.2 shows a simplified model of the received signal:

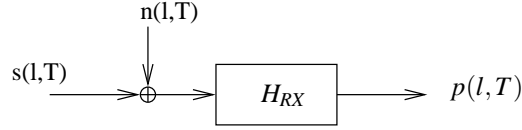


Figure 7.2: ASCAT received signal simplified model

$$p(l, T) = (s(l, T) + n(l, T)) * h(l, T) \quad (7.5)$$

Passing in the frequency domain leads to:

$$\underline{PSD}(l, T) = (P(l, T) + N(T)) H_{RX}(l, T) \quad (7.6)$$

with $\underline{PSD}(l, T)$ denoting the set of source packet echo samples associated with echo time T and with l indexing the source packet echo sample associated with discriminator frequency $f(l)$, the (estimated) corrected echo samples power $\hat{P}(l, T)$ can be, for each beam, expressed as:

$$\hat{P}(l, T) = \frac{1}{pg(l_0, T)} \left(\frac{\underline{PSD}(l, T)}{\hat{H}_{RX}(l, T)} - \hat{N}(T) \right) \quad (7.7)$$

where $pg(l_0, T)$ is the power gain estimation, $\hat{H}_{RX}(l, T)$ is the (estimated) receiver filter shape and $\hat{N}(T)$ the (estimated) receiver noise power.

7.3 Sample geometric localisation

This computing step performs a coordinate transform from discriminator frequency/orbit time (f_P, T) to spatial coordinates $(x_{\gamma_P}, y_{\gamma_P}, z_{\gamma_P})$ leading to localization of the sample P in terms of along-track and across-track position. The details about the geometry parameter calculation can be found in Section 5.3.8. Only the basic steps are summarized in the following.

7.3.1 Exact solution

The sample position characterized by a discriminator frequency f_P and orbit time T corresponds to a vector \vec{r}_{γ_P} given in the inertial frame, also called γ -frame. The origin of the vector is the origin of the γ -frame, i.e. the Earth's centre, while the end-point of the vector is P . The sample position is determined by solving the following system composed of three equations:

Equation of the discriminator frequency The discriminator frequency f_P of the point P is function of the point position as given by eq. (6.7). For any point position \vec{r}_{γ_P} , this equation becomes:

$$f_P(\vec{r}_{\gamma_P}) = f_c - f_0 - f_{off} - K_c \frac{2|\vec{r}_{\gamma_P}|}{c} + f_D(\vec{r}_{\gamma_P}) \quad (7.8)$$

where f_c denotes the carrier frequency, f_0 the total down-conversion frequency (sum of the LO frequencies), f_{off} the chirp start frequency, K_c the chirp rate and $f_D(\vec{r}_{\gamma_P})$ is the mean Doppler shift due to the motion of the spacecraft and to Earth rotation

$$f_D(\vec{r}_{\gamma_P}) = \frac{2 f_t}{c} (\vec{v}_{\gamma_{sc}} - \vec{v}_{\gamma_P}) \cdot \vec{r}_{\gamma_1} \quad (7.9)$$

where

- f_t : RF carrier frequency
- c : speed of light
- $\vec{v}_{\gamma_{sc}}$: velocity vector of the satellite in γ -frame
- \vec{v}_{γ_P} : velocity vector of the point on Earth in γ -frame
- \vec{r}_{γ_1} : unit vector from the point on Earth to the satellite

$$\vec{r}_{\gamma_1} = \frac{\vec{r}_{\gamma_P} - \vec{r}_{\gamma_{sc}}}{\|\vec{r}_{\gamma_{sc}} - \vec{r}_{\gamma_P}\|} = \frac{\vec{r}_{\gamma_P} - \vec{r}_{\gamma_{sc}}}{R}$$

with $\vec{r}_{\gamma_{sc}}$ the vector position of the spacecraft in γ -frame.

Equation of the ellipsoid The ellipsoid equation models the Earth. It is given by the WSG84

$$\frac{x_{\gamma_P}^2 + y_{\gamma_P}^2}{a^2} + \frac{z_{\gamma_P}^2}{b^2} = 1 \quad (7.10)$$

with $a = 6378.137 \text{ km}$ and $b = a(1 - f)$ and $f = 1/298.2572 \text{ km}$.

Equation of the plane The plane of constant azimuth Φ is passing through the antenna's centre and is spanned by two vectors, given in the γ -frame, \vec{r}_{γ_1} and \vec{r}_{γ_2} so its equation is:

$$\vec{r}_{\gamma_P} = \vec{r}_{\gamma_{ac}} + m \vec{r}_{\gamma_1} + n \vec{r}_{\gamma_2} \quad (7.11)$$

where $\vec{r}_{\gamma_{ac}} = (x_{ac}, y_{ac}, z_{ac})$ is the antenna centre, m and n are two real parameters.

7.3.2 Approached solution

Equation (7.8) shows that the Doppler frequency depends on the range which in turns depends on the Doppler frequency. This equation can therefore resolved by iteration to find the range. The iteration involves an error in range, thus in the position of the sample.

An approximation to the exact solution avoiding the iteration processus, corresponding to a given discriminator frequency, could be obtained based on the linear interpolation between two exact solutions. Indeed, the Doppler frequency and discriminator frequency are easily determined from the range. Doing so for a set of ranges values, a set of corresponding parameters (range, Doppler frequency, discriminator frequency) is determined. For an arbitrary discriminator frequency, the method consists in interpolating the ranges between the two values whose discriminator frequencies frame the given discriminator frequency. From the given range, the point position is then easily computed.

7.4 Power to σ^0 conversion

Converting the signal power values to σ^0 values involves the use of a normalization function, which takes into account the antenna gain pattern and the samples' geometry as described in Section 5.3.6

$$\zeta_N(l) = \frac{R^3 \sin(\theta) e^{\frac{2 f_{atm}}{\cos(\theta)}}}{G_{el}^2(\theta_{el})} \quad (7.12)$$

where ζ_N is the normalization function, R is the slant range, θ is the incidence angle, f_{atm} is the one-way atmospheric loss and $G_{el}(\theta_{el})$ is the one-way antenna gain in the beam elevation plane at the angle θ_{el} .

7.5 Spatial filtering

Generating σ^o values at the desired spatial and radiometric resolution involves smoothing the full resolution σ^o data obtained after coordinate transform. Therefore a spatial filter, centered on the required node position, is applied on the full resolution data. The spatial filtering is actually performed in three steps, respectively by the antenna footprint, on-board and on ground. The antenna footprint is range dependent, leading to a range dependent filtering. The on-board filter is kept position invariant while the on ground filter is position dependent to match the required resolution.

7.5.1 Node geometry

The details concerning the node geometry computation such as the node position, the node incidence angles and the node look-angles can be found in Section 5.3.8.9 and in Chapter 11.

7.5.2 Sample selection

The appurtenance of the samples to a node is computed on the fly, to avoid having to rely on a pre-computed look-up-table. The appurtenance is computed in two step. The first step involves a rough pre-selection of the samples, based on the acquisition time and range. In the second step, the precise distance of each sample to the node centre is computed and used as appurtenance criterion. The details concerning the sample pre-selection and the sample selection, with the associated mathematical formulas such as the sample projections onto the tangential plane at the node position, can be found in Section 11.2.

7.5.3 Sample weight

The spatial weighting function consists in the product of two weighting functions respectively across-track and along-track, making the separability assumption. To ensure an uniform spatial resolution, the one-dimensional weighting functions used will have parameters α_x and α_y and window dimensions L_x and L_y varying with the across-track position of the node and with the beam. The two-dimensional function is given by:

$$w(x, y) = w_x(x) w_y(y) \quad (7.13)$$

where $w_x(x)$ and $w_y(y)$ are the one-dimensional functions respectively across-track and along-track:

$$w_x(x) = \begin{cases} \alpha_x + (1 - \alpha_x) \cos\left(\frac{2\pi x}{L_x}\right) & -L_x/2 < x < L_x/2 \\ 0 & \text{elsewhere} \end{cases}$$

$$w_y(y) = \begin{cases} \alpha_y + (1 - \alpha_y) \cos\left(\frac{2\pi y}{L_y}\right) & -L_y/2 < y < L_y/2 \\ 0 & \text{elsewhere} \end{cases}$$

For $\alpha_x = 1$ and $\alpha_y = 1$, one has a plain rectangular window; for $\alpha_x = 0.54$ and $\alpha_y = 0.54$, one has a Hamming window. The nominal spatial resolution is 50 km. A second product with an enhanced spatial resolution of 25 km can also be obtained using an adapted ground filter, at the expense of a reduced radiometric resolution.

7.6 K_p computation

The normalized standard deviation of σ^0 measurements, K_p , is commonly used to evaluate the accuracy of the σ^0 measurements (see [12]):

$$K_p = \frac{\sqrt{\text{var}(\sigma_{\text{meas}}^0)}}{\sigma^0} \quad (7.14)$$

Part III

SCATT/ERS algorithm review

Chapter 8

Preprocessing

8.1 ADC Non-linearity correction (signal)

The ADC non-linearity correction should be performed before any linear processing is performed on the signal. This can ideally be performed right after the ingestion step.

The correction factor is defined as the ratio of expected ADC output signal power to the expected ADC input signal power:

$$C_P(P_{out}) = \frac{P_{out}}{P_{in}(P_{out})} \quad (8.1)$$

and is deduced from a similar power-based look-up table. For each sample of each component of the signal, one has

$$s_c^I(n) = \frac{s^I(n)}{\sqrt{C_P(s^2(n))}} \quad (8.2)$$

$$s_c^Q(n) = \frac{s^Q(n)}{\sqrt{C_P(s^2(n))}} \quad (8.3)$$

where s_c^I and s^I denote respectively the corrected and uncorrected signal in-phase component. The Q exponents denote the in-quadrature component and $s^2(n)$ is the averaged along-track signal power

$$s^2(n) = \frac{\sum_{k=n-l}^{k=n+l} w(k) (s^I(k))^2 + (s^Q(k))^2}{\sum_{k=n-l}^{k=n+l} w(k)} \quad (8.4)$$

where l is the length of the across-track window and the $w(k)$ are the weights of the across-track window.

8.2 I/Q imbalance correction

Due to the imperfection of the synchronous demodulation on-board and to differences between the I and Q channels, a correction is required. The following correction is considered (see also [14] p94a), where the I and Q exponents denote the in-phase and in-quadrature signal samples and the i index indicates the corrected signal

$$\begin{cases} s_i^I(n) &= \frac{s^I(n) - G_{bias}^I}{1+G} \\ s_i^Q(n) &= \frac{s^Q(n) - G_{bias}^Q}{\cos \alpha (1-G)} - \tan \alpha s^I(n) \end{cases} \quad (8.5)$$

where α is the channel non-orthogonality, G is the I/Q channel gain imbalance and G_{bias}^I and G_{bias}^Q are respectively the I and Q channel DC biases. The channel non-orthogonality, α , is defined as the phase difference between the on-board local oscillators, where the phase of the Q channel is equal to $\frac{\pi}{2} + \alpha$.

A similar formula is used to correct the noise sample as follows

$$\begin{cases} p_i^I &= \left(\frac{\sqrt{p^I} - G_{\text{bias}}^I}{1+G} \right)^2 \\ p_i^Q &= \left(\frac{\sqrt{p^Q} - G_{\text{bias}}^Q}{\cos \alpha (1-G)} - \tan \alpha \sqrt{p^I} \right)^2 \end{cases} \quad (8.6)$$

where p^I and p^Q indicate the noise power before correction and the i index indicates the result after I/Q imbalance correction.

8.3 Theoretical modelling

If $h(t)$ designates the impulse response of the on-board anti-aliasing filter, $s(t)$ the true backscattered signal¹ and $s_h(t)$ the signal on-board after anti-aliasing filtering but before sampling, one has

$$s_h(t) = h(t) * s(t) \quad (8.7)$$

where one would like to recover $s(t)$ from (sampled versions of) $s_h(t)$. Due to the presence of noise, (8.7) should rather be written as

$$s_h(t) = h(t) * s(t) + n(t) \quad (8.8)$$

where $n(t)$ is the system noise (including the quantization noise) or in the Fourier domain

$$S_h(f) = H(f) * S(f) + N(f). \quad (8.9)$$

This kind of problems are termed ‘‘Inverse problems’’[8] and are known as being ill-conditioned what means that the trivial solution

$$\hat{S}(f) = S_h(f)/H(f) - N(f)/H(f) \quad (8.10)$$

does not yield usable results if it yields results at all.

One of the methods that is known to be simple and to yield acceptable results to inverse (8.8) is to use the Wiener filter [3]. This filter is obtained by minimizing the expectation of the mean-square error between the actual signal $s(t)$ (unknown) and the estimate $\hat{s}(t)$. The Wiener filter is optimum under the assumptions that 1) the signals (signal and noise) are stationary (weak stationnarity of the covariance) and 2) the power spectral densities of the original signal and of the noise are known. The stationnarity hypothesis is not verified for real-world signals. This leads to gibbs-like artefact around edges.

Under these assumptions, the Wiener filter is defined as

$$H_w(f) = \frac{H^*(f)P_s(f)}{|H(f)|^2P_s(f) + P_n(f)} \quad (8.11)$$

where $P_s(f)$ and $P_n(f)$ are the Power Spectral Densities (PSD) of the original signal and the noise respectively. An estimate of the original signal is thus obtained by

$$\hat{S}(f) = H_w(f)S_h(f) \quad (8.12)$$

Replacing $S_h(f)$ in (8.12) by its expression from (8.9), the global transfer function is obtained

$$\hat{S}(f) = H_w(f)H(f)S(f) + H_w(f)N(f) \quad (8.13)$$

The product $H_w(f)H(f)$ will be close to 1 where the signal to noise ratio $|H(f)|^2P_s(f)/P_n(f)$ is large. Where the noise dominates ($P_n(f) \gg |H(f)|^2P_s(f)$), $H_w(f)$ will be very small and thus filter the noise out.

¹The backscattered signal is itself the convolution of the emitted pulse with the ground reflexion function. Ideally, the bias introduced by the emitted pulse shape should also be compensated, in a similar way.

8.4 On-board anti-aliasing filter

The on-board anti-aliasing filter is modelled as a Bessel filter as described in section 5.2.1.1.

The figure 8.1 shows a comparison between the spectrum of the measured returned echo and the spectrum that would have been obtained in the absence of noise and if the ground reflexion function could be assumed to behave as white noise.

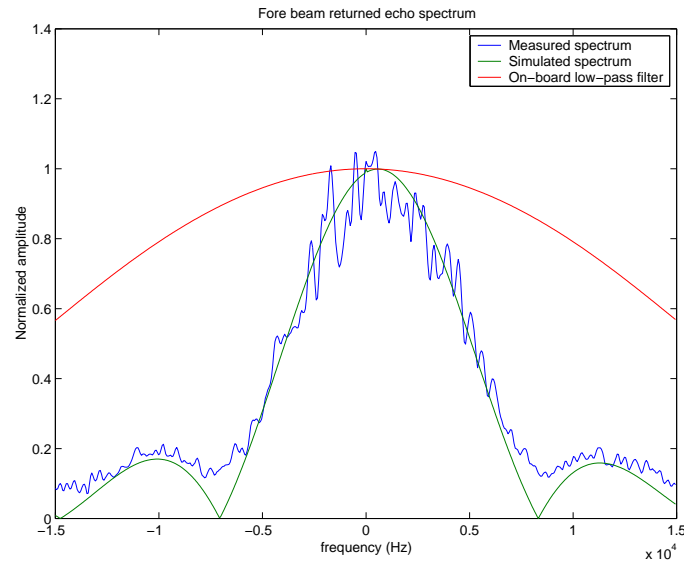


Figure 8.1: Fore-beam returned echo spectrum

One actually sees a good agreement, which shows that the on-board filter is quite well modelled by the Bessel filter.

8.5 Amplitude correction filter

The aim of this filter is to compensate for the spectral behavior of the on-board anti-aliasing filter and globally have a unit transfer function in the pass-band of the system.

A Wiener filter is best used to this end. To compute the Wiener filter from the expression (8.11), one needs the signal and noise power spectral densities. The noise power spectral density is usually assumed constant² (white noise) and equal to the noise variance. Several assumptions can be made regarding the power spectral density of the original signal yielding different filters. These assumptions and the corresponding filter are discussed in the next paragraphs.

8.5.1 Constant power spectral density

The filter resulting from the assumption of a constant PSD for the original signal is illustrated at figure 8.2

²the aliased components should be regarded as noise and be taken into account

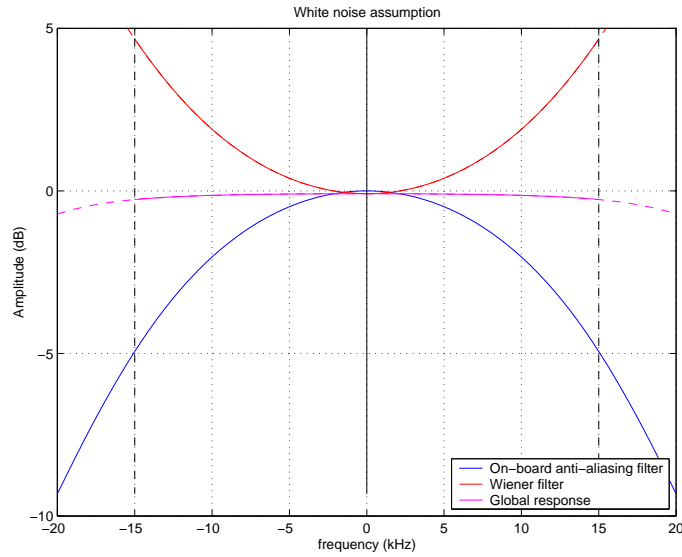


Figure 8.2: Wiener filter in the case of an assumed constant signal PSD

8.5.2 Pulse-power spectral density

For the PSD of the original signal, a white noise signal filtered by the emitted pulse will be assumed. Since the pulse length depends on the considered beam, two different filters will be obtained. This is illustrated in figures 8.3 and 8.4.

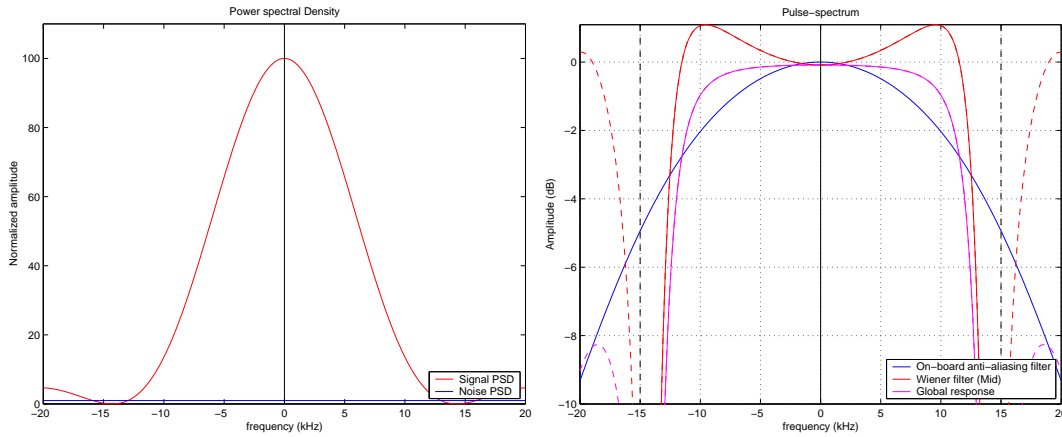


Figure 8.3: PSD (left) and resulting Wiener filter (right) in the case of a signal PSD assumed equal to the emitted pulse PSD (Mid beams)

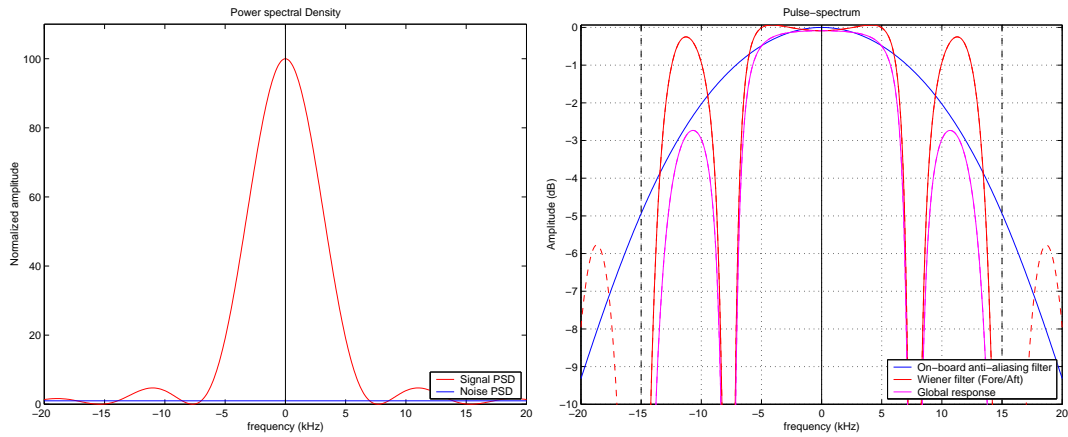


Figure 8.4: PSD (left) and resulting Wiener filter (right) in the case of a signal PSD assumed equal to the emitted pulse PSD (Fore/Aft beams)

Since the pulse PSD exhibits zeroes, meaning a total absence of signal at those frequencies, it is totally normal to find these zeroes back in the Wiener filter. Indeed, the signal to noise ratio of these frequencies is zero and so is the Wiener filter. This is particularly visible in the fore/aft case.

Moreover, due to the presence of a residual Doppler shift, the PSD of the original signal will also be shifted, as it is illustrated in figure 8.5.

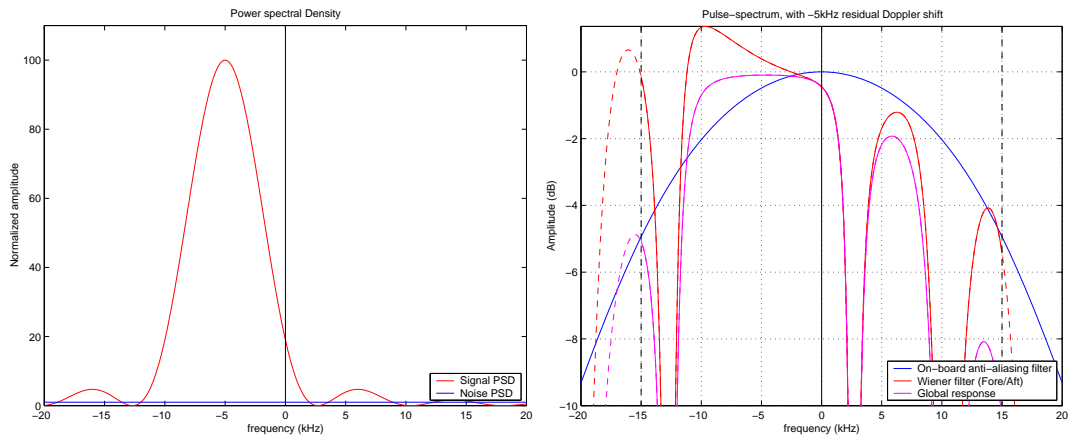


Figure 8.5: PSD (left) and resulting Wiener filter (right) in the case of a signal PSD assumed equal to the emitted pulse PSD (Fore/Aft beams) and with a residual Doppler shift of -5kHz

However, the situation depicted in figure 8.5 is only valid if the shift is constant across range. In reality, the residual frequency shift will vary across range and the corresponding signal PSD will rather be as depicted in figure 8.6.

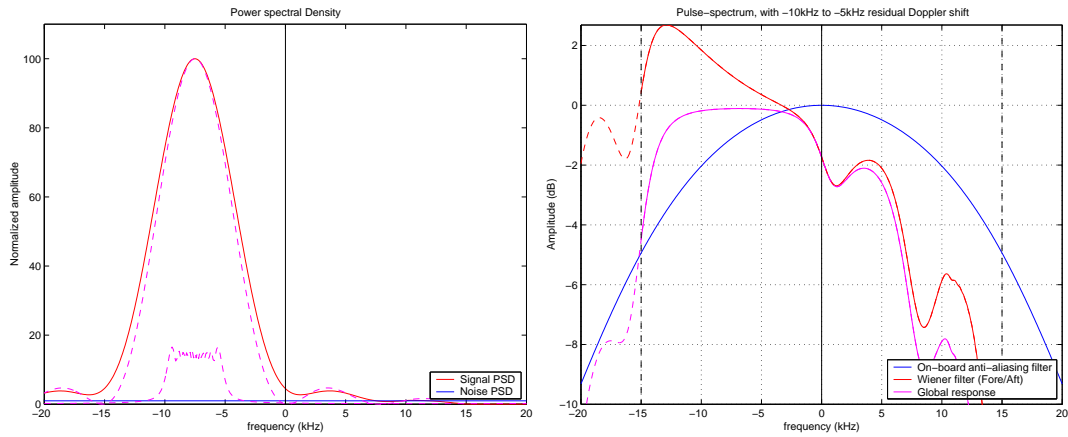


Figure 8.6: PSD (left) and resulting Wiener filter (right) in the case of a signal PSD assumed equal to the emitted pulse PSD (Fore/Aft beams) and with a residual Doppler shift ranging from -10kHz to -5kHz across track

8.5.3 Current filter

Using an appropriate signal PSD, it is possible to recover the filter used in the current ground processing chain.

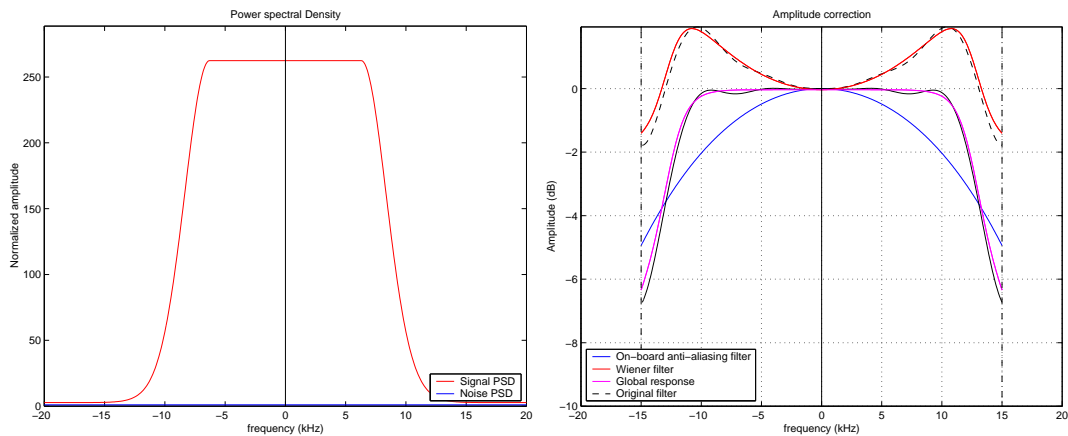


Figure 8.7: PSD considered (left) and resulting Wiener filter (right)

Since this filter does not take into account the spectral characteristics of the signal, it potentially amplifies the noise in certain frequency bands needlessly.

8.5.4 Discussion and comparison with the current filter

The three different assumptions regarding the PSD of the original signal yield filters with different characteristics. The most reasonable assumption is probably the one that assumes a returned echo PSD equal to a white noise, filtered by the emitted pulse.

The resulting filter exhibits zeroes, thus strongly contrasting with the amplitude-correction filter currently used. One might prefer having a flat spectrum, but this amounts to amplify components that only contain noise, and thus decreasing the SNR of the resulting signal.

8.6 Doppler compensation

The Doppler compensation is performed in the same way as described in section 5.2.2. However, since the yaw angle cannot anymore be assumed known in advance, the phasor $\theta = -2\pi F_g(\tau, T)$ and more precisely the residual Doppler frequency shift F_g (see equation [5.4]) will be computed on-the-fly, taking into account the estimated yaw angle.

The estimation of the yaw angle is described in chapter 9.

8.7 Low-pass filter

The aim of the low-pass filter after the Doppler compensation is to minimize the K_p by increasing the SNR. This is classically done using a low-pass filter whose cut-off frequency is chosen such that the SNR is maximized.

8.7.1 The signal bandwidth

Figure 8.8 shows the signal Power Spectral Density for the mid and the fore/aft beams together with the Butterworth low-pass filter.

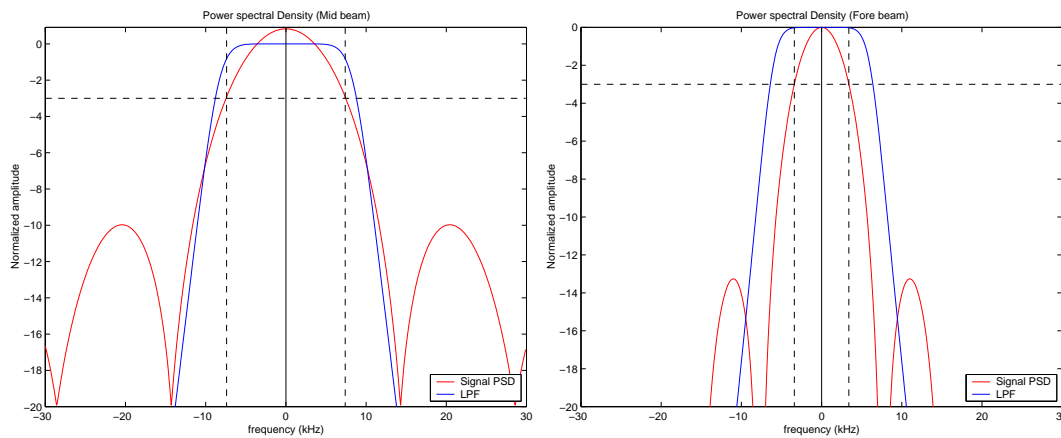


Figure 8.8: Post-amplitude correction and residual Doppler shift compensation signal Power Spectral Density for the mid-beam (left) and for the for/aft-beam (right)

As expected, since the pulse emitted by the mid-antenna is much shorter ($70\mu s$) than that emitted by the fore/aft-antennae ($130\mu s$), the PSD of the mid-beam signal is much wider than the PSD of the fore-beam signal.

8.7.2 The Butterworth filter

The current ground segment makes use of a 4th order Butterworth filter with cut-off frequency of 6.4kHz and 8.8kHz for respectively the fore/aft and mid beams. This type of filter is characterized by a maximally flat amplitude response in the passband and in the stopband. The discrete-time form of this filter, obtained by making the bilinear approximation [7] yields an IIR filter.

The filter is implemented in the Fourier-transformed domain. Figure 8.9 shows both the current implemented filter and the ideal Butterworth filter.

Deviations from the ideal Butterworth filter can be noticed, more precisely, a ripple in the pass-band and a perfectible attenuation in the stop-band. This is probably due to a bad implementation of the filter, and particularly due to a truncation of the impulse response.

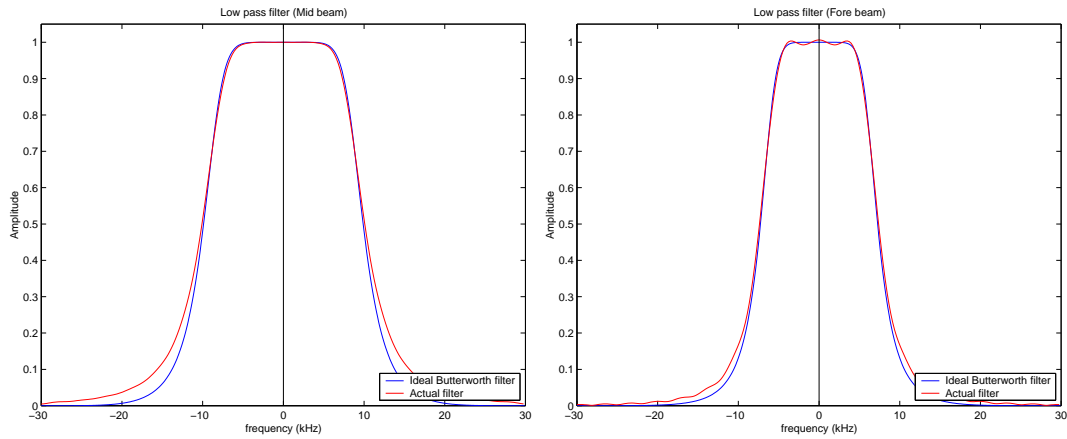


Figure 8.9: Current low-pass filters, mid-beam (left) and Fore-beam (right)

The Butterworth filter being an IIR filter should ideally be implemented in the time domain, using the corresponding recursive filter equation. Filter initialization (with zeroes) artefacts will be limited to the first few samples, given the fact that the filter impulse response energy is concentrated in the first coefficients.

A truncation of the IIR is also feasible, in view of an FFT-based implementation, provided the truncation window is taken long enough. Truncation artefacts can be minimized by using an appropriate weighting window (Hamming).

Chapter 9

Yaw angle estimation

9.1 Introduction

Due to the relative spacecraft-Earth-target velocity, the echoes received are affected by some range-dependent Doppler frequency shift. That frequency shift is directly affected by the spacecraft yaw angle. Hence, the yaw angle can be deduced by measuring the Doppler frequency shift of the returned echoes.

The next sections describe how the residual Doppler frequency shift can be measured and how the yaw angle can be obtained from that measurement. The effect of a misestimation of the yaw angle is finally discussed.

9.2 Doppler frequency shift measurements

9.2.1 Frequency-shift measurement

The spectrum of the returned echoes can be modeled as a $\sin(x)/x$ function, as is illustrated in figure 8.1.

The residual Doppler frequency shift, besides shifting the spectrum of the returned echo, also deforms it because the frequency shift is not constant across range.

The mean Doppler frequency shift can be measured by computing the best-fit of a gaussian window

$$m(f) = ae^{-\frac{(f-f_d)^2}{2\sigma^2}} + n \quad (9.1)$$

where a is the amplitude, σ is the variance of the gaussian, n is modelling the noise and f_d is the estimated Doppler frequency shift. This estimate is more robust than the one based on the computation of the center of gravity of the spectrum, particularly when, due to the frequency shift, a major part of the spectrum is shifted outside the anti-aliasing filter bandwidth. This is illustrated on figure 9.1.

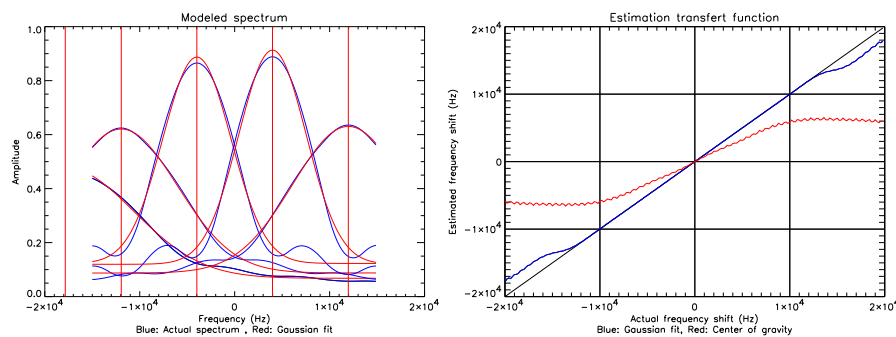


Figure 9.1: Shifted spectrum (left) and estimation validation (right)

The right graph¹ of figure 9.1 is obtained by shifting a model spectrum and measuring the frequency shift either by fitting a gaussian curve or by computing the center of gravity. The frequency shift considered simulates a linear frequency evolution between $\frac{f_c}{2}$ and $\frac{3f_c}{2}$, actually simulating a realistic residual Doppler shift. This graph shows that the gaussian fit is actually able to measure the Doppler shift. It also shows that on the contrary, the center of gravity is not a good measure of the Doppler frequency shift.

9.2.2 Spectral correction

The received echoes are low-pass filtered on board, before undergoing the A/D conversion in order to minimize frequency aliasing. This step distorts the spectrum of the echoes and introduces a bias on the measurement of the center of the spectrum as is shown in figure 9.2.

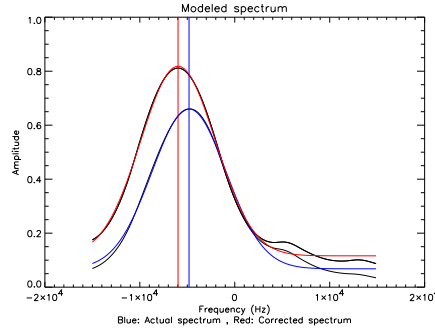


Figure 9.2: Illustration of the influence of the on-board low-pass filter on the shape of the spectrum. The center of the uncorrected spectrum is shifted right, leading to an under-estimation of the Doppler frequency shift.

The correction consists in dividing by the transfert function of the on-board anti-aliasing filter described in section 5.2.1.1. One thus obtains

$$S_{\text{corr}}(f) = \frac{S(f)}{H(f)} \quad (9.2)$$

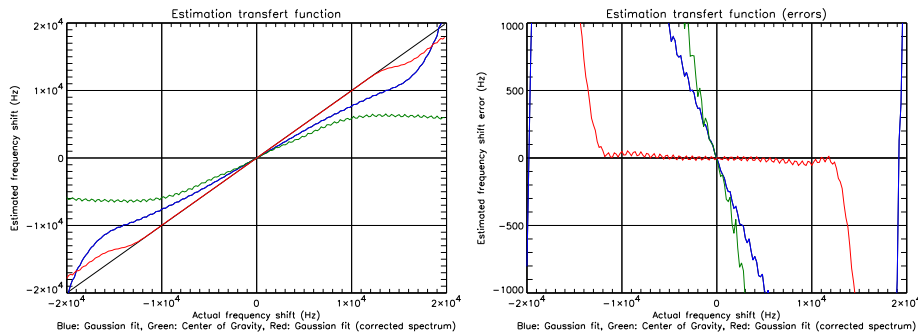


Figure 9.3: Illustration of the influence of the on-board low-pass filter on the Doppler frequency shift estimation. The graph right shows the estimation error.

Moreover, the antenna gain pattern and more generally the radiometric effect of the radar equation also introduce distortions, but these are much smaller. This is to be explained by the fact that the effect of the normalization consists in convolving the signal spectrum with a symmetric function and that doesn't move

¹The effect of the on-board anti-aliasing filter was not considered here

the center of gravity of the spectrum. Moreover, the corresponding convolution kernel is very narrow, close to a Dirac impulse as can be seen on figure 9.4.

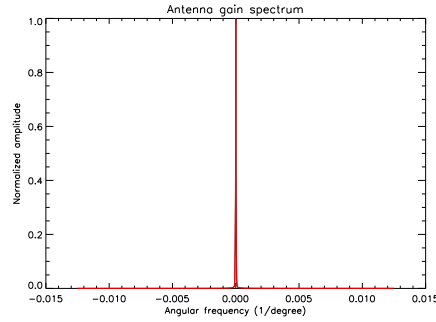


Figure 9.4: Angular spectrum of the mid-beam antenna gain pattern.

9.3 Yaw angle model

This section gives simplified relations between the yaw angle and the Doppler frequency shift. A comparison between these relations and the theoretical Doppler frequency shift is also shown.

9.3.1 Constant speed-field model

Making the assumption that the relative velocity between the satellite and the Earth target is independent of the yaw angle, one obtains the following formula

$$f_{\text{Doppler}} = \frac{2 v_r}{\lambda} \sin\theta \sin(\text{yaw} - \alpha) \quad (9.3)$$

where

- v_r is the relative velocity between the satellite and the Earth target = $|\vec{v}_{\gamma_{sc}} - \vec{v}_{\gamma_p}|$
- θ is the elevation angle
- $\alpha = 45^\circ, 0^\circ, -45^\circ$ respectively for the for-,mid- and aft-antennas

Making the hypothesis of very small yaw angle and keeping only the terms that depend on the yaw angle, one obtains an approximation of the residual Doppler frequency shift

$$f_{\text{residual Doppler}} = \frac{2 v_r}{\lambda} \text{yaw} \sin\theta \cos\alpha \quad (9.4)$$

These formulas are easily inverted and the yaw angle in function of the Doppler frequency shift (or in function of the residual Doppler frequency shift) is then easily obtained.

9.3.2 Circular-orbit model

The following model is extracted from [16]. The equation for the Doppler frequency shift is obtained by considering an oblate ellipsoidal Earth rotating around its z -axis and a circular orbit.

The resulting equation is:

$$f_{\text{Doppler}} = \frac{2 v_{sc}}{\lambda} \sin\theta \cos a [1 - (\omega_e/\omega)(\epsilon \cos u \sin i \tan a + \cos i)] \quad (9.5)$$

where (see also[16])

- v_{sc} is the velocity of the spacecraft along the orbit
- λ is the radar wavelength
- θ is the elevation angle (angle at spacecraft between the spacecraft position and the point position)
- a is the angle of the azimuth plane from the plane, plane formed by $(\vec{r}_{\gamma_{sc}}, \vec{v}_{\gamma_{sc}})$
- ω_e is the Earth's rotation rate
- ω is the spacecraft orbital rotation ($\omega = v_{sc}/|\vec{r}_{\gamma_{sc}}|$)
- $\varepsilon = +1$ since the radar looks to the right side of the spacecraft velocity vector
- u is the argument of latitude (angle measured between the ascending node and the spacecraft position in the orbit plane from the Earth's center)
- i is the orbit inclination measured from the Earth spin vector to the orbit rate vector

The inverse formula, giving the angle of the azimuth plane, is:

$$a = b + a \cos\left(\frac{A \cos b}{B}\right) \quad (9.6)$$

where

- $A = \frac{f_{Doppler} \lambda}{2 v_{sc} \sin \theta}$
- $B = 1 - \frac{\omega_e \cos i}{\omega}$
- $C = -\frac{\omega_e \cos u \sin i}{\omega}$
- $\tan b = C/B$

This angle is used to determine the yaw angle. First, the unit vector in the direction of the vector from the spacecraft to the point characterised by the a angle and in the azimuth plane is computed:

$$\vec{u}_{\gamma_{SC-P}} = -\cos(\theta) \vec{z} + \sin(\theta) \vec{u} \quad (9.7)$$

where

- $\vec{z} = \vec{r}_{\gamma_{sc}} / \|\vec{r}_{\gamma_{sc}}\|$
- $\vec{y} = \vec{z} \times \vec{v}_{\gamma_{sc}} / \|\vec{z} \times \vec{v}_{\gamma_{sc}}\|$
- $\vec{x} = \vec{y} \times \vec{z}$
- $\vec{u} = \cos(a) \vec{x} - \sin(a) \vec{y}$

Then, the unit vector in the antenna elevation plane pointing in the direction of the normal to the antenna's surface is computed in the γ frame:

$$\vec{z}_{el} = \mathcal{T}_{a2\gamma} \cdot [0, 0, 1]^t \quad (9.8)$$

With these two vectors and the local normal at the nadir point, we compute the normal to the elevation plane and the normal to the azimuth plane wrt the nadir normal.

$$\vec{n}_{az} = \frac{\vec{n}_{\gamma_{nadir}} \times \vec{u}_{\gamma_{SC-P}}}{\|\vec{n}_{\gamma_{nadir}} \times \vec{u}_{\gamma_{SC-P}}\|} \quad (9.9)$$

$$\vec{n}_{el} = \frac{\vec{n}_{\gamma_{nadir}} \times \vec{z}_{el}}{\|\vec{n}_{\gamma_{nadir}} \times \vec{z}_{el}\|} \quad (9.10)$$

From these two vectors, we deduced the yaw angle:

$$\text{If } \vec{n}_{\gamma_{nadir}} \cdot (\vec{n}_{az} \times \vec{n}_{el}) > 0 \text{ then yaw} = -\arccos(\vec{n}_{az} \cdot \vec{n}_{el}) \text{ else yaw} = \arccos(\vec{n}_{az} \cdot \vec{n}_{el}) \quad (9.11)$$

9.3.3 Comparison

Figure 9.5 presents a comparison of the various approximations to the true Doppler frequency shift. The discontinuity that can be observed is due to the change of on-board Doppler compensation coefficients. The best approximation seems to be the one deduced from eq. (9.5).

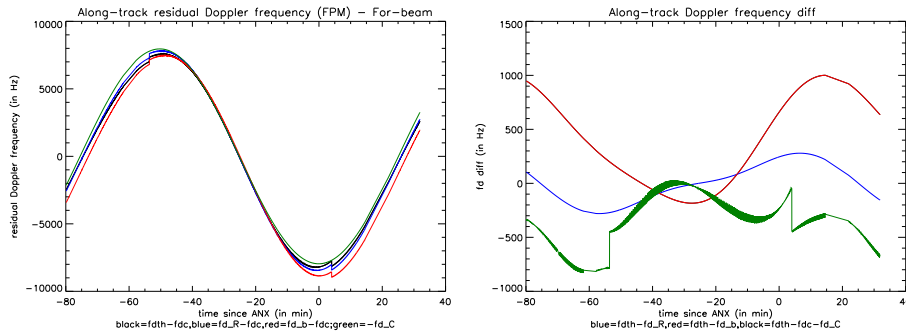


Figure 9.5: Comparison between the different models and the true value for the residual Doppler frequency shift. In black, the true value; in blue the residual Doppler frequency shift deduced from eq. (9.5); in red the residual Doppler frequency shift deduced from eq. (9.3) and in green the residual Doppler frequency shift given by eq. (9.4). The right graph presents the difference of Doppler frequency shift given by corresponding model with the theoretical value.

9.4 Influence of Yaw misestimation

9.4.1 Influence on the normalization factor

As can be seen on figure 9.6, a yaw error of 2^0 has very little influence on the normalization factor.

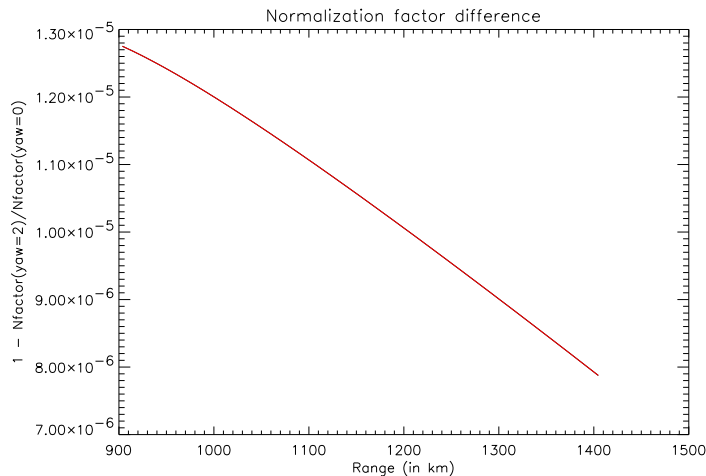


Figure 9.6: Normalized difference of normalization factors due to a yaw angle error of 2^0 .

This very small difference (less than $2 \cdot 10^{-6}$) is confirmed by the fact that the respective differences of the three parameters on which the normalization factor depends, due to a yaw error are also very small as can be seen on figure 9.7.

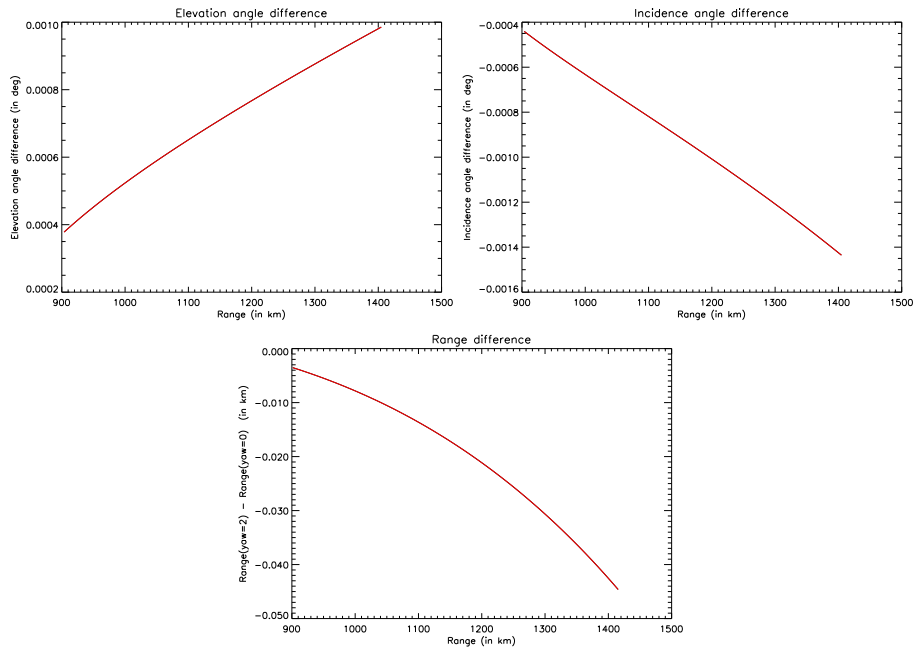


Figure 9.7: Difference in elevation angle, incidence angle and range for a yaw variation of 2^0 .

9.4.2 Geometric influence

The figure 9.8 shows the influence of yaw misestimation of 2^0 on the geometry.

node number: [005,09], beam = 2

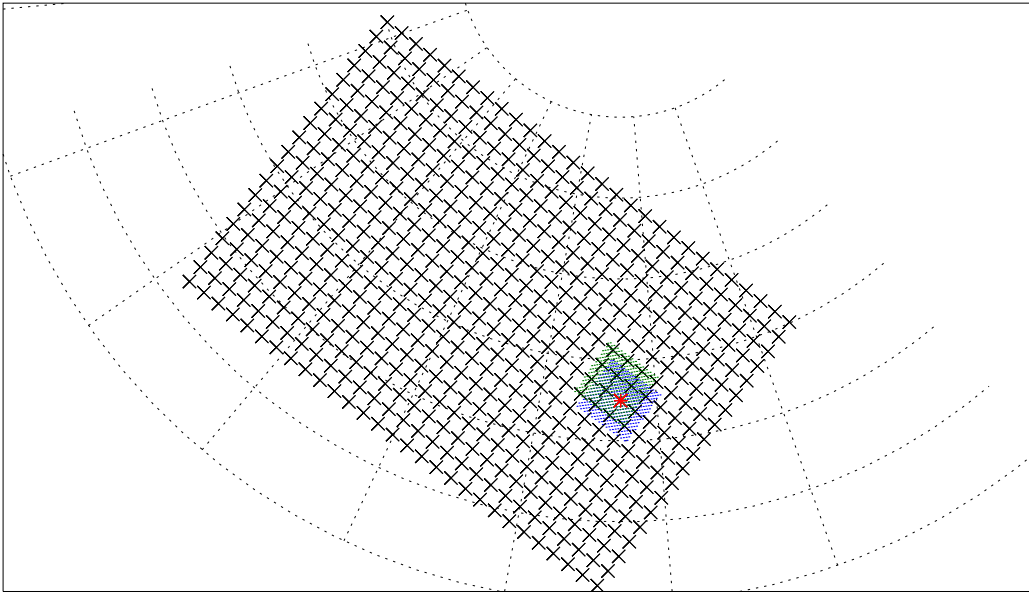


Figure 9.8: The node of interest is plotted in red. The samples belonging to the node when there is no yaw misestimation are plotted in blue. The green dots are these same selected samples affected by the yaw misestimation.

When there is no yaw misestimation, the samples belonging to the node are symmetrically positioned around the node. In presence of a yaw estimation error, the samples which influence the node value are not anymore symmetrically positioned around the node and the samples truly belonging to the node are unknown. According to the figure 9.8, it can be expected that a yaw estimation error of 2^0 will have a large influence on the node value.

Chapter 10

Along-track filtering

10.1 Introduction

Along-track filtering is used to smooth out along-track variations. This is used

- in the computation of the mean power in order to obtain the ADC non-linearity correction coefficient
- in the smoothing out of the estimated yaw angle, in order to take into account mechanical constraints imposed by the spacecraft inertial moment
- in the calibration pulse smoothing
- in the noise smoothing, although it is probably not really necessary here since the noise is already along-track averaged on-board

10.2 Filters

Unless explicitly mentioned, all filters are normalized to 1. This means that the filter actually used is $h_n(n)$ with

$$h_n(n) = \frac{h(n)}{N} \quad (10.1)$$

where

$$N = \sum_{n=-l_2}^{l_2} h(n). \quad (10.2)$$

where l_2 is the half length of the filter.

10.2.1 Gaussian filter

This filter is defined as

$$h(n) = e^{-\frac{(n-n_0)^2}{2\sigma^2}} \quad |n| \leq l_2 \quad (10.3)$$

and is depicted in figure 10.1.

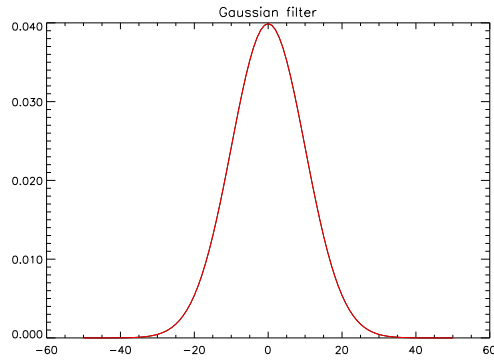


Figure 10.1: Gaussian filter, $n_0 = 0$, $\sigma = 10$, $l_2 = 50$

10.2.2 Moving-average filter

This filter is defined as

$$h(n) = 1 \quad |n| \leq l_2 \quad (10.4)$$

and is depicted in figure 10.2.

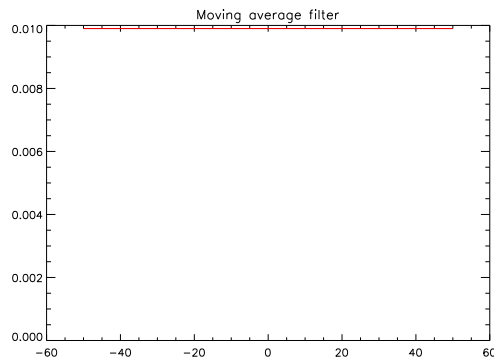


Figure 10.2: Moving-average filter, $l_2 = 50$

10.2.3 Dirac-filter

This filter is defined as

$$h(n) = \begin{cases} 0 & |n| \leq l_2, n \neq 0 \\ 1 & n = 0 \end{cases} \quad (10.5)$$

and is depicted in figure 10.3.

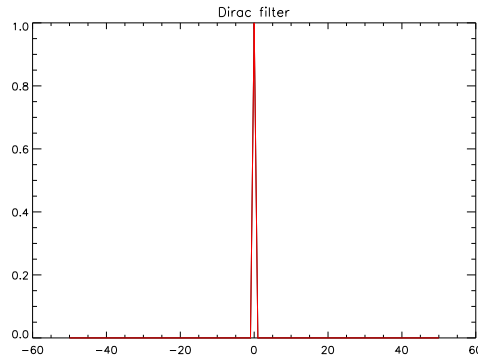


Figure 10.3: Dirac filter, $l_2 = 50$

For this particular filter, a filter length larger than 1 is useless. The parameter l_2 should thus be taken equal to 0.

10.2.4 Recursive filter

This filter is defined as

$$y(n) = (1 - \alpha)x(n) + \alpha y(n - 1) \quad (10.6)$$

where $x(n)$ and $y(n)$ are respectively the input and output signals. This filter has an infinite impulse response. A truncation as $h(n)$ vanishes is acceptable and leads to the following expression

$$h(n) = \alpha^n \quad 0 \leq n \leq l_2 \quad (10.7)$$

and is depicted in figure 10.4. It should be noticed that for this filter to converge, α must be strictly smaller than one.

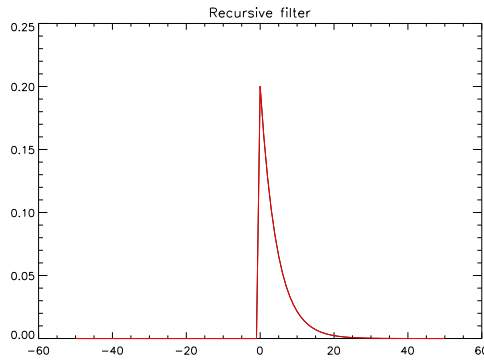


Figure 10.4: Recursive filter, $\alpha = 0.8$, $l_2 = 50$

This filter is the filter originally used in the along-track internal calibration energy averaging.

10.3 Gap-filling

The averaging requires that the data to be averaged be without gaps. The presence of gaps, if unhandled, would void the result of the averaging, at least around those gaps. Around the gaps, the filter used to perform

the averaging has to be modified in order not to take into account unknown values from within the gap. Equivalently, the gaps can be filled with sensible values and the normal averaging operation performed.

$$v_g(N_1 + n) = v(N_1 - n) \frac{\Delta N - n}{\Delta N} + v(N_2 + \Delta N - n) \frac{n}{\Delta N} \quad n = 1, \dots, \Delta N - 1 \quad (10.8)$$

where $v_g(n)$ and $v(n)$ respectively are the signals without (gap filled) and with gap, N_1 and N_2 are respectively the first and last indice of data around the gap and $\Delta N = N_2 - N_1$ is the number of points in the gap plus one. This is equivalent to perform a kind of mirroring of the data at the edge of the gap. The mirroring is weighted by the distance between the two edges of the gap. If the gap is infinitely large, the data is simply mirrored.

After filtering, the data inside the gap is discarded.

Chapter 11

Node geometry

In the first part, the mathematical formulas associated to the determination of the position of the nodes are presented. The latitude and the longitude of the node, located on the Earth, are then easily deduced. On the other hand, the incidence angle and the look-angle can not be estimated in advance since they depend on the actual yaw angle of the spacecraft. Their determination can only be done when all the samples influencing the σ^o of the node have been determined.

The backscattering coefficient σ^o of a node is a weighted summation of the backscattering coefficients of the samples belonging to the node. A sample is said to belong to a node when its backscattered coefficient has an influence on the backscattered coefficient of the node. In the second part, the mathematical formulas associated to the determination of the sample appurtenance are presented.

Since the yaw variation around the orbit is not predictable, the samples belonging to a node cannot be determined on advance. Due to run-time limitation it is impossible to apply the appurtenance criteria to all the samples to determine if they contribute or not to a node. A pre-selection of the samples is thus necessary. In the third part, the pre-selection method used in the implementation is presented, with the associated mathematical formulas. For each pre-selected sample, the appurtenance criteria is computed. The weight associated to the samples that actually belong to the node is then computed.

The fourth part describes how the location of the nodes rows are determined. The determination of the incidence angle and the look-angle of the nodes are presented in the fifth part.

11.1 Formulas for the node row geometry

The determination of the 19 measurement nodes position is detailed with the equations used in the implementation and presented in the order it is computed. The determination of the 19 nodes position is done in several steps. First the position of the node 10 is determined. Some constants are then computed for *all* nodes of the row and finally the 18 other nodes position are computed. The determination of the 19 nodes of the node row is based on [5], pp 449-455.

The nodes row is at the intersection of the Earth's ellipsoid and the plane perpendicular to the relative ground trace velocity at the nadir Earth's point. It is associated to exactly one time T .

11.1.1 The position of the node 10

This step consists in the determination of the position of the node 10 (see figure 11.1), as defined in section (5.3.8.9).

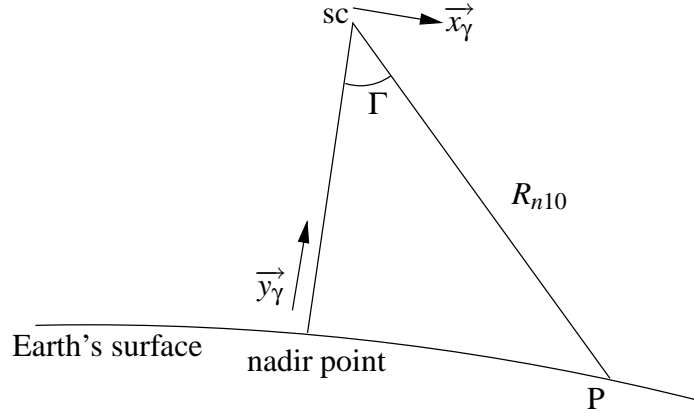


Figure 11.1: Determination of the node 10 position

The unit vector parallel to the Earth's normal at the subsatellite point and the unit vector parallel to the relative ground trace velocity are extracted from the orbit propagator, after a propagation to the node time. With the help of these two orthogonal (by definition) vectors, a right-handed Cartesian coordinate system is built. To have an orthonormal coordinate system, these vectors are normalized.

$$\vec{y}_\gamma = \frac{\vec{r}_{\gamma Nnadir}}{\|\vec{r}_{\gamma Nnadir}\|} \quad (11.1)$$

$$\vec{x}_\gamma = \frac{\vec{v}_\gamma}{\|\vec{v}_\gamma\|} \quad (11.2)$$

The third vector, completing the right-handed Cartesian coordinate system, is

$$\vec{z}_\gamma = \vec{x}_\gamma \times \vec{y}_\gamma \quad (11.3)$$

which is already normalized.

Given the elevation angle of the node 10, Γ , the unit vector, $\vec{u}_{\gamma sc2n10}$, parallel to the direction from the satellite's COG to the node 10 is easily deduced:

$$\vec{u}_{\gamma sc2n10} = \vec{z}_\gamma \sin \Gamma - \vec{y}_\gamma \cos \Gamma \quad (11.4)$$

and the position of the node 10 in the inertial frame, $\vec{r}_{\gamma n10}$, is thus:

$$\vec{r}_{\gamma n10} = \vec{r}_{\gamma sc} + R_{n10} \vec{u}_{\gamma sc2n10} \quad (11.5)$$

where R_{n10} is the range corresponding to the node 10.

11.1.2 The ellipse center in the g frame

The determination of the ellipse center position in the g frame, $\vec{u}_{gce} = (x_{gce}, y_{gce}, z_{gce})$, is done with the help of the unit vector, $\vec{u}_{g\gamma} = (x_{g\gamma}, y_{g\gamma}, z_{g\gamma})$, parallel to the relative ground trace velocity, in the g frame, and the nadir subsatellite point, \vec{r}_{gnadir} , which is the *geodetic subsatellite position*, in the g frame. The three components of the ellipse center in the g frame are:

$$x_{gce} = C_{ce} x_{g\gamma} \quad (11.6)$$

$$y_{gce} = C_{ce} y_{g\gamma} \quad (11.7)$$

$$z_{gce} = C_{ce} (b/a)^2 z_{g\gamma} \quad (11.8)$$

where $C_{ce} = (\vec{u}_{g\gamma} \cdot \vec{r}_{gnadir}) / (x_{g\gamma}^2 + y_{g\gamma}^2 + (b/a)^2 z_{g\gamma}^2)$, a and b are the GEM-6 parameters.

11.1.3 The unit vectors in the direction of the ellipse axes

This step consists in the determination of the two unit vectors, respectively in the direction of the semi-major axis and in the direction of the semi-minor axis.

The unit vector $\vec{u}_{gae} = (x_{gae}, y_{gae}, z_{gae})$ in the direction of the semi-major axis is:

$$\vec{u}_{gae} = (y_{g_{v'}}, -x_{g_{v'}}, 0) / \sqrt{x_{g_{v'}}^2 + y_{g_{v'}}^2} \quad (11.9)$$

and the unit vector $\vec{u}_{gbe} = (x_{gbe}, y_{gbe}, z_{gbe})$ in the direction of the semi-minor axis is:

$$\vec{u}_{gbe} = \vec{r}_{gbe} / \|\vec{r}_{gbe}\| \quad (11.10)$$

where $\vec{r}_{gbe} = (x_{g_{v'}}, z_{g_{v'}}, y_{g_{v'}}, z_{g_{v'}}, -x_{g_{v'}}^2 - y_{g_{v'}}^2)$

11.1.4 The lengths of the semi-axes

This step consists in the determination of the lengths of the semi-axes, respectively noted ae for the major axis and be for the minor axis.

$$ae = \sqrt{-a_M d} / a_M \quad (11.11)$$

$$be = \sqrt{-a_m d} / a_m \quad (11.12)$$

where

$$\begin{aligned} a_M &= (x_{gae}^2 + y_{gae}^2) / a^2 + z_{gae}^2 / b^2 \\ a_m &= (x_{gbe}^2 + y_{gbe}^2) / a^2 + z_{gbe}^2 / b^2 \\ d &= (x_{gce}^2 + y_{gce}^2) / a^2 + z_{gce}^2 / b^2 - 1 \end{aligned}$$

11.1.5 The other 18 nodes positions

This step consists in the determination of the other 18 nodes positions (see figure (11.2)), in the g frame.

$$\vec{r}_{gce2n10} = \vec{r}_{gn10} - \vec{r}_{gce} \quad (11.13)$$

is the vector from the ellipse center to the node 10, in the g frame.

The projections of this vector on the unit vectors in the direction of the semi-major axis and semi-minor axis are:

$$\begin{aligned} proj_a &= \vec{u}_{gae} \cdot \vec{r}_{gce2n10} \\ proj_b &= \vec{u}_{gbe} \cdot \vec{r}_{gce2n10} \end{aligned}$$

These scalar numbers are used to compute two angular constants of the nodes row: the angle, noted β , whose top is the ellipse center, angle from the major axis of the ellipse to the node 10, and an other angle, noted δ , being the angular distance between two nodes.

$$\beta = \text{atan}((proj_b / be) / (proj_a / ae)) \quad (11.14)$$

$$\delta = d_{ac} / \sqrt{(ae \sin \beta)^2 + (be \cos \beta)^2} \quad (11.15)$$

where d_{ac} is the desired across-track node distance, which is 25 km.

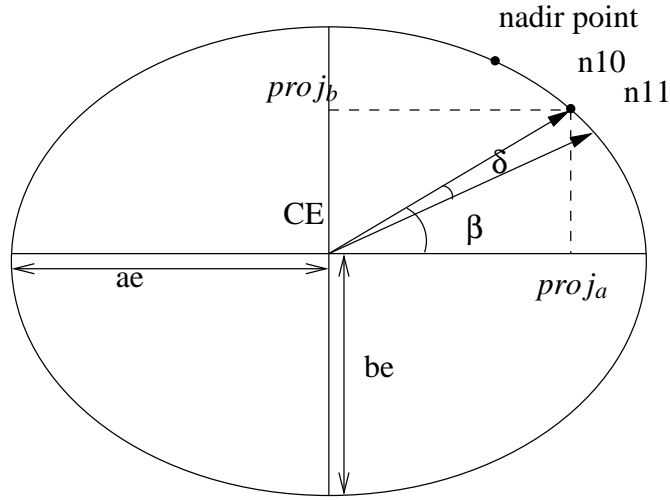


Figure 11.2: Determination of the 18 other nodes position. The ellipse is the intersection of the GEM-6 ellipsoid and the plane perpendicular to the relative ground trace velocity at the nadir Earth's point.

The positions of the 18 other nodes can then be computed:

$$\vec{r}_{gn(18-i)} = ae \cos\alpha \vec{u}_{gae} + be \sin\alpha \vec{u}_{gbe} + \vec{r}_{gce} \quad \alpha = \beta - (i-9)\delta \quad (11.16)$$

$$\vec{r}_{gn(8-i)} = ae \cos\alpha \vec{u}_{gae} + be \sin\alpha \vec{u}_{gbe} + \vec{r}_{gce} \quad \alpha = \beta - (i+1)\delta \quad (11.17)$$

with i varying from 0 until 8.

Given this formula, the constant across-track parameter for one row of 19 nodes is thus the across-track angular parameter, δ , and not the across-track distance. But since the across-track distance between the nodes does not vary much, it can be assumed constant in first approximation.

11.1.6 The latitude and the longitude

The determination of the latitude and the longitude of a point on Earth is described in [19]. The coordinates of the point P must be given in the g frame: $\vec{r}_{gp} = (x_{gp}, y_{gp}, z_{gp})$. The relation between the cartesian coordinates and the geographic ellipsoidal coordinates, the latitude ϕ and the longitude λ , are given by

$$\begin{pmatrix} x_{gp} \\ y_{gp} \\ z_{gp} \end{pmatrix} = \begin{pmatrix} C \cos\phi \cos\lambda \\ C \cos\phi \sin\lambda \\ (1-e^2)C \sin\phi \end{pmatrix} \quad (11.18)$$

where C is the radius of curvature in the prime vertical

$$C = \frac{a}{\sqrt{1-e^2 \sin^2\phi}} \quad (11.19)$$

The inversion of eq (11.18) gives

$$\phi = \arctan\left(\frac{z_{gp}}{\sqrt{x_{gp}^2 + y_{gp}^2}} \frac{1}{1-e^2}\right) \quad (11.20)$$

and

$$\lambda = \arctan\frac{y_{gp}}{x_{gp}} \quad (11.21)$$

Equations (11.19) and (11.20) need to be solved iteratively.

11.1.7 The subsatellite track heading

The determination of the subsatellite track heading (in radians) corresponding to the nodes row is here presented. Per definition, the subsatellite track heading is measured clockwise from a reference vector $\vec{r}_{\gamma_{ref}}$ and the relative nadir velocity $\vec{v}'_{\gamma} = (v'_x, v'_y, v'_z)$. The reference vector $\vec{r}_{\gamma_{ref}}$ is tangential to the local meridian at the nadir point position $\vec{r}_{\gamma_{nadir}} = (x_{nadir}, y_{nadir}, z_{nadir})$ (and thus is located into the tangential plane at the nadir) and is pointing north.

The local meridian at an Earth's point is only defined if the point is not exactly at the North pole or at the South pole. Consequently, the subsatellite track heading is only defined if the nadir position is not a pole position. The components of the vector $\vec{r}_{\gamma_{ref}}$ tangent to the meridian at the nadir point are, up to a multiplicative constant:

$$\begin{aligned} (x_{ref}, y_{ref}, z_{ref}) &= (-x_{nadir} \cdot n_z, -y_{nadir} \cdot n_z, x_{nadir} \cdot n_x + y_{nadir} \cdot n_y) \\ \text{If } (x_{nadir} \cdot n_x + y_{nadir} \cdot n_y) < 0 \text{ then } (x_{ref}, y_{ref}, z_{ref}) &= (x_{nadir} \cdot n_z, y_{nadir} \cdot n_z, -x_{nadir} \cdot n_x - y_{nadir} \cdot n_y) \end{aligned}$$

where $(n_x, n_y, n_z) = \vec{r}_{\gamma_{Nnadir}}$ is the unit normal vector at the nadir.

From the vector tangent to the local meridian and the local normal, a vector in the tangential plane, perpendicular to these vectors and pointing to the East is deduced:

$$\vec{r}_{perp} = \vec{r}_{ref} \times \vec{r}_{\gamma_{Nnadir}}$$

The subsatellite track heading is finally given by:

$$\text{If } P > 0 \text{ then } \omega = \text{acos}(R) \text{ else } \omega = 2\pi - \text{acos}(R) \quad (11.22)$$

where R (respectively P) is the cosine of the angle between the vector $\vec{r}_{\gamma_{P2scd}}$ and the reference vector \vec{r}_{ref} (respectively the vector \vec{r}_{perp} orthogonal to the reference vector).

$$\begin{aligned} R &= \frac{\vec{v}'_{\gamma} \cdot \vec{r}_{\gamma_{ref}}}{\|\vec{v}'_{\gamma}\| \cdot \|\vec{r}_{\gamma_{ref}}\|} \\ P &= \frac{\vec{v}'_{\gamma} \cdot \vec{r}_{\gamma_{perp}}}{\|\vec{v}'_{\gamma}\| \cdot \|\vec{r}_{\gamma_{perp}}\|} \end{aligned}$$

11.2 The sample selection

Not all the samples of a block have an influence on the σ^0 of a node, but there is more than one sample that influence the node value. The problem of the appurtenance of a sample to a node seems to be simple. If the sample is within the limits of the square window centered around the node then the sample will influence the node value. Unfortunately, the projection of a square plane surface on an ellipsoide or in other words, the determination of the perimetrical points of the node window is quite complex. The sample appurtenance to a node is consequently determined using the inverse way: the Earth's samples are projected onto the plane node window and their appurtenance is then easily determined with the help of a simple distance condition.

The planar square window centered around the node is kept and not projected onto the Earth's surface. This window is in the tangential plane, i.e. the plane whose normal vector is the normal to the Earth's surface at the node location. The window is oriented in such a way that one side is parallel to the relative nadir velocity. The other side is thus parallel to the vector which is the cross-product of the relative nadir velocity and the normal at the Earth's surface at the node. Thus, one side of all the windows associated with the 19 nodes of the same row will have the same direction.

The following formulas are used to determine the tangent plane at the node location, the two orthogonal directions into that plane, the sample projections onto these directions, and finally the sample appurtenance to the node (see figure (11.3)).

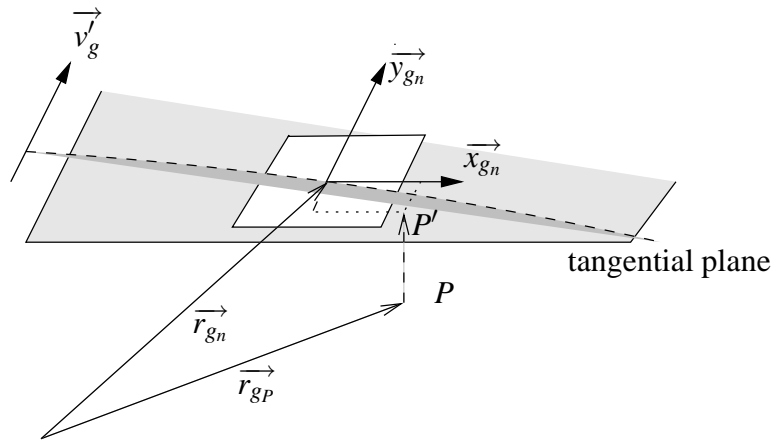


Figure 11.3: Sample selection

The two last steps, the sample projections and the sample appartenance determination, are repeated for all the samples that have been preselected for this node. The preselection of the samples is explained in the section 11.3.

The coordinate system to be used is the g frame.

11.2.1 The node local normal

When the node position $\vec{r}_{gn} = (x_n, y_n, z_n)$ is known in the g frame, it is easy¹ to deduce the local normal to the Earth at that point. The corresponding unit vector is:

$$\vec{uN}_{gn} = (x_n, y_n, (a/b)^2 z_n) / \sqrt{x_n^2 + y_n^2 + ((a/b)^2 z_n)^2} \quad (11.23)$$

11.2.2 The two square window unit vectors

These unit vectors are the vectors parallel to the sides of the square plane window, tangent at the node position at the Earth's surface.

$$\vec{y}_{gn} = \vec{v}'_g / \|\vec{v}'_g\| \quad (11.24)$$

$$\vec{x}_{gn} = \vec{y}_{gn} \times \vec{uN}_{gn} \quad (11.25)$$

where \vec{v}'_g is the satellite-Earth relative velocity at the nadir point. \vec{x}_{gn} is a unit vector because the two vectors of the cross-product are unit vectors and orthogonal.

11.2.3 The tangential plane

The plane which is tangent at the Earth's surface at the node point, $\vec{r}_{gn} = (x_n, y_n, z_n)$, has the following equation:

$$n_x \cdot x + n_y \cdot y + n_z \cdot z = D \quad (11.26)$$

where

- the unit normal at the Earth's surface at the node point is $\vec{uN}_{gn} = (n_x, n_y, n_z)$
- $D = n_x \cdot x_n + n_y \cdot y_n + n_z \cdot z_n = \vec{uN}_{gn} \cdot \vec{r}_{gn}$

The constant D is the projection of the node position onto the unit normal vector at the same position.

¹The calculation of the local normal unit vector at an Earth's point is done using the gradient operator of the function $f(x, y, z) = (x^2 + y^2)/a^2 + z^2/b^2$. Indeed, the GEM-6 surface equation forms an equipotential of this function. The normal vector at a point $\vec{r} = (x, y, z)$ on the GEM-6 can then be calculated by taking the gradient of f and then normalizing it: $\vec{uN} = \nabla f / \|\nabla f\| = (x, y, (a/b)^2 z) / \sqrt{x^2 + y^2 + ((a/b)^2 z)^2}$. This formula is valid for a vector expressed in the γ frame or in the g frame.

11.2.3.1 Determination of the projection point P'

The point P is the sample position $\vec{r}_{gP} = (x_P, y_P, z_P)$. The point P' is the projection of the point P onto the tangential plane. The vector between P and P' is parallel to the unit vector normal to the tangential plane. The location of the point P' , $\vec{r}_{gP'} = (x_{P'}, y_{P'}, z_{P'})$ is determined as follows, where a is unknown.

$$\begin{aligned}\vec{r}_{gP'} &= \vec{r}_{gP} + a \vec{uN}_{gn} \\ (x_{P'}, y_{P'}, z_{P'}) &= (x_P, y_P, z_P) + a(n_x, n_y, n_z) \\ &= (x_P + a n_x, y_P + a n_y, z_P + a n_z)\end{aligned}\quad (11.27)$$

Taking into account that P' belongs to the tangent plane, it has to satisfy (11.26):

$$\begin{aligned}n_x \cdot x_{P'} + n_y \cdot y_{P'} + n_z \cdot z_{P'} &= D \\ n_x \cdot (x_P + a n_x) + n_y \cdot (y_P + a n_y) + n_z \cdot (z_P + a n_z) &= D \\ (n_x x_P + n_y y_P + n_z z_P) + (n_x^2 + n_y^2 + n_z^2)a &= D\end{aligned}\quad (11.28)$$

But the normal vector is a unit vector, thus $n_x^2 + n_y^2 + n_z^2 = 1$ and (11.28) can be rewritten as

$$\begin{aligned}a &= D - (n_x x_P + n_y y_P + n_z z_P) \\ &= \vec{uN}_{gn} \cdot \vec{r}_{gn} - \vec{uN}_{gn} \cdot \vec{r}_{gP}\end{aligned}\quad (11.29)$$

Finally, the vector from the node to the projection point P' is thus:

$$\vec{r}_{gn2P'} = \vec{r}_{gP'} - \vec{r}_{gn} = \vec{r}_{gP} + a \vec{uN}_{gn} - \vec{r}_{gn}\quad (11.30)$$

11.2.4 The sample projections

The sample projections are the projections of the vector from the node to the sample, onto the two unit vectors. These projections correspond to the distance along, respectively, \vec{x}_{gn} and \vec{y}_{gn} , between the node and the projected sample location.

$$proj_x = \vec{r}_{gn2P'} \cdot \vec{x}_{gn}\quad (11.31)$$

$$proj_y = \vec{r}_{gn2P'} \cdot \vec{y}_{gn}\quad (11.32)$$

where $\vec{r}_{gn2P'}$ is the vector from the node to the point P' , projection of the sample point onto the tangential node plane:

$$\vec{r}_{gn2P'} = \vec{r}_{gP} + a \vec{uN}_{gn} - \vec{r}_{gn}\quad (11.33)$$

where $a = D - \vec{uN}_{gn} \cdot \vec{r}_{gP}$

11.2.5 The criteria of sample appartenance to a node

A sample is considered to contribute to a node if its projection fits into a rectangular window of sides s_{wl_x} across-track and s_{wl_y} along-track. If the absolute values of the projections of the vector $\vec{r}_{gn2P'}$ on the two unit vectors (belonging to the tangential node plane) are respectively smaller than their corresponding half window side length, the point P is said to belong to the node window.

Thus, if the condition

$$[(|proj_x| \leq s_{wl_x}/2) \text{ and } (|proj_y| \leq s_{wl_y}/2)]\quad (11.34)$$

is true, then the sample value will be taken into account for a contribution to the σ^0 node value.

11.3 The samples pre-selection

Not all the blocks contribute to a node value and for the blocks which contribute to it, not all the samples contribute to the node value. Due to CPU constraints, it is necessary to find some rough limits, in term of time (along-track) and in term of sample indexes (across-track) of these pre-selected blocks, to avoid having to compute the distance between each sample and the node.

The formulas related to this pre-selection are presented below. The pre-selection must be conservative in order not to exclude any sample that would have contributed to the node. The coordinate system to be used is the g frame.

11.3.1 Hypothesis

Since only a rough pre-selection is sufficient, several simplifying assumptions can be made.

First, a simplified geometry is considered.

The second hypothesis is that the node window is a plane square window having one side parallel to the nadir ground track, vector expressed in the g frame. The window size should be chosen such that even with the maximum expected yaw variations, all the samples that will contribute to a node still belong to the corresponding pre-selection window. The size of this window should thus be larger than the actual spatial averaging window size.

The third hypothesis is that in first approximation the altitude and the velocity of the spacecraft when it acquired the measurement blocks of all the beams contributing to one node were the same.

11.3.2 The node parameters

The relative velocity of the nadir point corresponding to the same time as the node is

$$v_{nadir} = \|\vec{v}_g\| \quad (11.35)$$

and the altitude of the satellite at the nadir point

$$H_{nadir} = \|\vec{r}_{gnadir} - \vec{r}_{gsc}\| \quad (11.36)$$

These two parameters are the same for the 19 nodes of the row since they are supposed to correspond to the same nadir position.

The across-track distance, distance between the nadir point and the node, in km, measured on the Earth's surface, is:

$$d_0 = \|\vec{r}_{gnadir}\| \theta \quad (11.37)$$

where

$$\cos(\theta) = \frac{\vec{r}_{gnadir} \cdot \vec{r}_{gn}}{\|\vec{r}_{gnadir}\| \|\vec{r}_{gn}\|} \quad (11.38)$$

The range corresponding to the node is the distance between the satellite and the node:

$$R_n = \|\vec{r}_{gsc} - \vec{r}_{gn}\| \quad (11.39)$$

11.3.3 The node limits depending on the beam

The node limits on the blocks times and samples indexes are different depending the beam considered: a set of four limits, T_{min} , T_{max} , SI_{min} and SI_{max} , are associated to one beam, and each node will have three of these sets. The node time is noted T_n and p_{wlx} and p_{wly} are the preselection window lengths respectively across-track and along-track.

11.3.3.1 Determination of the Earth's point from a point of the tangential plane

This is used to determine the ranges corresponding to the sample index limits (see figure 11.4).

If $\vec{r}_{gP'} = (x', y', z')$ is a point belonging to the tangential plane at the node then the corresponding Earth's point, $\vec{r}_{gP} = (x, y, z)$, is obtained as follow:

$$\vec{r}_{gP} = \vec{r}_{gP'} - d \vec{uN}_{gn} \quad (11.40)$$

where d is the real number to be found and $\vec{uN}_{gn} = (n_x, n_y, n_z)$ is the unit normal vector at the node. Because P is an Earth's point, it can be written that

$$\frac{x^2}{a^2} + \frac{y^2}{a^2} + \frac{z^2}{b^2} = 1 \quad (11.41)$$

$$\frac{(x' - d n_x)^2}{a^2} + \frac{(y' - d n_y)^2}{a^2} + \frac{(z' - d n_z)^2}{b^2} = 1 \quad (11.42)$$

Developing the factors and regrouping the terms, one obtains a second order equation in d :

$$a d^2 - 2b d + c = 0 \quad (11.43)$$

where

$$a = \frac{n_x^2}{a^2} + \frac{n_y^2}{a^2} + \frac{n_z^2}{b^2} \quad (11.44)$$

$$b = \frac{(n_x \cdot x')^2}{a^2} + \frac{(n_y \cdot y')^2}{a^2} + \frac{(n_z \cdot z')^2}{b^2} \quad (11.45)$$

$$c = \frac{x'^2}{a^2} + \frac{y'^2}{a^2} + \frac{z'^2}{b^2} - 1 \quad (11.46)$$

The two solutions are $d = \frac{b + \sqrt{b^2 - a \cdot c}}{a}$ and $d = \frac{b - \sqrt{b^2 - a \cdot c}}{a}$, and the solution to be kept is the smallest.

11.3.3.2 Range to index conversion

The conversion from a range value to an index value depends on the beam. For a given range R , the index value is:

$$index(R) = round\left[\left(\frac{2R}{c} - t_7\right)/t_d\right] \quad (11.47)$$

where

- c is the speed of light
- t_7 is the Tx pulse to first echo sample time and depends on the beam
- $t_d = \frac{1}{2f_s}$ where f_s is the sampling frequency

11.3.3.3 Fore beam

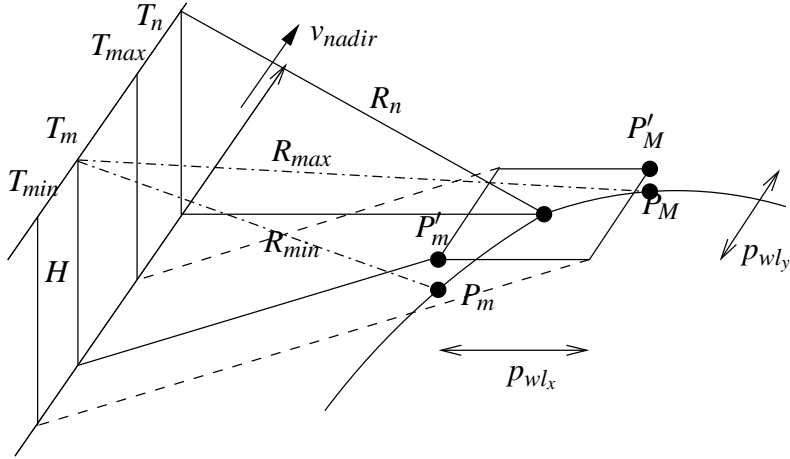


Figure 11.4: The determination of the node limits of the preselection for the fore beam blocks.

The time limits are (see figure 11.4):

$$T_{min} = T_n + (-p_{wlx}/2 - p_{wly}/2 - d_0)/v_{nadir} \quad (11.48)$$

$$T_{max} = T_n + (+p_{wlx}/2 + p_{wly}/2 - d_0)/v_{nadir} \quad (11.49)$$

The position, \vec{r}_{gscT_m} , of the satellite at the time $T_m = T_n - d_0/v_{nadir}$ is extracted from the orbit propagator to be used in the determination of the range limits.

For the determination of the range minimum, the point in the tangential plane to be considered is

$$\vec{r}_{gP'_m} = \vec{r}_{gn} - p_{wlx}/2 \vec{x}_{gn} - p_{wly}/2 \vec{y}_{gn} \quad (11.50)$$

with \vec{x}_{gn} and \vec{y}_{gn} being the two square window unit vectors.

The Earth's point, \vec{r}_{gP_m} , is then deduced as in 11.3.3.1. And the range minimum is then computed:

$$R_{min} = dist(\vec{r}_{gscT_m}, \vec{r}_{gP_m}) \quad (11.51)$$

For the determination of the range maximum, the point in the tangential plane to be considered is

$$\vec{r}_{gP'_M} = \vec{r}_{gn} + p_{wlx}/2 \vec{x}_{gn} + p_{wly}/2 \vec{y}_{gn} \quad (11.52)$$

The Earth's point, \vec{r}_{gP_M} , is then deduced as in 11.3.3.1. The range maximum is then computed:

$$R_{max} = dist(\vec{r}_{gscT_m}, \vec{r}_{gP_M}) \quad (11.53)$$

Consequently, the sample index limits are:

$$SI_{min} = \max[index(R_{min}), 0]$$

$$SI_{max} = \min[index(R_{max}), u \cdot 118 - 1]$$

where u is the upsampling factor (integer).

The result of the pre-selection and of the selection of the samples can be seen on the figure 11.5.

node number: [024,00], beam = 0

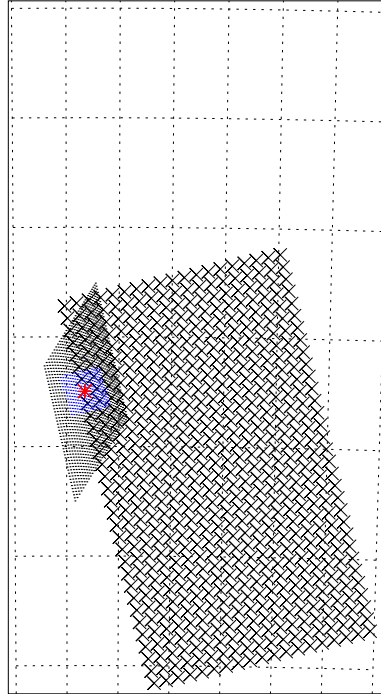


Figure 11.5: Fore beam: pre-selected and selected samples. The chosen node, marked as a red cross, is the 1st node of the 24th column of the node product. The other node of the product are marked as black crosses. The pre-selected samples for the node are marked as blue point while the samples belonging to the node are marked as black crosses. As it can be seen, the selection excludes data which have been pre-selected, and not the inverse. Some data are missing, because they are not available for the node processing.

11.3.3.4 Mid beam

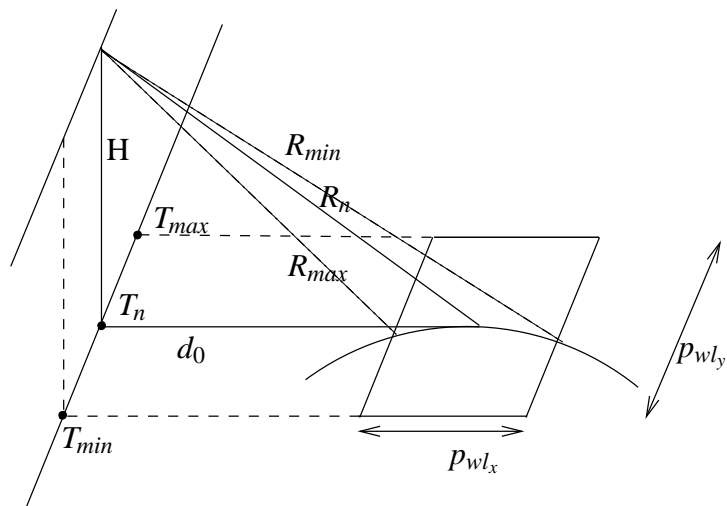


Figure 11.6: The determination of the node limits of the preselection

The time limits are (see figure 11.6):

$$T_{min} = T_n - (p_{wly}/2)/v_{nadir} \quad (11.54)$$

$$T_{max} = T_n + (p_{wly}/2)/v_{nadir} \quad (11.55)$$

The position, \vec{r}_{gscT_n} , of the satellite at the time T_n of the node is used in the determination of the range limits.

The ranges corresponding to the sample index limits are (see figure 11.6):

$$R_{min} = dist(\vec{r}_{gscT_n}, \vec{r}_{gP_m}) \quad (11.56)$$

$$R_{max} = dist(\vec{r}_{gscT_n}, \vec{r}_{gP_M}) \quad (11.57)$$

where

$$\vec{r}_{gP_m} = \vec{r}_{g_n} - p_{wlx}/2 \vec{x}_{g_n} \quad (11.58)$$

$$\vec{r}_{gP_M} = \vec{r}_{g_n} + p_{wlx}/2 \vec{x}_{g_n} \quad (11.59)$$

The sample index limits are:

$$SI_{min} = max[index(R_{min}), 0]$$

$$SI_{max} = min[index(R_{max}), u.74 - 1]$$

where u is the upsampling factor (integer).

The result of the pre-selection and of the selection of the samples can be seen on the figure 11.7.

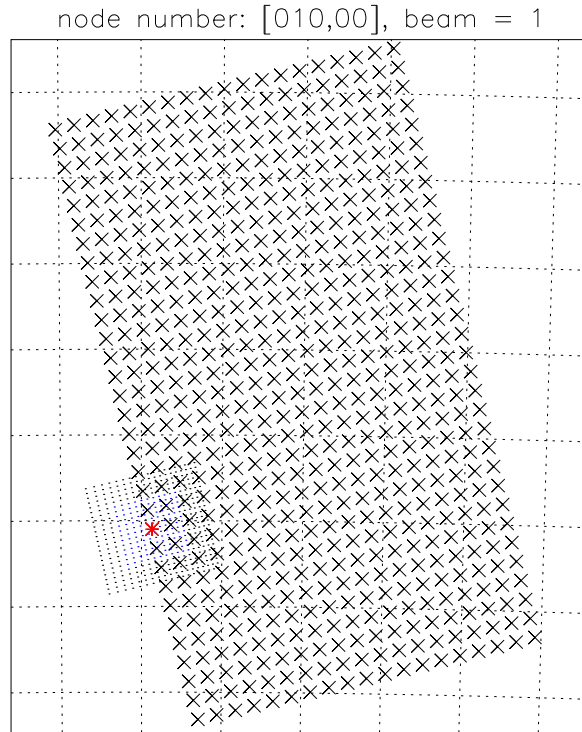


Figure 11.7: mid beam: pre-selection and selection

11.3.3.5 Aft beam

The time limits are:

$$T_{min} = T_n + (-p_{wlx} - p_{wly} + d_0)/v_{nadir} \quad (11.60)$$

$$T_{max} = T_n + (+p_{wlx} + p_{wly} + d_0)/v_{nadir} \quad (11.61)$$

The position, \vec{r}_{gscT_m} , of the satellite at the time $T_m = T_n + d_0/v_{nadir}$ is used in the determination of the range limits.

The ranges corresponding to the sample index limits are (see figure 11.6):

$$R_{min} = dist(\vec{r}_{gscT_n}, \vec{r}_{gP_m}) \quad (11.62)$$

$$R_{max} = dist(\vec{r}_{gscT_n}, \vec{r}_{gP_M}) \quad (11.63)$$

where

$$\vec{r}_{gP_m} = \vec{r}_{g_n} - p_{wl_x}/2 \vec{x}_{g_n} + p_{wl_y}/2 \vec{y}_{g_n} \quad (11.64)$$

$$\vec{r}_{gP_M} = \vec{r}_{g_n} + p_{wl_x}/2 \vec{x}_{g_n} - p_{wl_y}/2 \vec{y}_{g_n} \quad (11.65)$$

The sample index limits are:

$$SI_{min} = max[index(R_{min}), 0]$$

$$SI_{max} = min[index(R_{max}), u.118 - 1]$$

where u is the upsampling factor (integer).

The result of the pre-selection and of the selection of the samples can be seen on the figure 11.8.

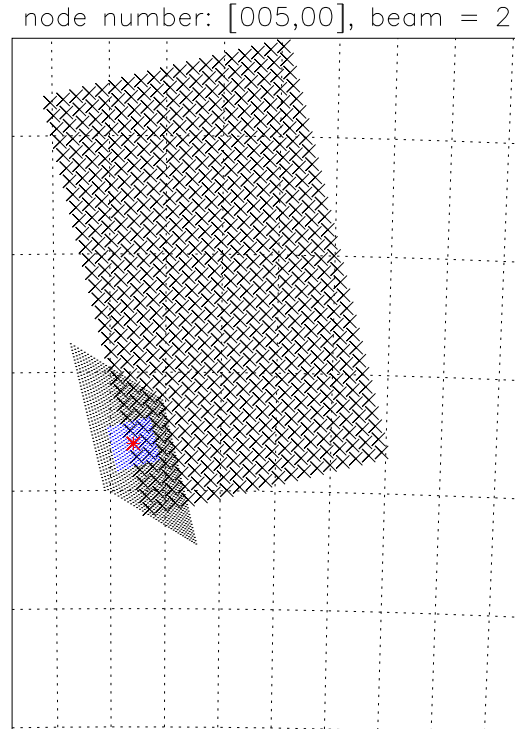


Figure 11.8: aft beam: pre-selected and selected samples.

11.4 The location of the nodes rows

The nodes rows are located on a line perpendicular to the satellite's ground trace. The rows of nodes are referenced in time. Given that reference time, the actual location of the intersection of the perpendicular line with the ground trace is computed as the nadir position of the spacecraft at the reference time.

The time of the nodes row of reference is defined as the time when the first mid-beam was acquired². The other rows of nodes are placed at the position of every 4th mid-beam, counted from the reference nodes row. Nodes rows are placed even in case of missing mid-beams source packets.

11.5 Incidence angle and look-angle

The definitions of the incidence angle and the look-angle of a point located on the Earth's surface are presented in the document [5], p 65.

All the vectors and their components are expressed in the γ frame. The point P located on the Earth's surface is characterized by a vector position noted $\vec{r}_{\gamma P} = (x_P, y_P, z_P)$. The unit vector local normal to the Earth's surface at the point P is written $\vec{uN}_{\gamma} = (n_x, n_y, n_z)$ with $n_x^2 + n_y^2 + n_z^2 = 1$. The satellite position is noted: $\vec{r}_{\gamma sc} = (x_{sc}, y_{sc}, z_{sc})$.

11.5.1 The incidence angle of an Earth's point

The incidence angle at the point P on the Earth's surface is defined as the angle between the vector $\vec{r}_{\gamma sc2P}$ from the satellite position to the point P , and the unit vector local normal at the Earth's surface at the point P .

$$\theta = \text{acos} \left(\frac{\vec{r}_{\gamma sc2P}}{\|\vec{r}_{\gamma sc2P}\|} \cdot \frac{\vec{uN}_{\gamma}}{\|\vec{uN}_{\gamma}\|} \right) = \text{acos} \left(\frac{(\vec{r}_{\gamma P} - \vec{r}_{\gamma sc})}{\|(\vec{r}_{\gamma P} - \vec{r}_{\gamma sc})\|} \cdot \vec{uN}_{\gamma P} \right) \quad (11.66)$$

11.5.2 The incidence angle of a node

The incidence angle at an Earth's point depends thus on the satellite's position at which the point on Earth has been seen by the satellite. This definition is not usable for the characterization of the incidence angle of a node and must be adapted.

A node is characterized by a triplet of incidence angles because the incidence angle is beam dependant. For each beam, the incidence angle associated to the node is the incidence angle of the sample for which the distance to the node position is the shortest, the distance to the node being the distance between the projection of the Earth's point onto the tangential plane at the node and the node position.

11.5.3 The look-angle of an Earth's point

Per definition, the look-angle at the point P on the Earth's surface is measured clockwise from a reference vector $\vec{r}_{\gamma ref}$ and the projection of the vector $\vec{r}_{\gamma P2sc}$ from the point P to the satellite's position, onto the local tangential plane. The reference vector $\vec{r}_{\gamma ref}$ is tangential to the local meridian at the point P (and thus is located to the tangential plane) and is pointing north.

11.5.3.1 Projection of the vector from the satellite position to P onto the local tangential plane

The vector from the point P to the projection of the satellite position onto the tangential plane at the point P is given by the formula (11.30):

$$\vec{r}_{\gamma P2sc'} = \vec{r}_{\gamma sc'} - \vec{r}_{\gamma P} = \vec{r}_{\gamma sc} + a \vec{uN}_{\gamma P} - \vec{r}_{\gamma P}$$

where $a = \vec{uN}_{\gamma P} \cdot \vec{r}_{\gamma P} - \vec{uN}_{\gamma P} \cdot \vec{r}_{\gamma sc}$

²Actually, as the time when the first valid mid-beam source packet is found in the data

11.5.3.2 Vector tangent to the local meridian at an Earth's point

The local meridian at an Earth's point is only defined if the point is not exactly at the North pole or at the South pole. If the point position is not a pole position, the local meridian at this point is defined as the curve, intersection of the Earth's surface and the plane containing the Earth's poles and the point.

The vector tangent to the meridian at the Earth's point P is thus at the intersection of the tangential plane at the Earth's surface in P and the plane containing the Earth's poles and the point.

The cartesian equation of the tangential plane is given by the formula (11.26):

$$n_x \cdot x + n_y \cdot y + n_z \cdot z = n_x \cdot x_P + n_y \cdot y_P + n_z \cdot z_P$$

The cartesian equation of the plane containing the local meridian is given by the following equation:

$$x_m \cdot x + y_m \cdot y + z_m \cdot z = 0$$

where (x_m, y_m, z_m) are the components of the vector \vec{r}_{γ_m} normal to this plane. This vector is parallel to the vector cross-product between the vector position of the point P and the unit vector from the South pole to the North pole:

$$\begin{aligned} \vec{r}_{\gamma_m} &= \vec{r}_{\gamma_P} \times \vec{z}_{\gamma} \\ (x_m, y_m, z_m) &= (y_P, -x_P, 0) \end{aligned}$$

The cartesian equation of the plane containing the local meridian is thus:

$$y_P \cdot x - x_P \cdot y = 0$$

The components of the vector $\vec{r}_{\gamma_{ref}}$ tangent to the meridian at the Earth's point are thus solution of the following system:

$$n_x \cdot x + n_y \cdot y + n_z \cdot z = n_x \cdot x_n + n_y \cdot y_n + n_z \cdot z_n \quad (11.67)$$

$$y_P \cdot x - x_P \cdot y = 0 \quad (11.68)$$

Or up to a multiplicative constant

$$\begin{aligned} (x_{ref}, y_{ref}, z_{ref}) &= (-x_P \cdot n_z, -y_P \cdot n_z, x_P \cdot n_x + y_P \cdot n_y) \\ \text{If } (x_P \cdot n_x + y_P \cdot n_y) < 0 \text{ then } (x_{ref}, y_{ref}, z_{ref}) &= (x_P \cdot n_z, y_P \cdot n_z, -x_P \cdot n_x - y_P \cdot n_y) \end{aligned} \quad (11.69)$$

11.5.3.3 The look-angle of an Earth's point

From the vector tangent to the local meridian and the local normal, a vector in the tangential plane, perpendicular to these vectors and pointing to the East is deduced:

$$\vec{r}_{perp} = \vec{r}_{ref} \times \vec{n}_{\gamma}$$

The look-angle is finally given by:

$$\text{If } P > 0 \text{ then } \omega = \text{acos}(R) \text{ else } \omega = 2\pi - \text{acos}(R) \quad (11.70)$$

where R (respectively P) is the cosine of the angle between the vector $\vec{r}_{\gamma_{P2sc'}}$ and the reference vector \vec{r}_{ref} (respectively the vector \vec{r}_{perp} orthogonal to the reference vector).

$$\begin{aligned} R &= \frac{\vec{r}_{\gamma_{P2sc'}} \cdot \vec{r}_{ref}}{\|\vec{r}_{\gamma_{P2sc'}}\| \cdot \|\vec{r}_{ref}\|} \\ P &= \frac{\vec{r}_{\gamma_{P2sc'}} \cdot \vec{r}_{perp}}{\|\vec{r}_{\gamma_{P2sc'}}\| \cdot \|\vec{r}_{perp}\|} \end{aligned}$$

11.5.4 The look-angle of a node

The beam-dependent look-angle at a node cannot be pre-computed since it depends on the yaw angle which is a priori unknown. In stead, the satellite position at a node is defined as the satellite position when the beam corresponding to the sample closest to the center of the node was acquired. The satellite position used is expressed in the g frame and corresponds thus to the UTCT of the closest sample. From that definition of the satellite position at a node, the node look angle is computed as described above, but with the node position expressed in the g frame (corresponding to the UTCT of the node row), the formulas being the same if all the vectors are expressed in the γ frame or in the g frame.

Chapter 12

K_p computation

12.1 Introduction

The normalized standard deviation of σ^0 measurements, K_p , is commonly used to evaluate the accuracy of the σ^0 measurements (see [12]):

$$K_p = \frac{\sqrt{\text{var}\{\sigma_{\text{meas}}^0\}}}{\sigma^0} \quad (12.1)$$

12.2 Expected σ^0 value

12.2.1 Sample value σ_{ij}^0

The signal actually measured by the scatterometer comprises the actual backscattered signal and noise contribution

$$s_{ijp} = \xi_{ijp} + \eta_{ijp} \quad (12.2)$$

where η_{ijp} denotes the noise contribution, ξ_{ijp} the contribution due to the backscattered signal. The indices i and j denote the spatial location where the measurement took place (resp. the along-track location and the range location) and the indice $p = 1, \dots, 32$ indicates the measurement number.

After detection, one has

$$P_{ijp} = N(i, j)\sigma_{ijp}^0 + n_{ijp} + 2\eta_{ijp}\xi_{ijp} \quad (12.3)$$

where $P_{ijp} = s_{ijp}^2$, $N(i, j)\sigma_{ijp}^0 = \xi_{ijp}^2$ and $n_{ijp} = \eta_{ijp}^2$. $N(i, j)$ is a normalization coefficient, converting the backscattered power to a backscattering coefficient as defined in section 5.3.6. This normalization factor of course depends on the location on Earth of the measurement. The noise power n_{ijp} is assumed constant across track and equal to n_i .

The local backscattering coefficient σ_{ij}^0 can thus be estimated by taking the average of the 32 measurements σ_{ijp}^0 :

$$\sigma_{ij}^0 = \frac{1}{32} \sum_{p=1}^{32} \sigma_{ijp}^0 = \frac{1}{N(i, j)} \left(\frac{1}{32} \sum_{p=1}^{32} P_{ijp} - n_i \right) \quad (12.4)$$

It is easy to show that this estimation is unbiased.

Equivalently, one has

$$\sigma_{ij}^0 = \frac{1}{N(i, j)} (P_{ij} - n_i) \quad (12.5)$$

where

$$P_{ij} = \frac{1}{32} \sum_{p=1}^{32} P_{ijp} \quad (12.6)$$

The unbiased estimator of the variance of σ_{ijp}^0 is given by

$$S_{\sigma_{ijp}^0} = \frac{1}{31} \sum_{p=1}^{32} (\sigma_{ijp}^0 - \sigma_{ij}^0)^2 \quad (12.7)$$

and making the assumption that the random variables σ_{ijp}^0 are independent, the variance of σ_{ij}^0 can be obtained by

$$S_{\sigma_{ij}^0} = \frac{1}{32} S_{\sigma_{ijp}^0} \quad (12.8)$$

12.2.2 Node value σ^0

The σ^0 value at a node is obtained by taking the weighted average of the σ_{ij}^0 values obtained at the different measurement samples inside the weighting window:

$$\sigma^0 = \sum_{(i,j) \in \mathcal{D}} a_{ij} \sigma_{ij}^0 \quad (12.9)$$

where \mathcal{D} denotes the domain inside which the weighting window is not zero.

12.3 Variance of σ^0

The value of σ^0 is to be seen as one particular realization of a random process. Since only one realization is available, the variance of σ^0 cannot be estimated using the classical expression.

12.3.1 Direct estimation

The variance of σ_p^0 is given by

$$S_{\sigma_p^0}^2 = \frac{1}{31} \sum_{p=1}^{32} (\sigma_p^0 - \sigma^0)^2 \quad (12.10)$$

Making the assumption that the different realizations of σ_{ijp} (different p) are independent from each other, one has that the different realizations of σ_p^0 are also independent. Since σ^0 is the mean of the realizations σ_p^0 , its variance is simply obtained by

$$S_{\sigma^0}^2 = \frac{1}{32} \sum_{p=1}^{32} S_{\sigma_p^0}^2 \quad (12.11)$$

12.3.2 Indirect estimation

Introducing the expressions of σ_p^0 and σ^0 in the expression of the variance of equation (12.10), one obtains

$$S_{\sigma_p^0}^2 = \frac{1}{31} \sum_{p=1}^{32} \left(\sum_{(i,j) \in \mathcal{D}} a_{ij} \sigma_{ijp}^0 - \frac{1}{32} \sum_{p=1}^{32} \sum_{(i,j) \in \mathcal{D}} a_{ij} \sigma_{ijp}^0 \right)^2 \quad (12.12)$$

or, isolating the common terms

$$S_{\sigma_p^0}^2 = \frac{1}{31} \sum_{p=1}^{32} \left(\sum_{(i,j) \in \mathcal{D}} a_{ij} \left(\sigma_{ijp}^0 - \frac{1}{32} \sum_{p=1}^{32} \sigma_{ijp}^0 \right) \right)^2 \quad (12.13)$$

and introducing σ_{ij}^0

$$S_{\sigma_p^0}^2 = \frac{1}{31} \sum_{p=1}^{32} \sum_{(i,j) \in \mathcal{D}} a_{ij}^2 (\sigma_{ijp}^0 - \sigma_{ij}^0)^2 + \frac{1}{31} \sum_{p=1}^{32} \sum_{(i,j) \neq (k,l) \in \mathcal{D}} \left(a_{ij} a_{kl} (\sigma_{ijp}^0 - \sigma_{ij}^0) (\sigma_{klp}^0 - \sigma_{kl}^0) \right) \quad (12.14)$$

or, reverting the order of the summation

$$S_{\sigma_p^0}^2 = \sum_{(i,j) \in \mathcal{D}} a_{ij}^2 \frac{1}{31} \sum_{p=1}^{32} (\sigma_{ijp}^0 - \sigma_{ij}^0)^2 + \sum_{(i,j) \neq (k,l) \in \mathcal{D}} a_{ij} a_{kl} \frac{1}{31} \sum_{p=1}^{32} ((\sigma_{ijp}^0 - \sigma_{ij}^0)(\sigma_{klp}^0 - \sigma_{kl}^0)) \quad (12.15)$$

The first term of this expression is the variance of σ_{ijp}^0 while the second term is the covariance of the random variables σ_{ijp}^0 and σ_{klp}^0 . The covariance can be expressed in function of the correlation coefficient and the variance of the random variables which finally yields

$$S_{\sigma_p^0}^2 = \sum_{(i,j) \in \mathcal{D}} a_{ij}^2 S_{\sigma_{ijp}^0}^2 + \sum_{(i,j) \neq (k,l) \in \mathcal{D}} \rho_{ijklp} \sqrt{S_{\sigma_{ijp}^0}^2 S_{\sigma_{klp}^0}^2} \quad (12.16)$$

with the correlation coefficient ρ_{ijklp} being defined as

$$\rho_{ijklp} = \frac{1}{31} \sum_{p=1}^{32} \frac{\sigma_{ijp}^0 - \sigma_{ij}^0}{\sqrt{S_{\sigma_{ijp}^0}^2}} \frac{\sigma_{klp}^0 - \sigma_{kl}^0}{\sqrt{S_{\sigma_{klp}^0}^2}} \quad (12.17)$$

Chapter 13

Ingestion

13.1 Introduction

The ingestion consists in reading the EWIC files and storing the individual measurements, including calibration data, noise data and other QC information in the internal representation of the processor. The purpose of this chapter is to describe how possible source packet corruption is detected and what actions are taken, possibly to attempt to recover the corrupted packet or limit the effect of the corruption.

Source packets can be (partly) unusable due to two main effects

- data corruption, typically occurring during the downlink of the data.
- instrument malfunction such as arcing of the TWT or calibration sub-system failure.

If some packets are acquired twice (or more) by different ground stations, it is possible that only some of the packets will be affected by data corruption. However, instrument malfunction will always affect all the packets, regardless of the acquiring station.

When source packets are acquired by several reception stations at the same time, a selection of the “best” source packets is possible. This selection process is performed as a pre-processing of several EWIC files to yield one consolidated EWIC file containing the “best” packets from the provided EWIC files. This pre-processing is described in Section 13.2.

The quality control performed on the subsequent ingestion of the resulting EWIC file is described in Section 13.3.

13.2 EWIC file merging

13.2.1 Introduction

EWIC file merging consists in producing a consolidated EWIC file from several overlapping EWIC files. In principle, when overlapping EWIC files are available, the data in the overlapping areas should be identical. Corruption of the packets, in particular at the start (and end) of the acquisition is always possible. The merging processing consists in identifying the corrupted packets and in selecting the “best” packet from the overlapping packets. The “best” packet is the one that has the “least” corruption. The “best” packet is output and stored in the resulting output EWIC file.

The merging process can be subdivided in 4 phases:

1. Initialization phase, where dummy packets are dropped.
2. Timecode correction phase, where possible corruption of the satellite binary time is detected and corrected
3. Source packet quality assessment, where the quality of each source packet is measured.

4. The merging in itself, where SP coming from different EWIC files are combined, keeping the SP with the highest quality.

13.2.2 Initialization phase

The initialization phase consists in

- Reading a number of SP, silently dropping the dummy packets. Dummy packets are packets where the echo data is exactly 0.
- Deducing from these SP a reference timecode to be used to alleviate the timecode overflow issue. The reference timecode is the smallest timecode of a contiguous sequence (which can be assumed non corrupted).

13.2.3 Timecode correction phase

The timecode (satellite binary time) correction is required to cope with possible timecode corruption. The corruption of the timecode can be assessed by looking at the timecode of the neighbouring SP. Indeed, the timecode are assumed to be strictly monotonous (with the exception of the overflow).

The following decision tree is considered to detect corrupted timecodes:

- If the timecode of three successive SP (corresponding to one FMA sequence) are in sequence and have a nominal increment w.r.t. each other, these timecodes are assumed to be valid.
- Corrupted timecode is detected by comparison with valid timecodes from neighboring SP. A timecode is corrupted if it is smaller than the previous valid SP or larger than the next valid SP.
- If the timecode of a single SP in an otherwise continuous sequence is corrupted, the timecode is corrected by interpolation between the valid timecodes of the neighboring SP. In any case, the sequencing of the SP shall never be altered. The message ERR-TIMECODE-CORRUPTED-CORRECTED is logged.
- If a timecode is found to be corrupted and if the SP surrounding it are not nearly contiguous (i.e. there is a data gap), the SP is dropped. The message ERR-TIMECODE-CORRUPTED-DROPPED is logged.

This processing is performed separately for each EWIC file. After this processing, the timecode is assumed to be reliable and usable for further assessment of the validity of the other fields of the records.

13.2.4 Source packet quality assessment

13.2.4.1 Corrupted beam-field

Antenna sequences should always be complete. This is detected based on the sequencing of the timecode. If the timecode of the considered SP is in continuous sequence with the previous or the next SP while the beam-field is not, beam-field corruption is assumed and the field value is replaced by the correct value. The message ERR-BEAM-CORRUPTED-CORRECTED is logged. The SP is flagged as having been corrected, the flag being used in the merge process. If the considered SP is an isolated packet, the corruption cannot be detected.

13.2.4.2 Corrupted Doppler coefficients

Doppler coefficients should only change twice per orbit and should remain constant between these changes. The Doppler coefficients of one SP must always be equal to the Doppler coefficients of either the previous or the next SP of the same beam, unless right after or before a data gap.

In the case corrupted Doppler coefficients are noticed, their value is replaced by the value of the previous SP of the same beam. It should be noticed that this correction might be wrong if the corruption occurs

exactly when, along the orbit, the Doppler coefficients change. This is particularly true if the Doppler coefficients of several SP are affected. The message ERR-DOPPLER-COEF-CORRUPTED-CORRECTED is logged. The SP is flagged as having been corrected, the flag being used in the merge process.

13.2.4.3 Frame checksum flag set

The Frame Checksum flag is set when either bits 8-9 (Frame Synchronizer) of the EWIC MPH are equal to 1 and bits 10-11 (FS processor to I/F) of the EWIC MPH are equal to 1. If the bits are equal to 2 (unknown performance), the bits are reputed to either be 1 or zero depending on a configuration.

The message ERR-FRAME-CHEKCSUM-SET is logged. Additionnaly, noise power, calibration pulse and mode flag are replaced by default values read from a configuration file.

The flag is also used in the merge process.

13.2.5 Source packet selection and merging

If several SP corresponding to the same timecode are available, the SP with the least number of flags set is selected. If all available SP have the same number of flags set, the SP corresponding to the first EWIC file is selected.

Otherwise, the SP are output in sequence, regardless of the EWIC file the SP was extracted from.

13.3 EWIC file ingestion

13.3.1 Calibration packet rejection

SP acquired in calibration mode have the calibration flag set (see [2], page 4.4-102). The message NOTICE-CAL-SP is logged and the SP is dropped.

13.3.2 Dummy packet rejection

Dummy SP are characterized by having a zero echo data. The corresponding SP are silently dropped.

13.3.3 Corrupted noise power

A corrupted noise power is assumed when the noise power is above a configurable threshold.

In this case, the message ERR-CORRUPTED-NOISE-POWER is logged and the noise power is replaced with default values read from a configuration file.

13.3.4 Corrupted calibration pulses

A corrupted calibration pulse is assumed when the calibration pulse energy is above a configurable threshold.

In this case, the message ERR-CORRUPTED-CAL-PULSE is logged and the calibration pulse is replaced with default values read from a configuration file.

13.3.5 Calibration pulse missing

Failure of the calibration subsystem is detected when the echo signal power is larger than a configuratble threshold (that has to be larger than the thermal noise floor) and when the calibration pulse energy is smaller than a configurable threshold.

In this case, the message NOTICE-CAL-SUB-SUBSYSTEM-FAILURE is logged. The calibration pulse energy is replaced with the an energy computed using a linear formula. The terms of the linear extrapolation are read from a configuration file.

13.3.6 Wave gap

Data gaps between successive complete FMA sequences

- having the duration of two FMA sequences
- occurring when in wind/wave mode

are assumed to be wave gaps. In this case, the message NOTICE-WAVE-GAP is logged and the gap is filled by copying the neighbouring FMA sequences.

13.3.7 Data gap

When a data gap that is not a wave gap is detected, the message NOTICE-DATA-GAP is logged. No other action is performed.

13.3.8 Arcing event

Arcing events are detected when the echo signal is smaller than a certain threshold (but larger than zero) and the calibration pulse energy is smaller than a configurable threshold.

In this case, the message NOTICE-ARCING-EVENT is logged. No other action is performed.

Part IV

User provided grid processing

Chapter 14

Introduction

In the current ERS wind product (and most scatterometers) the nodes are defined relative to the satellite ground track. A new data-independent grid is introduced, where the nodes may have arbitrary positions. Typically, the nodes would be defined on an earth-fixed grid rather than the usual satellite swath-related grid.

Level 2 processing involves spatial averaging and resampling to output the data at node locations. This averaging and resampling is best performed with data at the highest available spatial resolution, i.e. raw-resolution level 2 data. Providing a data product with user-specified node location avoids having the user resampling and interpolating level 2 data at the nominal resolution. Such an operation would necessarily degrade product quality due to the inherent interpolation involved. This permits a direct use and/or comparison of data from different remote sensing instruments.

In addition, this provides some additional level of uniformity between scatterometer data among different instruments.

Chapter 15

Nodes generation and pre-selection

15.1 Generation of the grid nodes

The nodes are assumed to be externally provided. By way of an example, an earth-fixed grid of nodes is described below.

The example grid is part of so-called Discrete Global Grids (DGG). A number of grids are analyzed in [18] for conformality, isotropy, global coverage, adjacency and the minimization of the inter-cell distance variation. The Icosahedron Snyder Equal Area (ISEA) partitioned with hexagons at aperture 4 resolution 9 (ISEA4H9) presents uniform adjacency with a mean inter-cell distance of 15.072 km and a standard deviation of 0.9 km [18, 20]. Therefore, this grid was chosen for the processing of SMOS level 1C data.

15.2 Selection of the grid nodes

As user-provided grids typically contain many (several millions) nodes, a pre-selection of the nodes that may possibly contain data is performed in order to optimize the processing.

Only the nodes inside the full resolution swath of the scatterometer are selected for further processing. The pre-selection method is based on the great circle distance between the grid nodes and the middle of the satellite swath. This distance is selected such that the pre-selected nodes fall inside the scatterometer swath.

15.3 User-provided grid input format

The locations of the nodes are provided via an external text file. Each line in the file corresponds to one node. And each line is composed of 4 comma-separated numbers. The first number is an integer and indexes the node, the second number is an unused integer, the third floating point number is the longitude (in decimal degrees) and the fourth field is a floating point number with the latitude (in decimal degrees). An extract of a sample user-provided grid file is shown in Table 15.1.

```
1, 0000000000, 11.250000, 58.282526
2, 0100000000, -168.750000, 58.282526
3, 0100000001, -168.750000, 58.518418
4, 0100000010, -168.750000, 58.754575
5, 0100000011, -168.750000, 58.990994
```

Table 15.1: Extract of a sample user-provided grid file (only the first 5 nodes are shown).

Chapter 16

Sample pre-selection and selection

The pre-selection and selection of the samples prior to spatial averaging is performed to optimize the processing speed. The method used for the nominal product (ASPS2.0) is retained and is briefly reviewed below.

Only a group of source packets and set of samples within these source packets contribute to a node. To avoid having to compute the distance between each sample and the node, a pre-selection of potentially contributing samples is performed. The pre-selection area must be larger than the size of the spatial averaging window. The pre-selection of the source packets is based on the timing of each source packet and the pre-selection of the samples within a source packet is based on a rough geometric estimation, thus yielding a parallelogram-like pre-selection window. For further details about sample selection see [15]. From the pre-selected samples, the contributed samples are those that are within a certain radius from the node.

Figure 16.1 illustrates the sample selection. The grid nodes are plotted in blue, the samples of the pre-selected source packets are in black, the pre-selected samples are in green and the final contributing samples are in red.

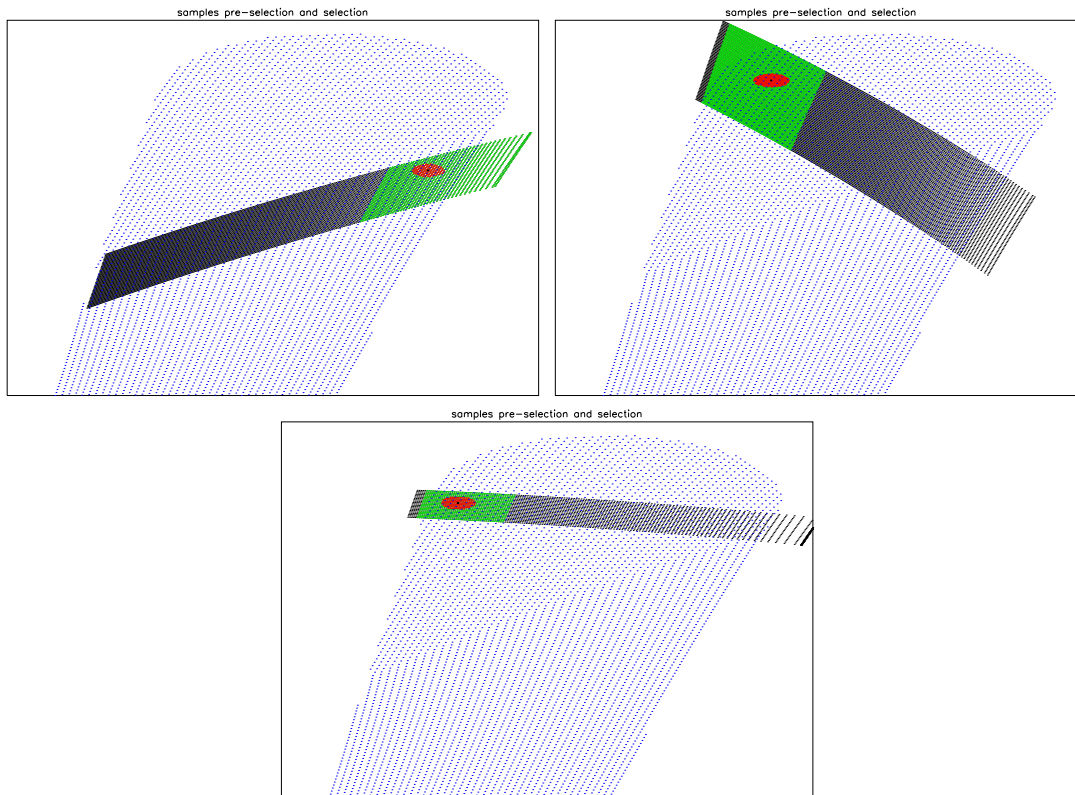


Figure 16.1: Sample selection and pre-selection around a node

Chapter 17

Spatial filtering

Spatial filtering consists in a weighted sum of samples belonging to an area around each node [10]. In the nominal ASPS processing, the grid is approximately square and the weighting function used is a two-dimensional separable Hamming window with axis parallel to the along and across-track directions. This rectangular filter is suitable for the current rectangular spatial sampling (lines of nodes perpendicular to the satellite ground track), where each cell has four (approximately) equidistant neighboring cells.

In a user-provided grid, one has to cope with general node positions. If the grid is approximately regular and interleaved, much like an ISEA4H9 grid, the spatial sampling is approximately hexagonal and the spectral replication (aliasing) grid is also (approximately) hexagonal [13, 22]. Therefore, the ideal low-pass spatial filter guaranteeing no frequency aliasing is hexagonal. Not taking into account differing cross- and along-track raw-signal spatial resolution (due respectively to chirp length and antenna azimuth pattern), the spatial averaging window may be approached by a circularly symmetric Hamming window

$$w(x, y) = w(r)$$

where $r = \sqrt{x^2 + y^2}$ is the radial distance between sample (x, y) and the node. Such a window also minimizes the introduction of privileged directions.

If however the differing cross- and along-track raw-signal spatial resolution may not be neglected, an elliptic window has to be considered. In this case, one has $r = \sqrt{x^2/a^2 + y^2/b^2}$ where a and b are window size parameters and the axis are assumed located across- and along-track.

17.1 Design of the spatial averaging window

The aim of this section is to design the shape and the dimensions of the spatial averaging window, which will be used in the spatial filtering of the fixed grid product. Part of the discussion is illustrated using Hamming windows. It is understood that other window functions (Blackman, rectangular, ...) may be used.

17.1.1 Separable Hamming window

The kernel of separable (Hamming) window is a result of the product of two one-dimensional (Hamming) windows. The weight of a sample with coordinates (x, y) is $w(x, y) = w(x)w(y)$.

An illustration of the spatial and spectral shape of the separable Hamming window is given in figure 17.1.

17.1.2 Circular Hamming window

The circular Hamming window is generated by circularly rotating a one-dimensional Hamming window. This produces a non-separable radially symmetric window. The region of support of such a window is a disk. The weight of a sample with coordinates (x, y) , such that $r = \sqrt{x^2 + y^2}$ is $w(x, y) = w(r)$.

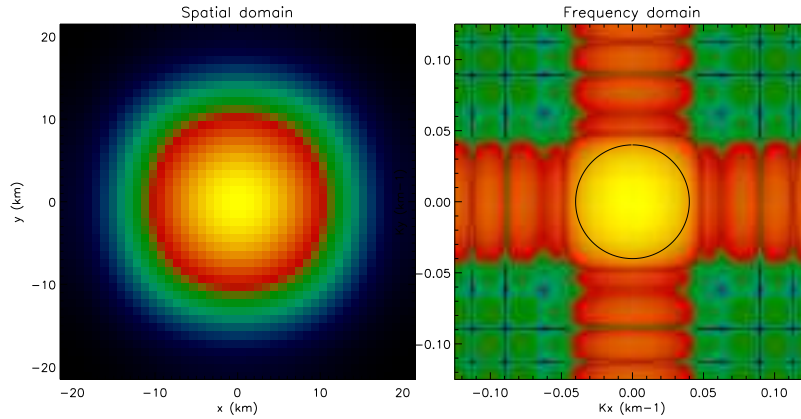


Figure 17.1: Separable Hamming window

An illustration of the spatial and spectral shape of the circularly symmetric Hamming window is given in figure 17.2.

17.2 Aliasing analysis

The grid of the nominal scatterometer product takes a form of lines of nodes (19/41) which have a $25/12.5$ km separation across and along track within the swath. Each node is centered within a resolution cell of $50 \times 50 \text{ km}^2 / 25 \times 25 \text{ km}^2$, for nominal and high resolution products respectively.

The size of the Hamming window is $84.5 \times 84.5 \text{ km}$ or $42.25 \times 42.25 \text{ km}$ across and along track for the fore and aft antennae, and $86 \times 86 \text{ km}$ or $43 \times 43 \text{ km}$ for the mid antenna, for nominal and high resolution products respectively.

The sigma naught (σ_0) of given a node is the average of the sigma naughts of all samples inside the region of support of the window (rectangle or circle) weighted by the value of the window at the spatial coordinates of the samples. The region of support of the window is limited in the spatial domain, this is not the case in the frequency domain and the windows exhibit spectral sidelobes. The level of the sidelobes at frequencies higher than the Nyquist frequency will determine the amount of contaminating energy from neighboring spectral cells.

We define here the SNR as the energy contributing to the cell of interest E_s to the energy aliased from neighboring cells E_n where a uniform power spectrum is considered¹. By symmetry the energy outside the spectral cell centered at the origin is assumed to be the same as the energy aliased by the neighboring spectral cells.

$$SNR = \frac{E_s}{E_n} \quad (17.1)$$

A comparison of the SNR which would result from each window using the same radius and grid spacing is presented in Table 17.1. As can be seen the separable Hamming window presents the best SNR followed by the circularly symmetric Blackman, while the worst SNR is provided by the rectangular window, as expected.

¹The power spectrum is of course not uniform but the point here is to perform a comparison of the aliasing-rejection properties of the windows

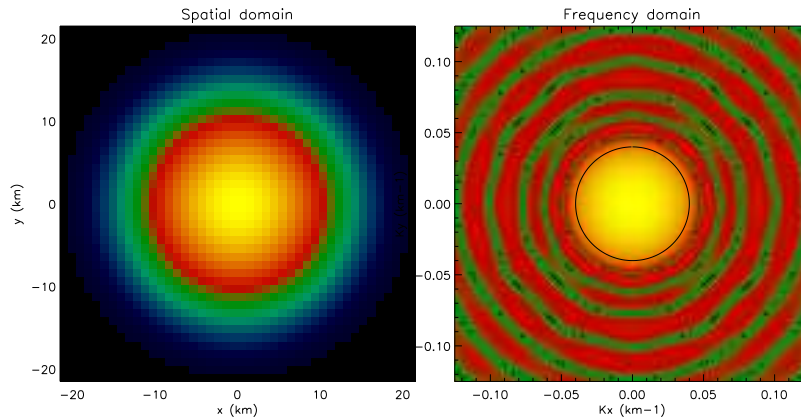


Figure 17.2: Circularly symmetric Hamming

Window type	Grid spacing (km)	Window diameter (km)	SNR
Rectangular Hamming	12.5	43	5.6768
Circular Hamming	12.5	43	1.9280
Circular Blackman	12.5	43	4.5227
Circular rectangle	12.5	43	0.2417
Circular Blackman	15	60	9.9715

Table 17.1: SNR comparison

For a ISEA4H9 grid with node spacing of 15km, a circularly symmetric Blackman window with 60 km radius would be used and the SNR corresponding to this window would be 9.97.

17.3 Spatial resolution

The ERS-2 scatterometer resolution is determined by the antenna beam width in azimuth and by the pulse length in across-track. The azimuth antenna beam width is 0.9° for the fore/aft antenna and 1.4° for the mid antenna [4]. The emitted pulse width is $130 \mu\text{sec}$ for the side antennas and $70 \mu\text{sec}$ for the mid antenna. Given the projection of the azimuth antenna pattern and the pulse on ground varies with range, the spatial resolution depends on range (incidence angle).

Figure 17.3 shows the ERS-2 across-track and along-track theoretical resolution in function of the incidence angle. The worst resolution is ~ 46 km, performed by the side antennas in across-track at near swath, and 28 km by the mid antenna in along-track at far swath, The highest resolution is 14 km for mid antenna at far swath and side antenna at near swath respectively in across-track and along-track. The highest resolution of the mid antenna in across-track is due to the short pulse and the lower resolution in along-track is due to the broader beam.

The spatial resolution of a system is defined by the width of the impulse response function at 50 percent of its peak value. The Hamming window used in the spatial averaging step dominates the form of the scatterometer impulse response function. Therefore the final resolution of the scatterometer product depends mainly on the characteristics of this window.

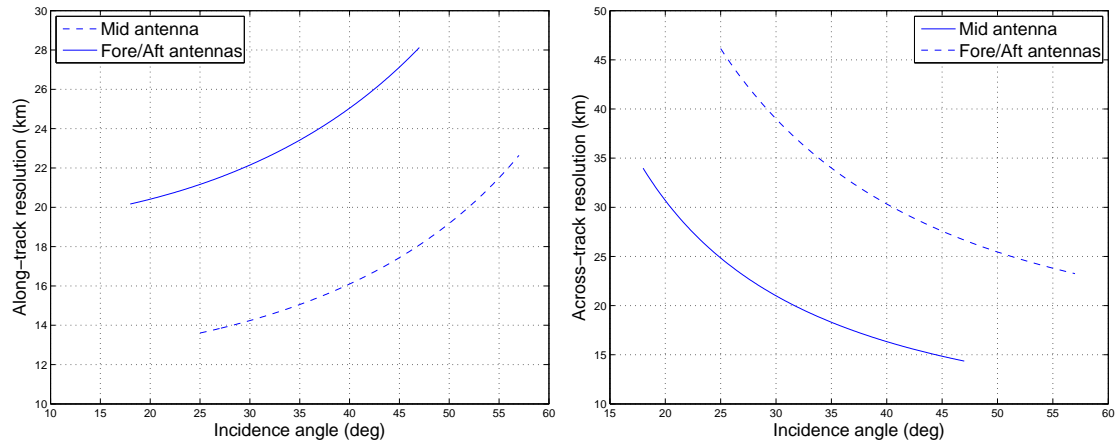


Figure 17.3: ERS-2 spatial resolution - along-track resolution (left) - across-track resolution (right)

The width of the Hamming window used for the nominal product is 84.5 km for the side antenna and 86 km for the mid antenna. The spatial resolution corresponding to this window is ~ 45 km. This resolution corresponds to the worst case (see figure 17.3), i.e., the resolution is normalized across and along-track.

ERS-2 scatterometer was designed for ocean wind field retrieval from the measured backscatter, which require a high radiometric resolution. The radiometric resolution (called K_p) is the standard deviation of the averaged sigma noughts inside the integration area, i.e., the spatial filtering window size. Increasing integration area will decrease the K_p but on the other hand decreases the spatial resolution. Moreover the aliasing effect should be taken into account (as discussed in the previous section), which depends on both the grid spacing and the window spectrum.

Figure 17.4 show a comparison of three filters with respect to the actual one (Hamming). All the filters are chosen to have the same spatial resolution as the actual Hamming window. The vertical dashed bars show the half width power of the windows in space domain and -3 dB magnitude in spatial frequency domain. It can be noticed that for the same resolution, Both Hamming and Blackman windows have low sidelobes level (~ -20 dB). While the rectangular window has the highest sidelobes, this is in line with SNR values shown above. Table 17.2 summarizes the performances of the different windows.

Window type	Window length (km)	Resolution (km)	Relative sidelobe attenuation (dB)
Boxcar	46	~ 45	-13.2
Hamming	86	~ 45	-42.6
Blackman	110	~ 45	-58.1

Table 17.2: Spatial resolution comparison

In the UPG processing chain a radial window is used to cope with the differing pre-existing spatial filtering inherent to the instrument respectively in azimuth and range. This yields a spatial filter with an elliptic region of support. The length of the semi-major and semi-minor axis are configurable. The circularly symmetric window shown in 17.2 is a particular case of the radial window, when the difference in azimuth and range are neglected. The user can choose between Hamming and Blackman window. However the separable Hamming window still can be used by the processor.

If the provided grid is regular i.e., with a fix grid spacing, The window size is determined by the grid spacing. The bandwidth of the used window (in spatial frequency space) must be smaller than Nyquist frequency. This bandwidth should be defined (-3, -10 dB ...), e.g., the magnitude of the spectrum of the actual window at Nyquist frequency (0.02 km^{-1}) is less than -10 dB. For instance for ISEA4H9, the magnitude of the 60 km Blackman window spectrum at Nyquist frequency (0.033 km^{-1}) is ~ -20 dB. In the case of an irregular grid, the window width can be normalized to worst resolution across and along

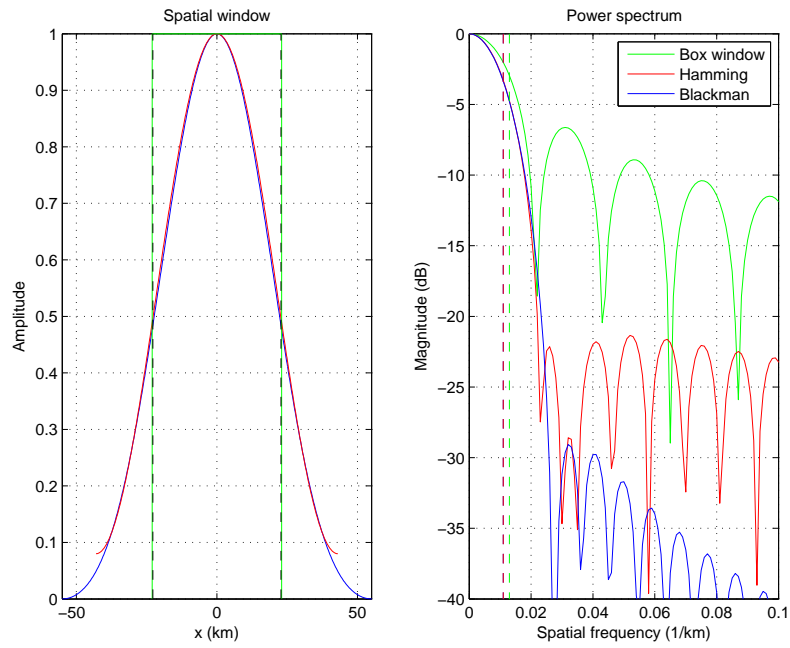


Figure 17.4: ERS-2 spatial filtering

track, respectively 46 km and 28 km, or size varying with varying resolution. However, the impact on the noise (K_p) should be assessed and probably a threshold fixed, particularly for small resolution cells (small integration area).